Energy efficient control of a low voltage motor to extend battery life

JOHAN MALGERUD
DANIEL SKARP

KTH Industrial Engineering
and Management

Master of Science Thesis
Stockholm, Sweden 2014

Energy efficient control of a low voltage motor to extend battery life

Johan Malgerud
Daniel Skarp

Master of Science Thesis MMK 2014:59 MDA 493
KTH Industrial Engineering and Management
Machine Design
SE-100 44 STOCKHOLM

KTH Industriell teknik och management

Examensarbete MMK 2014:59 MDA 493

Energieffektiv kontroll av en lågspänningsmotor för ökad batterilivslängd

Johan Malgerud

Daniel Skarp

Godkänt	Examinator	Handledare
2014-06-26	Jan Wikander	Bengt Eriksson
	Uppdragsgivare	Kontaktperson
	ASSA ABLOY	Daniel Garmén

Sammanfattning

Intresset för elektromekaniska lås ökar, på grund av dess många fördelar jämfört med de rent mekaniska låsen. Fördelar med elektromekaniska lås är, tillgång till online tillträdes hantering och billigare nycklar. Dessa applikationer är ofta batteridriven vilket ökar behovet av energibesparing för att förlänga batteriets livslängd.

Detta examensarbete har till syfte att minska energiförbrukningen i ASSA ABLOY lås, Aperio E100 med hjälp av mer intelligent motorstyrning, samt genom att välja lämpligare hårdvara. Avhandlingen börjar med att utvärdera olika ställdonstyper, och välja det mest lämpliga för Aperio E100 låset. En mer djupgående undersökning för denna motortyp genomförs sedan för att hitta nya energieffektiva styrmetoder samt en mer passande motor och motor brygga.

En borstlös DC motor valdes för att ersätta det nuvarande borst DC motorn i Aperio E100. En spänningsstegsmetod används för att minska energiförbrukningen, genom att simulera ingångssteg med hjälp av MATLAB Simulink. Den totala förbrukningen av borst DC motorn minskade med 33%, och den borstlösa DC motorn med 89%. Dessa minskningar av motorkonsumtionen ledde till en teoretisk förlägning av batteritiden på 8 respektive 17,6 månader.

KTH Industrial Engineering and Management

Master of Science Thesis MMK 2014:59 MDA 493

Energy efficient control of a low voltage motor to extend battery life

Johan Malgerud

Daniel Skarp

Approved	Examiner	Supervisor
2014-06-26	Jan Wikander	Bengt Eriksson
	Commissioner	Contact person
	ASSA ABLOY	Daniel Garmén

Abstract

The interest for electromechanical locks is constantly increasing, with its many advantages over the purely mechanical varieties, such as intelligent access schedules, online access handling, and cheaper credentials. These applications are often battery powered making the need for energy conservation crucial when extending the battery lifetime.

This master thesis will reduce the energy consumption of the ASSA ABLOY, Aperio E100 lock using more intelligent control of the motor, as well as by selecting more suitable hardware. The thesis starts out by evaluating different actuator types, and selecting the most suitable for the Aperio E100 application. An in depth study for this motor type then reveals new energy efficient control methods for this.

A brushless DC motor is chosen to replace the current brushed DC motor in the application. A voltage trajectory method is then used to reduce the consumption, by simulating input steps using MATLAB. The total consumption of the brushed DC motor was reduced with 33%, and the brushless DC motor with 89%. These reductions in the motor consumption lead to a theoretical increase in the battery life of 8 and 17,6months respectively.

Preface

This master thesis work, of 30 credits, is the last project of the mechatronics master program, at Machine design at the Royal Institute of Technology (KTH), in Stockholm, Sweden. The thesis was carried out at the locking company ASSA ABLOY in Stockholm Sweden.

First of all would we like to thank our supervisor Daniel Garmén and the technical expert of the thesis project Anders Cöster, at ASSA ABLOY, whom provided us with all the necessary background knowledge and guidance during the project as well as all the necessary tools. We would also like to thank our supervisor at KTH, Bengt Eriksson that assisted us through the thesis.

Thanks also to Frimann Sigurdsson that was of great help assisting in electrical hardware and guidance in the lab, and Charlie Dejus that help us with knowledge, and assistance at measuring the system. Also thanks to Tomas Jonsson who helped us with measurements for the evaluation of the final prototype. Finally thanks to everyone else at ASSA ABLOY and KTH whom were very helpful throughout the whole thesis.

Nomenclature

Abbreviations

RFID	Radio-frequency identification
MFF	Magnetomotive force
DC	Direct current
BDC	Brushed DC
BLDC	Brushless DC
MSM	Magnetic shape memory
PWM	Pulse width modulation
ZVS	Zero volt switching
Rpm	Revolutions per minute
FOC	Field-oriented control
DSP	Digital signal processor
NEMA	National Electrical Manufactures Association
EMDM	Electromagnetic design method
FCM	Field-circuit method
FEM	Finite element method
FEA	Finite element analysis
GA	Genetic algorithm
SQP	Sequential quadratic programming
PM	Permanent magnet
VSD	Variable speed drive
EMI	Electromagnetic interference
emf	Electromotive Force
ESR	Equivalent series resistance
GPIO	General-purpose input/output
ADC	Analogue/digital converter

Notations

R	Resistance
R_A	Armature resistance
R_e	Field resistance
R_{dson}	Transistor triode state on resistance
L	Inductance
U	Supply voltage
U_d	Transistor drain voltage
i	Motor current
I_A, I_B I_C	Armature winding current
I_D	Drain current
I_a	Stator current
I_e	Rotor armature current
U_{emf}	Back emf voltage
P	Power
P_a	Armature copper loss
P_e	Field copper loss
C_p	Parasitic winding capacitance

C_{oss}	Parasitic drain-source capacitance
f	Switching frequency
^oM	Mechanical degrees
^oE	Electrical degrees
T_p	Peak Torque
J_l	Load inertia
A_{cc}	Acceleration
T_l	Torque load
t_v	Mechanical time constant
t_f	Final time
k	Ratio of t_v/t_f
Z	Lever pivot
r_1	Locking pin, lever contact point radius
r_1+r_2	Lead screw, lever contact radius
F_s	Spring force
F	Nut load force
T_{load}	Torque load
T_{up}	Raising load torque
d	Screw diameter
P	Screw pitch
α	Screw pitch angle
W	Screw pushing force
N	Normal contact force
μ	Screw friction constant
u_i	Input voltage
u_R	Resistor voltage drop
K_{emf}	Back emf constant
$\dot{\varphi}$	Motor velocity
$\ddot{\varphi}$	Motor acceleration
u_l	Inductor voltage drop
T_m	Motor torque
K_m	Torque constant
T_l	Load torque
T_f	Friction torque
J_m	Motor inertia
T_{load}	Total load torque, Tl+Tf
Fc	Coulomb friction constant
b	*Viscous friction constant*
$A\ B\ C$	BLDC windings
$u_A\ u_B\ u_C$	Winding voltages
Θ_e	Electrical angle
Θ_m	Mechanical angle
p	Pole pairs
R_{in}	Current sensor in resistor
R_{out}	Current sensor out resistor
R_{sens}	Shunt sensing resistor
u_{shunt}	Shunt voltage
ΔTA	Acceleration time

ΔTC	Cruise time
ΔTD	Deceleration time
c	Exponent scale factor
t	Time
$\dot{\varphi}_s$	Starting speed
$\dot{\varphi}_f$	Final speed
t_0	Trajectory starting time
t_1	Trajectory cruise start time
t_2	Trajectory deceleration start time
E	Energy

Contents

1 Introduction

This chapter contains a short introduction of the ASSA ABLOY Aperio E100 locking system. It will also define the thesis purpose, scope and limitations, and finally present the chosen methodology. All theory and statements in this chapter are results of interviews and discussions with experts at ASSA ABLOY.

1.1 Background and problem description

Research question: "Is it possible to drive a low voltage motor energy efficiently by using intelligent control, feedback or more suitable motor"

Electromechanical locks are becoming a more interesting product for the locking market, with advantages such as; long distance communication, easier access handling, better security and cheaper keys manufacturing. These locks are often battery powered, making the energy a finite resource. This thesis investigates the possibility of extending the battery life in one of ASSA ABLOYs current locking systems, the Aperio E100, by reducing the energy consumed during the locking and unlocking sequence.

1.1.1 Aperio E100

The Aperio E100 lock is one of the most widely use electromechanical locks from ASSA ABLOY. It is designed for indoor use, and has a wireless communication system for both long distance (radio) and short distance (RFID) for opening the mechanical lock. Figure 1 shows the radio communication between the locking module and access control server (online access control) makes it possible to both open the lock remotely as well as with short distance RFID key cards. The Door controller is a communication register between the online access control and radio communication hub. The hub relays signals to the Aperio E100 that opens and locks the mechanism.

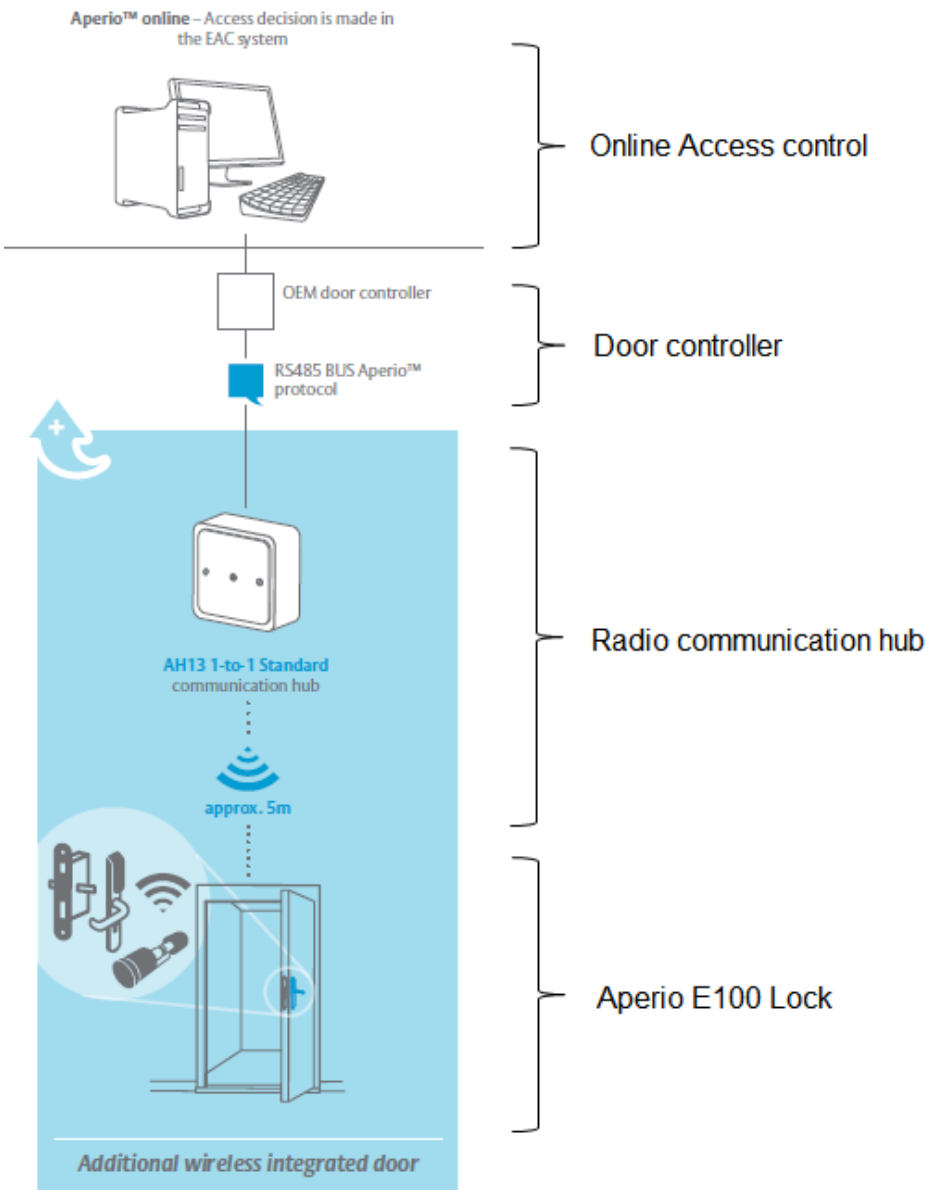

Figure 1 – Aperio E100 Communication [1]

The Aperio E100 locking mechanism shown in Figure 2 is driven by a 3V brushed DC (BDC) motor that transfers motor torque into linear motion via a threaded lead screw gear. The lead screw then transfers a force to the locking pin through the lever by completing a total of five revolutions, moving the leaver from the inner to outer positions. The curve shape of the lever is necessary in order to keep the locking pin pressed when the handle axle is rotated, as the door is opened, using the door handle. The locking pin engages the handle in the open state whilst in the locked state the handle is disconnected. When the locking pin is pressed, the motor and screw are in the inner state as shown in Figure 2, the system is locked.

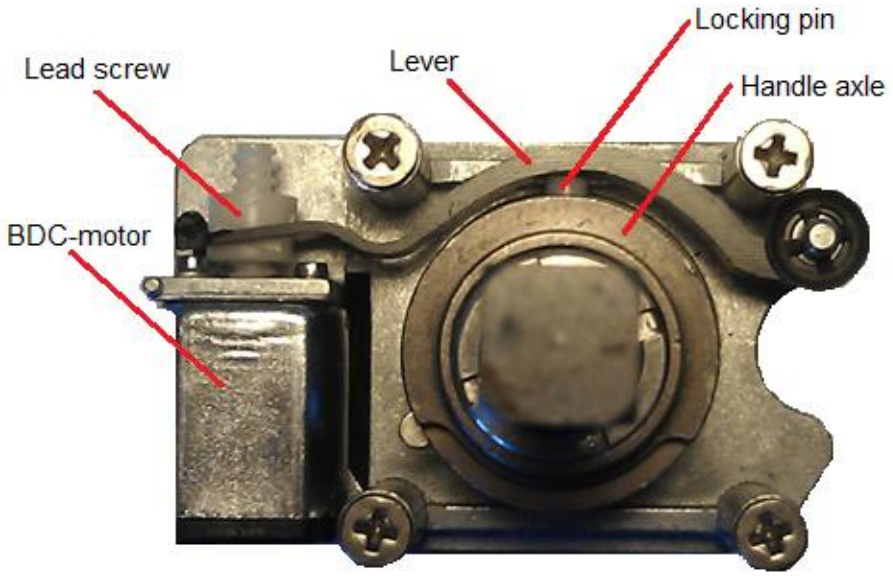

Figure 2 - Aperio E100:s locking mechanism

In this project the mechanism, which is activated by the locking pin, will be considered as a “black box”. The motor is currently driven at maximum speed, and is controlled/ shut off by two Hall-effect sensors at the end positions of the lead screw. The Hall-effect sensors sense a small magnet at the tip of the leaver that can be seen in Figure 3.

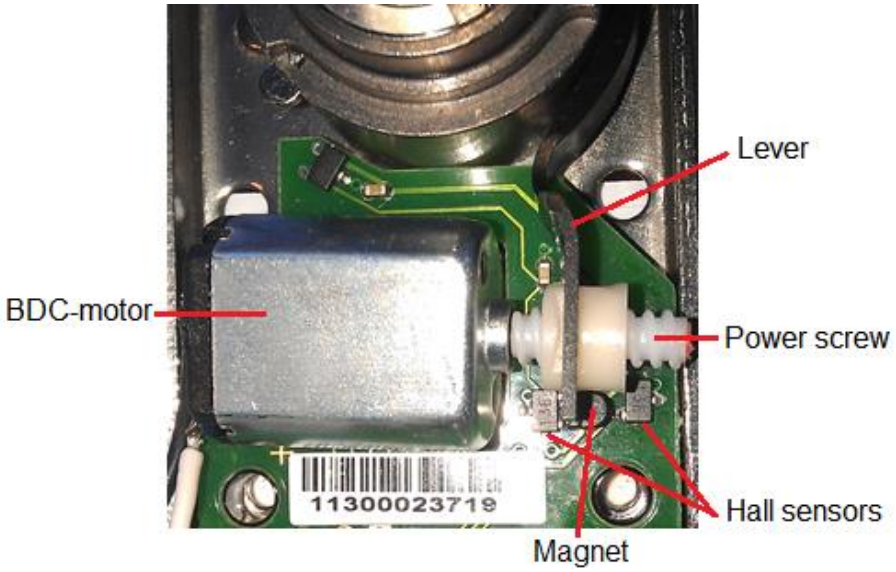

Figure 3 - Aperio E100 System

1.1.2 Energy consumption

The energy consumption in the Aperio E100 lock is caused by different components such as the processor, RFID/radio communication and motor drive. This thesis will focus on the consumption of the motor and its drive, neglecting consumption of radio communication due to time limitation of the thesis. Figure 4 shows the current consumption of one running cycle of the Aperio E100 system. It starts with a 0,85 second consumption caused by the RFID

communication followed by the motor drive of the unlocking sequence of approx. 100-200ms. After this the processor goes down in sleep mode for three seconds before it starts up and the motor locks the mechanism. As seen in the Figure 4 the motor drive causes a major part of the consumption. The total consumption of the motor drive for the unlocking and locking phase together is about 55.5mJ.

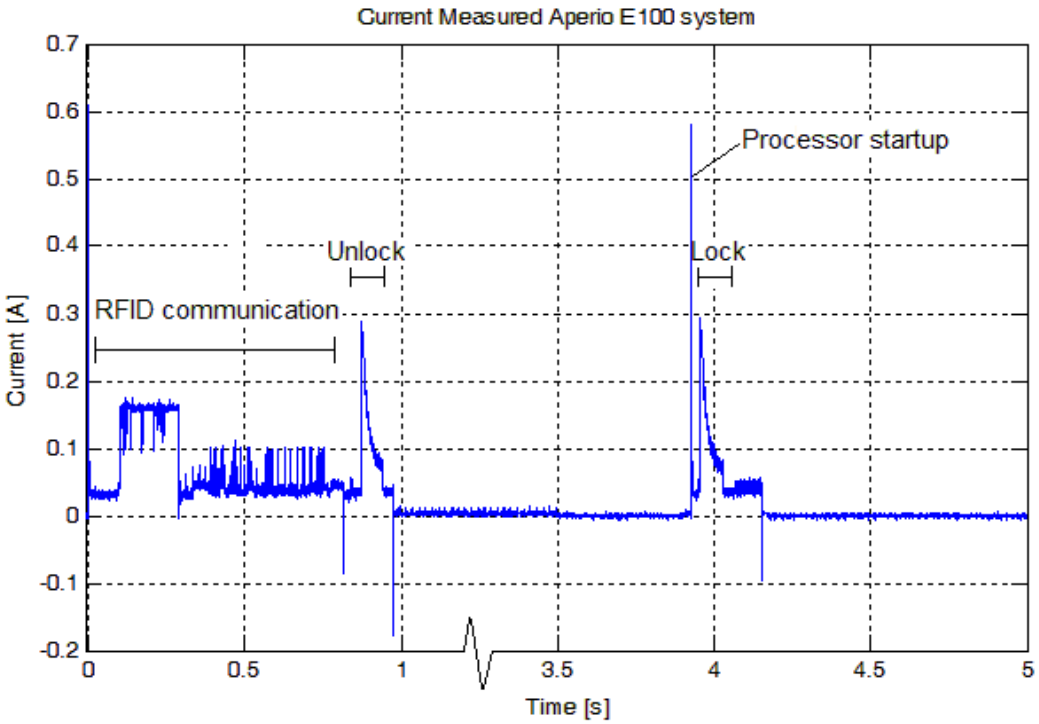

Figure 4 - Current consumption of the Aperio E100

At the moment, the lock has a battery runtime life of around three years, with about 66 000 openings. The standby current consumption of the system is about 10µA.

1.2 Purpose

The purpose of this project is to lower the energy consumed of the motor and its drive, for the Aperio E100 lock, to extend battery life. The thesis will present a prototype for a new actuator and control method that extends the battery life compared to the current Aperio E100 system. The purpose of extending the battery life is to reduce the need and cost of maintenance when batteries run out of power.

1.3 Research scope

Improvements to the current BDC motor system will be investigated, as well as new actuator types, algorithms, driving circuits and necessary measurement techniques. The actuator needs to be small enough to fit inside the mechanism, whilst still being able to generate sufficient torque to drive the locking mechanism in an efficient manner. The research should include algorithms for both efficient drive and optimal control for the system.

To limit the thesis scope, the research was split into two parts; first a general comparison between different actuators was conducted, followed by an in depth research about behaviors, control, and efficient motor drives for the most promising actuator.

1.3.1 Limitations

The limitations done in this thesis were:

- Only consider the motor and its drive when reducing the energy consumption and excluding processor and RFID communication due to time limitation of 20 weeks for the thesis.
- No inclusion of energy harvesting techniques to extend the battery life. This due to time limitations and the fact that reduced energy consumption is preferable before harvesting.
- The thesis group will use a constant 3V voltage source and not a battery. The reason of this is to have a consistent voltage which facilitates accurate measurements.
- No battery management techniques will be used. The project focuses on just the motor and its drive and no other energy saving areas.
- No changes or modifications of the locking mechanism, including: leaver, lead screw and locking pin, as not to compromise the security and reliability of the lock. This with the exception of using a linear motor, where it would be possible to remove the lead screw.

1.3.2 Sources

The major part of the research of this thesis has been found from the Royal Institute of Technology's database Primo. This database contains; journals, books, conference proceedings, theses and dissertations. In this database frequently used search words were combinations of: "efficient", "optimal", "power", "energy", "minimum", "BLDC", "BDC", "brushless", "control", "design", "loss-minimization", "ripple", "trajectory", "selection", "commutation", "drive", "switching", "low voltage". Apart from using the Primo search engine, Google Books was also used in finding literature with similar search words.

1.4 Hypothesis/ Goal

The goal of this project is to reduce the energy consumption of the opening/locking routines with 50%. This goal is based on the fact that other locks ASSA ABLOY distributes have a significantly smaller consumption than the Aperio E100. These locks however have a different mechanism and motor. The goal was developed together with experts at ASSA ABLOY from their previous understanding of the mechanism.

1.5 Methodology

The thesis started with a project and a product break down structure, to be able to identify key functionalities of the product as well as interesting areas of research. As project management method, a key point phase method, according to KTHs Department of machine design [2], has been used in this thesis. This method divides the project into four consecutive phases, see Figure 5.

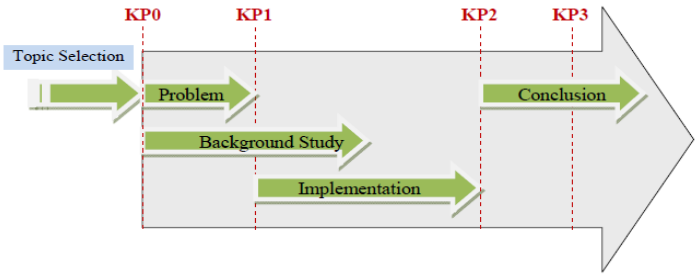

Figure 5 – Method [2]

An introductory problem definition phase (started at KP0), where the background and purpose of the thesis is discussed, and developed together with all the stakeholders and experts in relevant fields. Alongside this a thorough background study is done (started at KP0), investigating what has currently been done in similar applications and fields. What motor types are available, interesting control algorithms, feedback sensing, and new developments in energy efficient processors and motor drive technology will be investigated. This research will start very broad and will later be refined. After the research phase, an implementation phase will start (KP1). This will include testing of the current Aperio E100 system and an implementation based on the tried and tested methods discovered in the research. A prototype will then be developed and performance tests done. Finally the conclusion phase (started at KP2) where the results are discussed. The reason of using the key point phase method was to ensure that the project would run on schedule and that internal deadlines were met. KP3 is set as the presentation day of the thesis work. The key point phase method was structured in the form of a Gantt chart, which was executed in KP0.

Weekly project meetings with the supervisor and technical expert at ASSA ABLOY were held as well as continuous updates via email to the supervisor at KTH to ensure a valid final conclusion was reached. Verifications of the results and measurements were made by comparing to the current Aperio E100 system, the ASSA ABLOYs measurement methods and by discussing with experts at the company.

2 Pre-Study

To limit the scope of this project, a general comparison and investigation into different actuators was carried out in this pre-study, to identify possible actuators that could be used to replace the current Aperio E100 motor. This was done by researching actuator types, and looking into published reports showing the possibilities, advantages and drawbacks of the different actuators. Finally a comparison and decision of the best actuators was presented in this chapter. After the pre-study, further research was conducted on the most feasible actuators. These findings will be presented in the next chapter: Frame of reference.

2.1 Available motor types

The initial actuator research showed some interesting motor types such as; brushed DC, brushless DC, piezo ultrasonic motors, stepper motors, solenoid and magnetic shape memory motors. These actuator types were selected, for this pre-study, based on research and discussion with experts at KTH and ASSA ABLOY, and are described shortly below.

2.1.1 BDC (Brushed DC)

The current motor in the Aperio E100 system is a BDC motor. This type of motor uses mechanical commutation of brushes in the motor, i.e. they do not require any control to switch current for running. In a BDC motor, the armature windings are set on the rotor, and typically surrounded by permanent magnets.

The advantage of a brushed motor is that no current control is necessary and that they are very cheap according to Condit [3]. The negative factor is the actual brushes that causes increased maintenance, due to brush erosion discussed by Nikolic et al. [4] pp.1 and decreased efficiency due to the voltage drop in the commutation shown in Cross et al. [5]

2.1.2 Rotational BLDC (Brushless DC)

BLDC motors are often built with a permanent magnet rotor and a static armature that contains the stator windings. Commutation is achieved electronically via the stator instead of brushes. Without the brushes, friction is reduced making the motor more efficient and giving it a longer lifetime, Aghili [6]. A drawback with removing the brushes is that commutation is more complex to control, Wang [7] to get the motor running.

BLDC motors also run quieter, have a better speed/torque characteristic, and produce lower EMI than brushed motors. They also have better cooling since the windings are now in the stator. The energy density of a brushless motor is also higher and they can therefore be made smaller than BDC motors. However, they are also more expensive than the BDC [4] pp.23.

2.1.3 Linear BLDC

Boldea & Nasar [8] describe a linear motor as a rotary motor that has been rolled out flat. The principle of driving a linear brushless motor according to Crowde [9]pp188 is the same as for a rotational. Magnets are attached to the track, and coils and sensors are fitted to the moving assembly. As in rotational driving of brushless motors, positional feedback is needed in order to control velocity. Deceleration of brushless motors is done by running the motor as

a generator, inducing a negative torque. However electrical braking cannot hold the motor stationary as discussed by Rakesh & Narasimham [10]pp785.

2.1.4 Piezo Motor

Piezoelectric elements, or ceramics, can be excited and cause motion when a voltage is applied to them. This phenomenon has been used in a variety of different piezo motor types. There are two main types, a slip stick type, and an ultrasonic, McMahon [11].

The stick slip principle described by Nguyen et al. [12], works by a piezo elements (stick) that creates slow deformation in one direction and the runner moves together with the guiding system due to static friction. In the next step the element quickly returns to the initial position and the runner slips on the contact elements, which results in a small forward step after a back step, as seen in figure Figure 6.

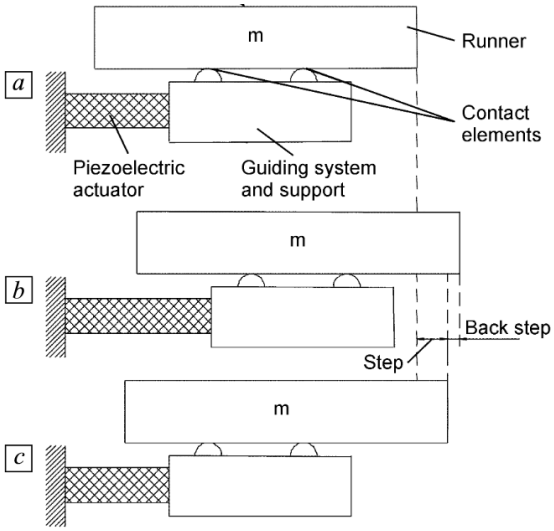

Figure 6 - Piezo Stick Slip

For the ultrasonic types, a high frequency signal excites the piezo element at its resonance frequency, causing a moving wave through the element. Motion is transferred to the motor axis via drive pads attached to the element, which push the motor forward [11].

Piezo motors have a high energy density, meaning they can still generate a proportionally large torque even though they are made small considered by Jeong et al. [13]pp.1. They are also more energy efficient than BLDC. However piezo motors also need more complex control to drive them. An advantage of all piezoelectric motors is the no-power locking feature, where the motor will still hold a load, due to friction, without drawing power [11]. Piezoelectric ultrasonic motors have the advantage that they can be produced small without losing efficiency as regular DC motors do.

2.1.5 Stepper Motor

Stepper motors work like PMBLDC motors however, teeth on the stators and rotor are aligned when a voltage is fed to the stator winding, stepping the motor, shown by Shah [14]

pp.10.This gives a possibility of open loop position control by counting pulses sent to the stators. This is however not without some problems, such a resonance stepping, and miss counted steps [14] pp.86.

2.1.6 MSM (Magnetic Shape Memory)

As piezoelectric elements are excited and change shape when a voltage is applied to them, MSM alloys are altered when they are subjected to a longitudinal magnetic field, Claeyssen et al. [15] pp.1. A linear MSM motor can be made by enclosing the alloy in a series of coils that generate magnetic fields when power is applied. The control of these fields can be done digitally, moving the alloy like a worm inside the stator coil. When not powered, the motor will lock into its current position, shown by Claeyssen et al. [16].

2.1.7 Self-latching solenoid

To use a solenoid, it is necessary to have one that is stable at its end positions without any holding power consumption. This is the case for self-latching solenoids.

A self-latching solenoid can act in various ways according to Pawlak [17] pp.173, one type of a self-latching solenoid uses a permanent magnet (PM) that attracts a plunger when sending a short current pulse through the coil. The attraction makes the PM latches to the second position without further power. To return the plunger, an opposite current pulse is sent which will unlatch the magnet and a spring will force the plunger back to initial position. This makes the solenoid bi-stable as described by Struman [18]. Another way is to have two coils, one on each side of a PM. When a current runs through one of the coils, it will attract the PM and the PM will latch in the end position, [17] pp.174, without any need of current, also discussed by Yatchev et al. [19]pp.208. The two coils can be connected in series in a way that they create opposite magnetic field. The direction of the electromagnetic force will depend on the direction of the current. [19]

Latching solenoids fits well in applications where power is limited, such as battery applications, because it requires just a short pulse and have a bi-stable feature. [18] Latching actuators consumes little power and are therefore a good alternative in portable devices. [17] pp.174

2.2 Motors type selection

The following section contains a short discussion about the different actuator types and the reasons for their compatibility in the Aperio E100 system. The purpose of this discussion is to exclude some motor type, to be able carry on with more thorough research for one of the types.

2.2.1 MSM

Magnetic shape memory motors have been described as very similar to piezoelectric motors and will therefore be compared to these. Shape memory alloys can provide a higher force and strain than piezoelectric. However, due to much lower time constants, their performance is inferior to piezoelectric elements as described in Claeyssen et al. [20]pp.194. To drive a MSM motor, a coil needs to surround the alloy in order to provide a magnetic field. This makes the MSM motors larger than a piezo motor. Even though MSM motors have been

developed and improved recently, they are still not used in industries and this could be due to the fact that piezoelectric motors have lower power consumption and a higher energy density [20]pp.195-198.

These drawbacks of MSM motors against piezoelectric actuators and the fact that the thesis group couldn't find a single product that fulfilled the requirements cause the elimination of them for further study in this thesis.

2.2.2 Linear brushless motors

Linear brushless motors would have been an interesting choice in this case where it would have been possible to remove the energy loss of the lead screw. However, due to the fact that these motors have little internal friction, they will not provide a "power off holding torque". This makes them unusable in this thesis application.

2.2.3 Stepper motor

During the research of stepper motors it was found that they were very similar to BLDC with the advantage of open loop control. However, under normal open-loop running conditions of a stepper motor, changes in the load torque and rapid accelerations will cause unintentional displacements in the rotor. This can after a while lead to the loss of synchronization which can't be corrected nor detected according to Grimbleby [21]pp5. Due to this inefficiency of the open-loop control, which is otherwise an advantage of a stepper motor, it was eliminated from further research in this thesis.

2.2.4 Selection table

The rest of the actuators types where compared in Table 1. To do the comparison one of each different motor type that satisfied the requirements the best was found. In the table three important requirements; stroke length, size and torque load, and three important factors, power efficiency, availability and cost, were used as selection criteria. The three factors where developed together with the supervisors at ASSA ABLOY in a way that the end prototype would also be of interest for the company. In Table 1, the scoring for the important requirements is one (1) for actuators that fulfill the requirement and zero (0) for those that don't. For the factor requirement, five (5) is the best score and a zero (0) means that it wasn't sufficient.

Table 1 – Actuator selection table

Requirment / Motor	Actuator type	Stroke with acceptable housing length	Size	Torque/ Force	Power Efficiency	Availability	Cost
		7mm (0/1)	20, 15,12mm (0-1)	2mNm/0.35N (0-1)	(0-5)	(0-5)	(0-5)
Brushed DC (Current System)	QX-FF-030	1	1	1	2	5	5
BLDC rotational	EC 9.2 flat Ø10 mm	1	1	1	4	5	2
Linear Piezo	Piezo wave	1	1	0	5	1	0
Piezo rotational	Squiggle	1	1	1	5	1	0
Self-Latching solenoid	Not found	0	0	-	-	-	-

2.2.5 Self-Latching solenoid

The problem with linear actuations is to find one that has a small housing size but still has a relatively long stroke as well as having a supply voltage of 3V. The required stroke in this application is 7mm, whilst the maximum housing length is restricted to 20mm. This proved to be a problem when looking at products and after taking contact with suppliers there were no latching actuator that fulfilled both of these requirements and had the right supply voltage. These facts gave the self-latching solenoid 0 at size and stroke.

2.2.6 Piezo motors

The fact that piezoelectric motors are a fairly new technology is the main drawback of this motor type. This means that there are a very limited number of suppliers (availability 1) that produce this motor type in larger quantities, making them expensive even in theoretical larger quantities, which gives a zero at cost in Table 1. The price of the Piezo Wave® (Linear 0.1N) was 650kr/unit and the Squiggle (SQL-RV-1.8) was 850kr/unit, (buying 1000 products) which makes the use of a piezoelectric motor unrealistic and unwanted for ASSA ABLOY.

2.2.7 Brushed

Brush DC motors are not as efficient as BLDC and piezo motors but since a BDC motor is already in use in the current Aperio E100 mechanism, it is still interesting to see what improvements can be done on the control of this motor to improve the energy efficiency of the motor drive. These motors are also cheap and easy to control [22].

2.2.8 Rotational Brushless

BLDC motors are of a similar build as brushed. They are however more expensive. On the other hand, BLDC motors have shown better performance, longer lifetimes and keep a higher efficiency even when made smaller than the brushed equivalents. BLDC motors are often of similar size as brushed and will therefore simplify the integration with the current mechanical hardware. Brushless motors can be controlled and commutated in a wide variety of ways, and this will be interesting for further investigation.

3 Frame- of-reference

The previous research showed BDC and BLDC motors to have the most promising features required for this project and the following research will focus on these types. The research was continued to deepen the understanding for those actuators, focusing on function, behaviors, design, and control methods.

3.1 Motor Theory

This section shortly describes how both a brushed and brushless DC motor works and the motors equivalent electrical circuit. Motor behaviors such as losses and inrush currents are also discussed.

3.1.1 How a DC motor works

A DC motor works due to the fact that a force is generated when a conductor carries a current through a magnetic field. To maximize the force generated, a strong magnetic field is needed as well as a large current. The magnetic fields can be generated either by using permanent magnets, or by wrapping field coils around a ferromagnetic core, creating an electromagnet. Hughes [23] discusses how to increase the magnetic flux density and defines a coils magnetomotive force (MFF) as the number of turns in the coil times the current going through it.

When a high flux density magnetic field has been generated, this force can be used to induce another force on the current carrying conductor, creating motion. However, the magnetic field first needs to be controlled, directed, and allow an air-gap for the conductor to pass through. The size of this gap is important since the reluctance of air is much higher than that of the ferromagnetic core, weakening the field. Another effect of a large air gap is that the magnetic field becomes “ballooned” out, and weaker [23].

Once the magnetic field and air gaps are determined, the conductors are wound in this case around the rotor (Figure 7) where the positive current at the top of the image (using tangential magnetic force F=*B i l*) are forced to the left, and at the bottom to the right, creating a rotating motor.

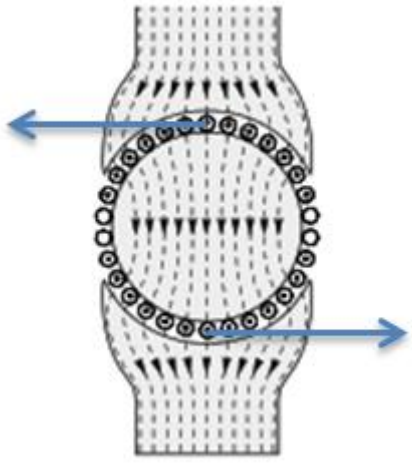

Figure 7 - DC Torque generation [23]

Electrically a dc motor circuit can be set up as in Figure 8, where *R* is the winding resistance, *L* motor inductance, U is the supply voltage, and U_{emf} is the back emf.

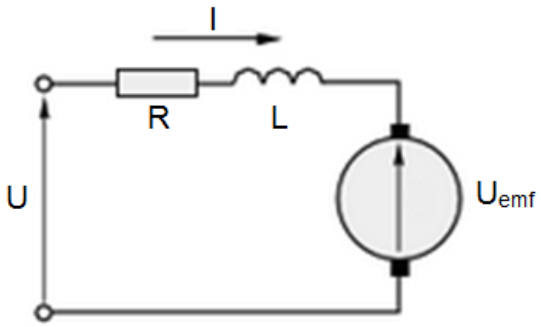

Figure 8 - DC electric circuit [23]pp94

Figure 9 shows the basic mechanical build of a separately excited brushed DC motor.

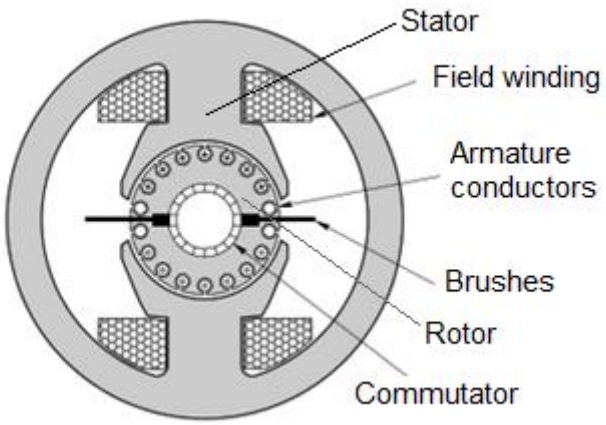

Figure 9 - Basic motor construction [23]pp83

3.1.1.1 Losses

When driving a DC motor, losses will occur in the windings as disturbances to the magnetic fields and as friction. These losses are dependent on rotor speed, currents and temperatures. These are all comprehensively discussed by De Angelo et al. [24], Sergaki et al. [25] and Kusko & Galler [26] and are summarized below.

Copper losses are caused by a current passing through windings. These can be divided into two parts, armature- (P_a) and field (P_e) copper losses. Armature losses occur as a current passes through the stator windings, with the stator current i_a, and the rotor resistance, R_a. The loss is given by equation (1).

$$P_a = {i_a}^2 R_a \tag{1}$$

Field copper losses occur as a current runs through the rotor windings, shown in equation (2):

$$P_e = {i_e}^2 R_e \quad (2)$$

where,i_e is the rotor current, and R_e is the field resistance:

Iron losses or magnetic losses described by Bakshi & Bakshi [27]pp5-2 occur in the form of eddy currents. These are created as the rotating magnetic field of the rotor cuts the magnetic stator field, which induces a back emf in the core. This induced current creates a power loss as well as hysteresis losses caused by the changing magnetic field of the stator core.

Friction and windage losses are caused by the motor being physically held together, as friction in bearings and other contact surfaces as well as the inertia of air moving through the motor.

Stray load losses, according to Kusko & Galler [26], are caused by the uneven distribution of the air gap, stator slot effects and skin effects in the conductor. It can be calculated as a function of torque, stator voltage, frequency and temperature.

Brushed contact losses are caused by a voltage drop across the brushes as a BDC motor is commutated mechanically.

3.1.1.2 Loss minimization

Loss minimization is described by De Angelo et al. [24], and all the internal losses are identified and calculated. An algorithm to minimize DC motor drive losses is proposed, independently controlling the armature and field currents. The method described is modeled with simplifications and experimentally tested for a motor in steady state (assuming that the torque and speed constant).

3.1.2 Motor effects

DC motors have several different properties that affect its performance. In this section torque ripple, cogging, motor size and inrush current will be explained.

3.1.2.1 Torque ripples

Torque ripples are peaks in the motor torque and current. There are three main causes of this ripple effect. One cause of ripples can be described by variations in the motor and construction imperfections. Another cause can be ripples induced by PWM switching the motor for variable speed drive. The last cause, which only occurs for BLDC motors, is commutation ripples. Shi & Li [28]pp2139 discuss the actual cause of the commutation ripples as differences in the rate of change of the current during commutation switching.

3.1.2.2 Cogging

Cogging is a phenomenon that happens when the number of the motors stator slots is an integral multiple of its rotor slots. Then a case of magnetic locking happens when the stator and rotor teeth are aligned as in Bando [29]pp.263, which gives an effect of torque ripples shown by Krawczyk et al. [30]pp.290.

3.1.2.3 Motor size

Motor efficiency is calculated as the ratio between the mechanical output power and the electrical input power as shown in a report by the U.S. Department of Energy [31]. Figure 10

shows efficiency variations of energy efficient and standard efficiency motors. As the figure shows, smaller motors become less efficient.

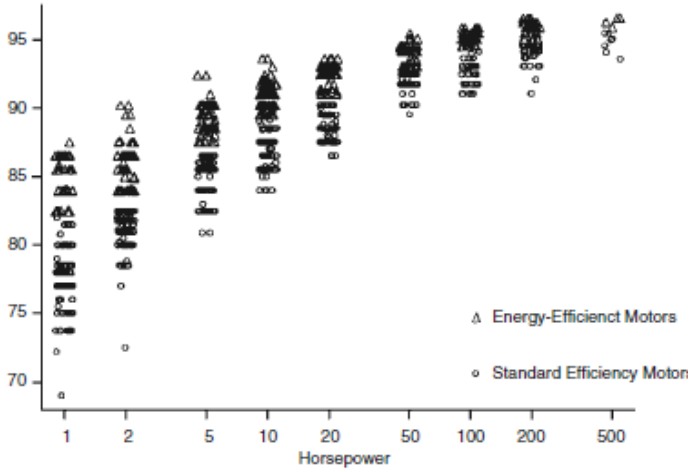

Figure 10 - Motor size and efficiency [31]

3.1.2.4 DC motor acceleration and inrush current

Bhattachrya & Singh [32]pp.145-147 and Xia [33]pp.47 describe the characteristics of the current of a DC motor during the initial starting phase as well as the stall phase. During acceleration of a brushed DC motor the inrush current is normally very large, often more than ten times the normal operating current. This is due to the fact that when the armature is at rest, no back emf voltage is generated, and usually DC motors have a very little resistance. Equation (3) shows the armature current, I_A given as:

$$I_A = \frac{U - U_{emf}}{R_A} \tag{3}$$

At startup, and when stalling the motor, the back emf, U_{emf} is reduced to zero, generating an inrush current equal to the supply voltage, U divided by the armature resistance R_A. Inductance in the motor will delay the current buildup, allowing time for a counter emf to be generated, slightly lowering the inrush.

The starting of a BLDC motor is very similar to a BDC, however Xia [33]pp47 introduces a voltage drop over the power switches of the bridge inverter U_d. This then gives the armature inrush current I_A as shown in equation (4):

$$I_A = \frac{U - U_d}{R_A}\ , \tag{4}$$

with the supply voltage U, and resistance R_A. This inrush current is still very large due to the fact that the power switch voltage drop *Ud* is typically very small.

Batarseh [34]pp51 gives equation (5), the transistor drain voltage drop U_D, which describes a power transistor in the triode state having a constant resistance $R_{DS(on)}$ *and* I_D is the drain current.

$$U_D = R_{Ds(on)} I_D \quad (5)$$

An advantage of the large inrush current is that a very large acceleration is generated in the motor. This can however also damage the motor.

3.2 Brushless DC motors

This section includes research regarding BLDC motor characteristics, motor drive, motor drive losses, as well as the commutation methods used to drive a BLDC motor.

3.2.1 Characteristics

The key parameters that influence a BLDC motors behavior will be identified in this section. These are necessary to understand when selecting and optimizing a motor.

3.2.1.1 Radial flux vs Axial flux

BLDC motors can be according to Yilmaz [35]pp17-18, classified upon the direction of the magnetic flux. Most BLDC motors are radial flux, meaning that the magnetic field axis goes perpendicularly to the motor axle. These motors are longer and have lower rotor inertia, giving them a quicker response to load changes.

Axial flux motors are designed with the rotor outside the stators making it have a magnetic field axis which is parallel to the motor axle. These motors are more “disc like”, short with a larger radius. Results from this study [35]pp.194 show that axial flux motors have a higher efficiency, torque/volume, and torque/mass than radial flux motors.

According to Hanselman [36]pp.121-122, axial motor generates more torque but also higher axial forces. Axial motors also have increased manufacturing costs.

3.2.1.2 Inner and outer rotor

In Hanselman [36]pp120-121 the difference between outer and inner rotor is also explained. Inner rotor means that the rotor is inside the stator while the outer, also called “inside out” motors, has the opposite stator/rotor configuration. Most motors have an inner rotor as these have better heat dissipation, and better containment of the rotating elements. However a larger torque can be produced with an outer rotor motor compared with an inner rotor motor with the same radius.

3.2.1.3 Slotted vs Slotless BLDC

Mitchell et al. [37]*pp.699* describes two different armature types, slotted and slotless, shown in Figure 11. The main advantage of the slotless type is that it no longer has any cogging torque. This effect can however, also be counteracted with a slotted armature by using skew magnetization as discussed by Xia [33]pp129-130, however, the stator design becomes more complex, causing increased stray losses and more sinusoidal back emf. The result of this decreases the output torque. The slotless armature air gap is larger than the slotted, leading to reduced magnetic loading, which forces this motor type to become longer if it is to have the same torque.

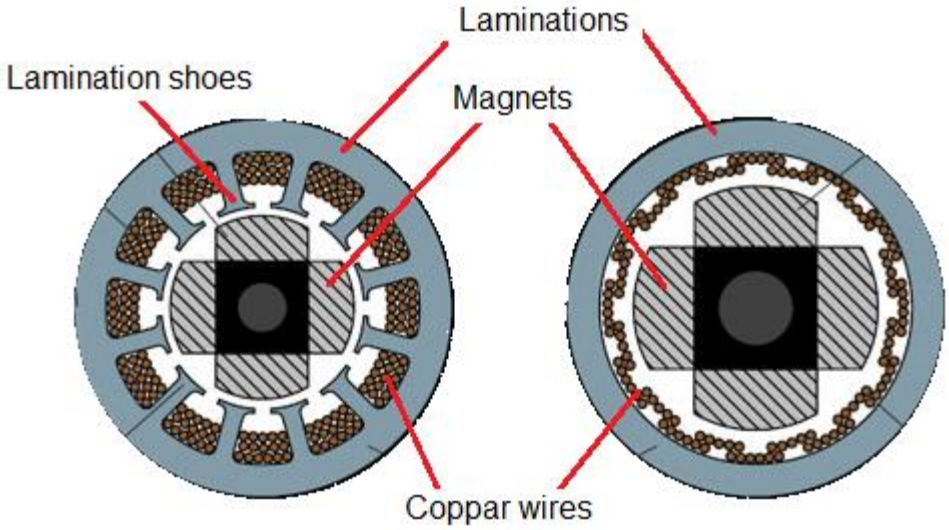

Figure 11 - Slotted and slotless, Pittman [38]

According to Hanselman [36]pp.120, slotless motor can fit more windings inside but has almost always a lower performance than slotted. The reason of this is that the slotted stator ferromagnetic material gives good heat conduction that removes heat, and since slotted stators have a smaller magnetic air gap. This results in higher permeance coefficient and a greater flux density.

3.2.2 Motor drive

This section includes research about different motor drive methods of BLDC motors. It also handles different motor drive-losses and methods of reducing them.

3.2.2.1 Bipolar

In Gieras [39]6.1-6.2 bipolar or full-wave brushless motor drives are explained as a six switching drive that is capable of providing the motor with both positive and negative current. This drive technique is used in a six step commutation with only two phases active at a time, seen in Figure 12 where S_1 to S_6 are six transistors, and A, B and C are the three phases.

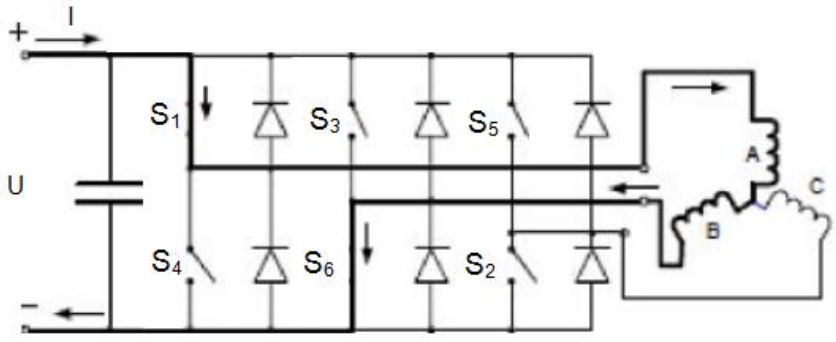

Figure 12 – Bipolar Motor Drive [39]6.1-6.2

3.2.2.2 Unipolar

Gieras [39] also explains the unipolar or half wave drive for brushless motors which has three switches S_1, S_2 and S_3. Having three switches instead of six makes the drive only able to provide the phases *A, B* and *C* with positive currents as seen in Figure 13.

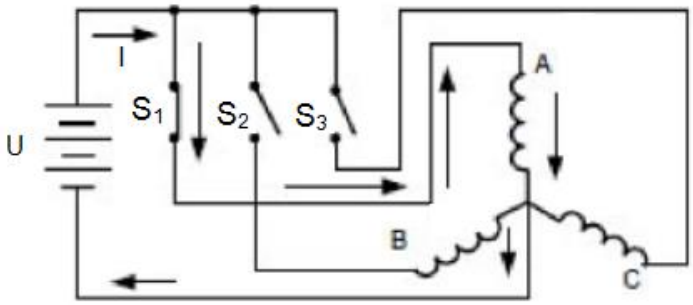

Figure 13 – Unipolar Motor Drive [39]6.1-6.2

The direction of the rotor is then dependent on the sequence in which the different stators are turned on.

Yan & Serteller [40] state that the advantage with bipolar drive is that the torque constant is higher. Unipolar drive on the other hand produces a higher speed in steady state. Therefor the source says that unipolar is mostly used in applications where high speed is required and bipolar is used to move loads in the starting sequence because it has twice the starting torque with the same speed. A drawback with unipolar motor drive is that it runs more noisily than bipolar.

Upon the fact that bipolar motor drives generate higher starting torques, while unipolar drives generate higher speeds, Jang, Kim & Kim [41] suggests a method where a brushless DC motor is driven using bipolar drive in the starting sequence and unipolar drive at steady state. The reason that unipolar has better steady state performance is due to magnetic saturation. The torque constant is reduced for bipolar motor drives, giving unipolar higher operating speed.

3.2.2.3 Transistor losses

The power losses in transistors are described by Smith [42], and two main reasons are discussed. Firstly the internal resistance of the MOSFET dissipates power when current passes through it. Secondly due to the capacitive properties of the MOSFET losses, caused by switching. This switching loss is proportional to the switching frequency and is more significant in low power applications. Equation (6) shows the turn-on loss.

$$Turn - on\ Loss = \frac{(C_{oss} + C_p){U_d}^2 f}{2} \tag{6}$$

Where U_d is the drain voltage, C_p and C_{oos} are the parasitic winding- and drain-source capacitances respectively. The switching frequency is given by *f*.

3.2.2.4 Soft switch

Reducing the switching losses can be done using hardware, and Shahbazi et al. [43] describes a soft switching method where three capacitors and one inductor are integrated

into the switching circuit driving a battery powered BLDC drive system. These components have the effect of slowing down the rise rate of the voltage which results in reduced turn-off power losses and voltage spikes are eliminated.

This method however requires three additional switches, one per phase, three snubber capacitors placed over the low side switches, an inductor between the power source and the midpoint of the new switches as well as a free-wheeling diode placed between ground and the resonant inductor.

Pan & Lou [44] introduces as a similar resonant inverter solution however using a 12-switch inverter instead. The main goal with both these types is to only switch at zero voltage (ZVS). The three added switches are controlled in such a way as to generate resonance between the inductor and the capacitors, which makes ZVS possible, reducing switching losses.

3.2.3 Commutation

Commutation is the procedure for knowing which stator the current should run through, depending up on the rotor position. This is necessary to get a DC motor running and for BDC motors the commutation is done automatically (mechanically) which makes them easy to drive. For BLDC motor though, this has to be done manually (electrically) Aghili [6].
In this section, different commutation methods for BLDC motors, with different pros and cons, will be described.

3.2.3.1 Mechanical vs Electrical position

To understand commutations it is necessary to know the difference between mechanical and electrical degrees.

Mechanical position is a reference to the rotors rotation and is measured in mechanical degrees (º M), one complete revolution is obtained by the rotor at 360º, putting the rotor back in its original position. Electrical degrees (º E) describe the rotation required for the rotor to encounter an identical magnetic field. These two angles are related by the number of poles the motor has Hanselman [36]pp.11.

3.2.3.2 Trapezoidal commutation

According to Herrington [45]*pp.282* trapezoidal control of a three-phase motor is a six step commutation method with a new interval every 60 electrical degrees. Combinations of three Hall-effect sensors decide the position of the rotor and thereby which of the six commutations steps that should be executed. The steps consists of an on and off states of the transistors in an h-bridge.

3.2.3.3 Sinusoidal commutation

Herrington [45]*pp.283* also describes the sinusoidal control method. It is a newer method that was introduced for smoother operations for motors running at slow speed (approx. 100 rpm). The principle of sinusoidal commutation is to have a wave formed input current and back emf. The advantage of sinusoidal compared with trapezoidal is that, in the theory, one gets rid of the torque ripple that can occur for trapezoidal commutation. On the other hand, the sinusoidal control can only produce 91 percent of the peak torque compared to the trapezoidal.

3.2.3.4 FOC (Field-oriented control)

In John. et al. [46]*pp.348* FOC as commutation method is described. The goal of controlling a brushless DC-motor with FOC is to optimize the torque compared to the power usage. To maximize the torque, the angle between the rotors magnetic field and the stators should be orthogonal. In FOC this condition is held all the time by sequentially update the rotor angle. FOC include a change of reference system from a three phase static reference frame to a two axis rotational frame, these calculations require a fast processor such as a DSP.

In Chan et al. [47] a method of constant power operation, similar to FOC is described where Hall-effect sensors are used for rotor detection and an encoder is used for rotor position feedback. The FOC method generates the optimal flux/current angle and therefore generates the maximum torque, while the major disadvantage being that a fast processor is needed due to complex calculations. The constant power operation method is easier to implement than FOC and doesn't require any high speed processor, with the downside that it doesn't maximize the produced torque.

3.2.3.5 Sensorless BLDC Commutation

In Hung et al. [48] Back emf is used as feedback instead of Hall-effect sensors which has the drawback that a starting sequence has to be performed, reaching speeds of 750 rpm, before sensing of the position is possible.

In this paper by Ungurean et al. [49] a sensorless controller for a BLDCPM is made by monitoring the back emf zero crossing, generated in the different motor windings. It also discusses the advantages of using a sensorless BLDC motor control such as reduced cost, better reliability, and reduced mechanical size, as well as the advantage of not having position sensors when a motor rotor is submerged in liquid. Starting of a sensorless controller is normally done by open loop "Align and go" strategies, where the rotor is accelerated by not knowing where the rotor actually is. This starting process takes time, and this paper focuses on a new method of I-f starting to reduce this time.

For successful I-f sensorless starting, first alignment needs to be done, followed by a startup sequence before back emf zero crossing detection can be done, followed by sensorless back emf speed control. In the alignment phase two motor phases are charged with a low duty cycle for a short time. The start-up sequence then calculates the reference position as the integral of the reference speed and the duty cycle is calculated from the current. Ideally this should create the correct commutation sequence. However, due to damping in the motor this is not the case. This sequence is then followed by an I-f to back emf switching phase when the motor has significant velocity to generate usable back emfs. Here the zero crossing detection is introduced and the commutation aligned as usable emfs are detected. Once this is achieved the motor can be speed controlled. A drawback with this method is that PWM duty cycles below 20% don't produce usable back emf zero crossings.

3.3 DC- DC conversion

According to Czarkowski [50]pp257-258, losses associated with DC-DC converters are voltage ripples and efficiency losses due to parasitic resistances and capacitances. The resistance is due to resistance of leads and connectors. The total efficiency of a boost converter is describes as in equation (7):

$$\eta = \frac{R(1-D)^2}{R(1-D)^2\left(1+\left(\frac{V_D}{V_O}\right)+fC_OR\right)+r_L+D_{rs}+(1-D)r_D+D(1-D)r_C} \quad (7)$$

Where *R* is the load resistance, *D* is the diode, V_D *is the forward voltage drop over the diode,* V_O is the output voltage*, f* is the frequency, C_O is the output capacitance, r_L is the ESR of the inductor D_{rs} is the r_D is the forward on resistance of the diode, and finally r_C is the capacitance resistance. The term fC_OR show the switching losses in the converter, also discussed in section 3.2.2.3

3.4 Measure current

A common method of measuring current is to connect a shunt resistor in series to the system. The voltage is measured over the shunt resistor and converted to a current with ohm law Pop et al. [51]pp 151. To maintain a low voltage drop (power dissipation) over the shunt the resistor should be very small. To measure small currents that are generated over a small resistor, it is required to have a high quality amplifier such as an instrumental amplifier. Sozanski [52]pp.30.

3.5 State of the art: Motor selection and design

To know which motor that is optimal to use in an application, two different techniques are presented in this section. A selection method from available motors can be done, or the motor can be designed and construct the optimally oneself. This section first includes different selection methods, and then different design and optimization techniques for DC motor are presented.

3.5.1 Selection

This section presents relevant selection methods for finding efficient motors. When selecting a motor there are several factors to take into account and a few different methods that can be implemented.

In Roos et al. [53]pp.65, three main factors to consider if a DC motor can drive a given load are described. The first is that the “root mean square value of the required motor torque has to be lower than the motor’s continuous torque rating”. Secondly, the motors peak torque value has to be higher than the required motor torque. Finally the peak motor speed needs to be lower than the maximum speed of the motor. Apart from this, this report focuses on a method of optimizing the motor and gearhead selection by using MATLAB software.

According to Poulin [54] motor selection should be done by first comparing the peak torque, T_p requirements shown in equation (8):

$$T_p = J_l A_{cc} + T_l, \quad (8)$$

where J_l is the load inertia, A_{cc} the acceleration, and T_l, is the torque load due to friction. Motor peak torque should be selected at 10-15 higher than T_p, as a safety margin. Secondly

one should compare speed/torque requirements by looking at data sheets and curves to determine safe torque and speed limits. Also the windings need to be selected, different windings gives the motor different torque constants, back emf constants and armature resistance. After these steps, the writer makes some calculations to determine requirements of the power, current peak and voltage and the effects of the temperature.

3.5.1.1 NEMA

NEMA (National Electrical Manufactures Association) has developed a standard for efficiency of electrical motors and the standard is designed as a help to compare different motors. Most motors are qualified as high efficiency but if selecting a premium NEMA motor one can be sure of quality and saving efficiency. McCoy et al. [55]pp.5-9

3.5.2 Motor design

To be able to get the best motor that fits a specific product, another approach is to design the motor oneself. This section discusses some overall design considerations of a DC motor, followed by different techniques to optimize their design for improved performance such as increased torque, speed, or efficiency.

3.5.2.1 General motor design

In Xia [33]pp.28 two general methods of BLDC motor design are discussed. The first method EMDM, electromagnetic design method, is used more often than FCM, field-circuit method, due to its simplicity even though the FCM method produces more accurate results. The EMDM includes four steps, determining the rotor structure, magnetic load, electric load, and size. The FCM uses FEM, finite element analysis to calculate the magnetic field. This highly accurate calculation of the magnetic field is the main advantage of this method. The paper discusses optimization of a BLDC motor to reduce commutation torque ripples, as well as cost and thereby improve the motor efficiency. However the same algorithms could be used to optimize for other aspects such as torque and speed.

Chapter 6 in Hanselman [36]pp.127-150 thoroughly describes the design of a three-phase brushless permanent magnet DC motor. Firstly it discusses the best combinations of magnetic poles and slots in order to efficiently produce torque. Secondly the coil span, to maximize flux linkage and induced back emf, is discussed. It then covers winding layout, and identifies the double layer lap winding as the most efficient layout. After winding layout, coil connections are discussed, as windings of the same phase need to be connected. Here care needs to be taken if coils are coupled in parallel to not cause current circulations and thereby reduce motor performance. Series connection is the most common method used. The winding factor is explained as the phase back emf dependent on the individual coil back emfs, and how the distribution and difference in phase of these can generate harmonics, contributing to a lower, less sinusoidal total phase back emf. Finally the chapter provides calculations for the phase inductance, using the air gap inductance, slot leakage inductance, as well as the end turn inductances.

3.5.2.2 Number of phases

BLDC motors with an increased number of phases have an increased fault-tolerance according to George et al. [56]. If a single phase becomes defective, the remaining phases can still be used to drive the motor efficiently. The paper proceeds to discuss that increased torque can be achieved with an increased number of phases for the same current and motor

volume. The optimization of the number of phases is then done by simulating the flux densities generated by different phased motors using finite element analysis (FEA) software.

3.5.2.3 Flux weakening/strengthening

Electrical motors and efficient motor drive for electrical vehicles are becoming important in order for them to become competitive regular combustion engine vehicles. A flux controlled permanent magnet brushless motor is described in Zhang [57]. This motor is wound like a doubly salient PM motor, having two types of stator windings; the regular three-phase armature windings, and DC field windings which control the air gap flux. The air-gap flux can then be strengthened to increase starting torque, and weakened to deliver a better constant-power operation range. After experimentation, a faster rise time was achieved at a slight reduction in efficiency.

3.5.3 Motor design optimization

This section presents optimization methods needed when designing DC motors.

The paper by Markovic et al. [58] describes the modelling and optimization of a slotless brushless DC motor using built in MATLAB optimization algorithms. In the study, algorithms are compared and it was found that the optimal solution was a combination of a genetic algorithm (GA) and sequential quadratic programming (SQP), a gradient-based method. The GA determines the direction towards the optimum, and the SQP algorithm finds the optimum. A drawback discovered with using the MATLAB functions was the difficulty to tune algorithm parameters.

According to Rahideh et al. [59]pp.3680 the optimal design of a BLDC can be achieved by using a genetic algorithm. The paper describes the necessary equations for the design of a motor when considering torque, speed, cost as well as mechanical factors. The geometry of the motor is optimized, and here they consider; the number of poles pairs, pole-arc per pole-pitch ratio, magnetic thickness, stator/rotor core thickness, winding thickness, mechanical air gap, rotor radius, current density, wire gauge and stator/rotor axial length.

Messine et al. [60] discuss optimization based on the branch and bound algorithm, guaranteeing finding the global optimum (if it exists). The paper however also acknowledges the fact that the optimized parameters do not always match those of experienced machine designers.

In the paper Markovic et al. [61] a slotted BLDC motor is optimized using genetic algorithm and FEM. To generate the motor model, FEM software [62] is used together with MATLAB motor code which is changed during the optimization process.

The paper Ishak & Hassan [63] has presented the analytical modeling of PM excited brushed DC motor for low-cost applications. The analytical model is employed to predict the air-gap flux density distributions, the flux linkage waveform seen by each armature coils, the individual induced voltage in each coil and the net induced voltage available at the brush terminals. Two DC motors have been used for the analytical model i.e. 12-slot armature and 10-slot armature. The analytical results for these two DC motors have been validated by

FEM. Optimal magnet pole arc for minimum torque ripple can also be estimated quite rapidly by the proposed analytical model.

3.6 State of the art: Control

This section describes methods of efficiently controlling DC motors using different techniques such as speed trajectory control and loss minimization optimization, as well as BLDC specific control.

3.6.1 Trajectory generation

In order to drive a motor efficiently for a set distance minimum energy and minimum loss trajectory planning can be implemented. These methods reduce energy consumption, and are therefore relevant for this thesis.

3.6.1.1 3-step velocity control

In Kim & Kim [64]*pp.2375-2380* a 3-step velocity control algorithm is implemented on a wheeled mobile robot in order to generate a velocity profile for acceleration, cruise and deceleration, in order to reduce battery consumption. The profiles discussed are exponential and trapezoidal, both for acceleration and deceleration. A constant cruise speed is always desirable. The study combines the different profiles to find the optimum. Figure 14 shows four different speed trajectories that where tested. They all consist of an acceleration phase ΔT_A, a cruise phase ΔT_C and a deceleration phase ΔT_D.

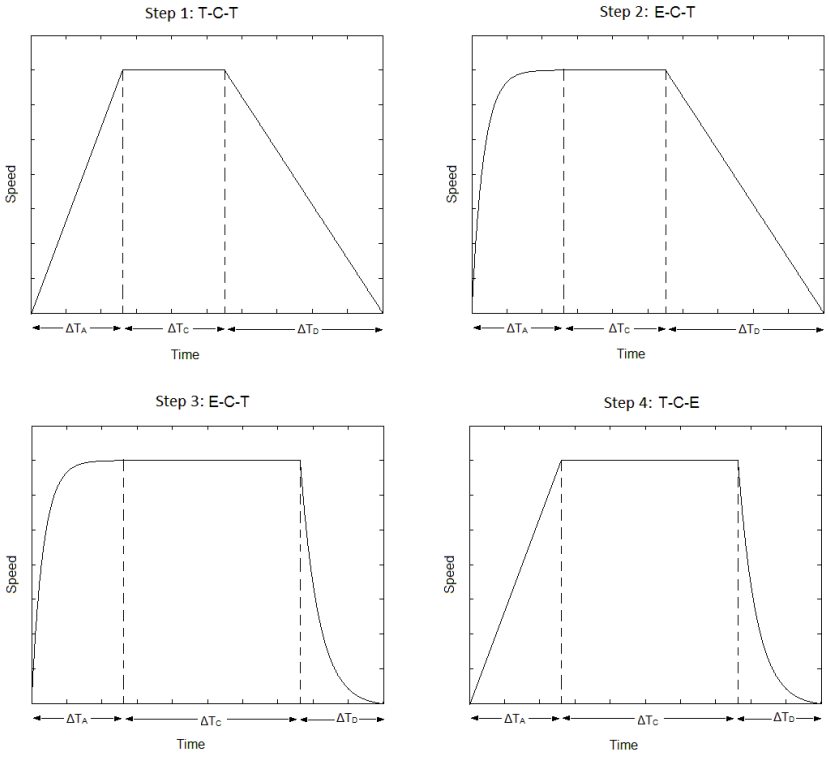

Figure 14 – Trajectory Steps

A search algorithm is also implemented. The study found that with 3-step velocity control and planning, a 30% increase in battery life could be achieved using exponential acceleration and trapezoidal deceleration compared to a purely trapezoidal profile.

3.6.1.2 Loss minimization trajectory

Another method proposed by Kim & Kim [65]pp.369 describes the optimal velocity trajectory of a two wheeled robot, to reduce energy consumption from the battery power supply by actually measuring the energy consumption and using this as a cost function. This method also uses regenerative braking to reduce energy consumption. It discusses the drawback of loss-minimization control as relatively complex due to the difficulty of measuring the parameters of the different loss components. Some research has reduced the complexity by removing some components however this makes the loss-minimization control inefficient.

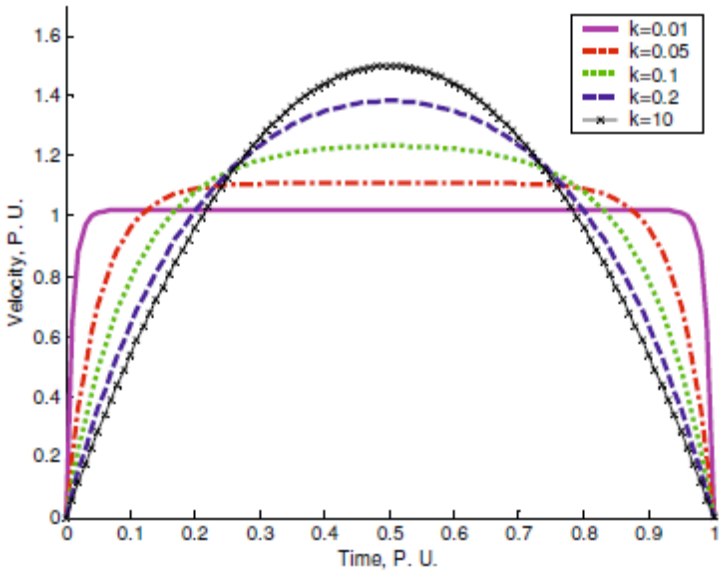

Figure 15 - Minimum energy trajectories at different *k values* [65]pp.369

The paper discusses the shape of the velocity trajectory, Figure 15, as dependent on the mechanical time constants (t_v) and the time it takes to complete the step (t_f) shown in equation (9)

$$k = \frac{t_v}{t_f} \tag{9}$$

In the end after both simulations and actual tests the paper concluded that a 9-10% reduced energy consumption could be achieved by using this method instead of loss minimization or trapezoidal trajectory planning respectively.

A combination of both trajectory planning and loss minimization is put forward in Sergaki & Stavrakakis [25]. The paper investigates a robot application with separate excitation BDC motor drive. The calculations for the excitation needed required complete knowledge of all the motor parameters as well as a complete motor loss model.

3.6.2 Efficient feedback control

Apart from trajectory planning, other methods of controlling motors efficiently are by using feedback to vary the motors behavior depending on its current state. Discussed here are variable speed/frequency control, and feed forward current control. Both these methods increase the motor efficiency and thereby also reduce the energy consumption.

3.6.2.1 Variable speed/frequency control

One idea of variable speed drive according to Saidur et al. [66] is to vary the motors speed to its optimum, depending on the load, to increase the motors efficiency. The author mentions several different techniques of using variable speed drive (VSD) but concludes that the most common method is to change the speed using a PWM input. A VSD system consists of three components, the motor, a power converter and a control system.

3.6.2.2 Feed-forward current control

Watanabe & Yuta [67] mentions common methods of reducing copper losses from torque ripples by increasing the input PWM frequency or add external inductors. The authors then propose a new method where no external inductor or frequency changes are necessary to reduce current in a mobile robot. This is achieved by using a switching method where the current in closed state is loaded in the motors inductance and when opened the current freewheels with a diode. This way the current and current ripples are reduced. The report also proposes a current feed-forward method to control the current know what current each phase (in a small three-phase BLDC motor) should be fed with. This is done by doing calculation for knowing desired current for all angle and rotational speeds. The current is translated to a PWM ratio for the input. This way, one can know the optimal current in all running cases. The reason of using a feed-forward method is due to difficulties and complexity to measure current directly. The results show a small power reduction.

3.6.3 Overcome Inrush current

The inrush current of a DC motor described previously in section 3.1.2.4 will be of major consideration when designing an energy efficient system. There are several soft starting techniques to reduce the inrush, however with the consequence of reduced acceleration which leads to longer inrush periods.

3.6.3.1 Soft start

Soft starters on the market are according to Zhang et al. [57] mainly mechanical and usually consist of thyristors. The soft starter, put forward by Zhang et al. [57], consists of a PWM chopper on the supply voltage, regulating the average voltage, and thereby also the current supplied to the motor. The paper concludes that by using an increasing PWM duty cycle from 20-100% over 10 seconds, the inrush current was more than halved. The same result has also been shown in Lü & Sun [68].

Adjustments of the voltage and changes of the chopper PWM duty cycle are discussed in Tie & Le-jia [69], and are considered hard to do. Some solutions presented previously are closed loop speed feedback, which requires extra sensors. This method proposes to use adaptive neuro fuzzy soft starting pulse modulation without using extra sensors. The network uses the previous duty cycle and the armature current to calculate the new optimal duty cycle. Results are however only simulated in MATLAB, but the author feels that this method

of implementing a soft starter would reduce the complexity of on line calculations of the duty cycle.

3.6.3.2 Resistor soft start

Bhattacharya & Singh [32] suggest a five step starter method where four acceleration resistors is connected in series and gradually switched off during acceleration. This gives the effect of a higher resistance in the start and according to ohm's law, also described in section 3.1.2.4, this give a lower inrush current. However, also as described in section 3.1.1.1, increased losses will occur before the resistors are switched off. In Figure 16 one can see a DC motor connected in series with the acceleration resistors.

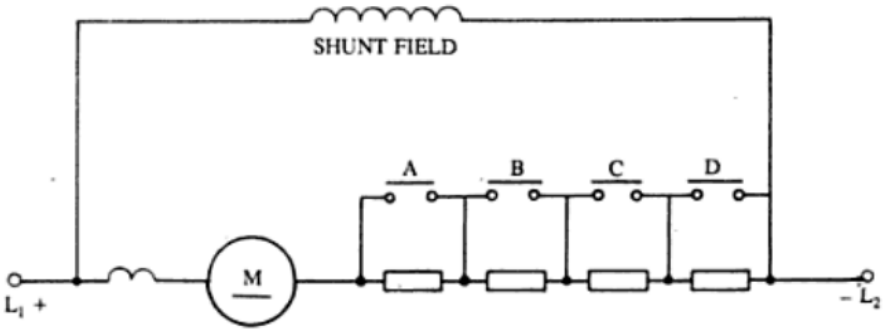

Figure 16 – Automatic resistor switching setup [32]

4 Implementation

To extend the battery life time of Aperio E100 a modeling optimization approach was selected, where the energy was compared between different trajectory steps. This was done on the current system motor as well as on an optimally selected BLDC motor. This was done to compare the new prototype with the current Aperio E100 lock.

In this chapter the implementation of this thesis will be described by first stating the requirements and describing the overall concept before discussing the hardware selection, modeling and software more thoroughly.

4.1 Requirements

When developing the new prototype for the Aperio E100 lock, certain requirements for the product had to be met. Some of these were set by the company whilst others were limitations on the hardware:

- The voltage supply for the system is 3V DC, limited by the RFID and communication circuit on the E100.
- The final application is battery powered so a current limit was set at 500mA.
- The motor size could not exceed the limited space inside the lock housing of 20x15x12mm.
- A maximum locking and unlocking time was set to 300ms each, as times longer than this would cause noticeable delays for the users.
- The locking mechanism (lever, lead screw, locking pin and handle) are seen as black box and are not to be altered.
- The minimum torque required by a motor is set at 0.45mNm as measured and calculated in section 4.4.1.1.

A list of all the requirements can be found in Appendix A.

4.2 System Breakdown

The two selected actuators to work with in this thesis were the BDC motor from the Aperio E100 system as well as a new BLDC motor. Both systems use the same mechanism as the E100, which is a requirement (Appendix A) and uses Hall-effect sensors to sense the end positions of the leaver.

4.2.1 BDC

The structure of the Brushed DC circuit, seen in Figure 17, was driven by a 3V supply. Two PWM signals from the processor control the motor drive, which is used to control the motor in both directions. The motor shaft drives the load of the locking mechanism. The Hall-effect sensors from the Aperio E100 are connected to the processor and are necessary for knowing the leavers end positions.

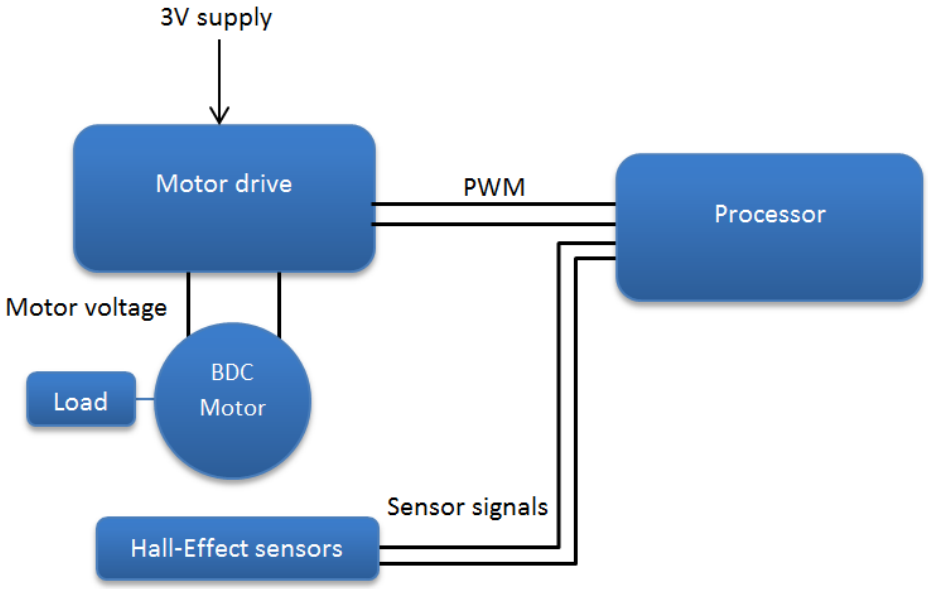

Figure 17 - BDC System overview

4.2.2 BLDC

The BLDC motor selected in this thesis was a three-phase motor and the HW-structure of the system can be seen in Figure 18. The motor is driven by a three-phase motor drive using signals from the processor. The application has three Hall-effect sensors from the motor sensing the rotor position and two sensing the end positions of the leaver. The motor drives the same load as the Aperio E100 system.

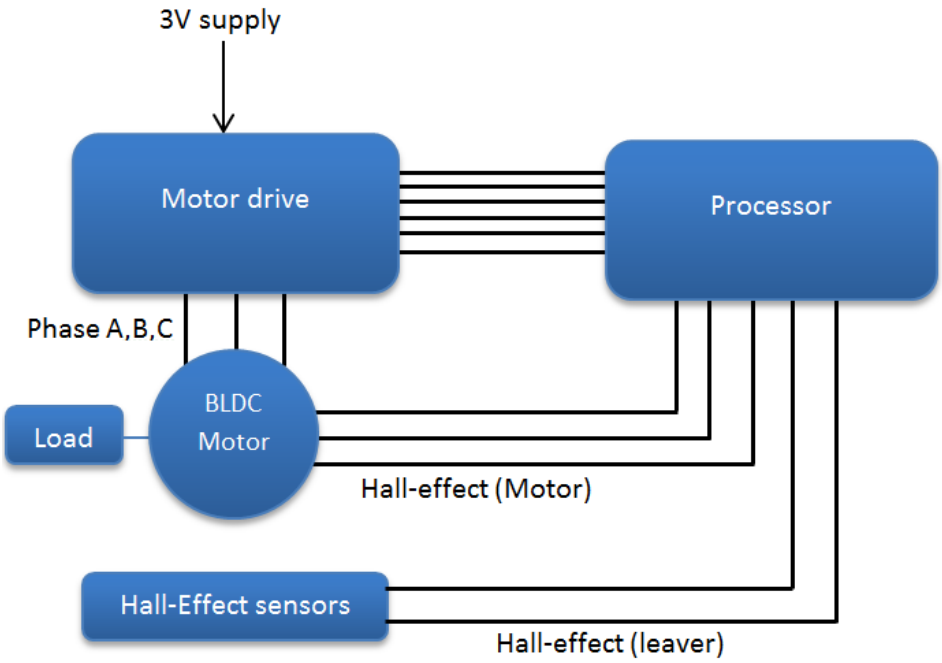

Figure 18 - BLDC System overview

4.3 Hardware BDC Prototype

The Aperio E100 lock has a processor and a motor drive which controls the motor, however time constrains made access to these not possible. Therefore new hardware was chosen, and this section describes these choices.

4.3.1 Processor

In this thesis an mbed LPC1768 (Appendix C.10) platform was used. It is a 32bit processor that runs at 96MHz, with preprogramed functions from the mbed library. This was used because it's easy to get started and great for rapid prototyping. To use LPC1768 was a recommendation from the expert at ASSA ABLOY. This is however not an optimal selection for a finished product due to price, high energy consumption and large size.

4.3.2 BDC Motor and driver

The motor for the Aperio E100 system is a QX-FF-030 (Appendix C.1) from QX Motor. It has a nominal voltage of 2.5V but runs in the Aperio E100 lock at 3V. The motor has a stall current of about 0.2 A, a maximum efficiency just under 40% and a measured resistance of 12.8Ω. The motor has two connections that during running mode are connected to the supply voltage U and ground.

To drive the brushed DC motor in both directions a motor drive is necessary. In this thesis a Texas instruments DRV8837EVM (Appendix C.2) was used. It has a maximum internal resistance of 330mΩ and the motor has a resistance of 12.8 Ω, which gives a voltage drop ratio shown in equation (10) of 2.5%.

$$\frac{0.33}{12.8} = 2.5\% \qquad (10)$$

4.4 Hardware BLDC Prototype

This section explains the method of selecting a BLDC motor and presents the BLDC and motor driver hardware implemented in this thesis. This prototype uses the same mbed processor as the BDC prototype, presented in section 4.3.1.

4.4.1 Motor Selection

In section 3.5.2 several methods of motor design were presented which could provide the optimal motor needed for this product, however due to time limitations a selection method of already existing motors was conducted instead. When selecting a BLDC motor there are several factors that needs to be considered. The first test, as discussed by Roos in section 3.5.1, was to verify that the motor torque is higher than the peak load torque. To perform this test, the torque load of the mechanism must first be measured, followed by a look at the inrush current, supply voltage, motor size, motor configuration and finally sensors.

4.4.1.1 Load measurements

To calculate the torque load of the locking mechanism firstly the translational force, required on the leaver to compress the locking pin, needs to be measured. Here a load cell, “Phidgets Micro Load Cell (0-100g)” (Appendix C.7), together with a driver “PhidgetBridge 4-inputs” (Appendix C.6), was used to measure the translational force. Figure 19 shows the load cell mounted sideways at the same height as the center of the leaver (Locking mechanism), and attached at the same radius as where the lead screw normally acts. The mechanism was then compressed incrementally and the force measured at 1 mm intervals.

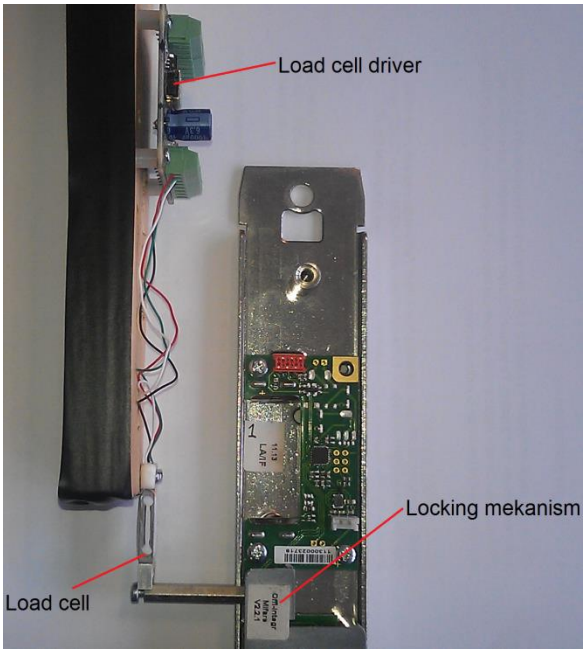

Figure 19 - Force measurement setup

From the measured force the torque load on the motor was calculated. A free body diagram was drawn, shown in Figure 20. The radius of the leaver from the pivot A, to the locking pin is r_1, and the force generated here by the locking pin spring is F_S. This force corresponds to the force F which acts at the distance r_1+r_2 from the pivot. The locking pin is in all test cases and measurements in this thesis adjusted to a position perpendicular to the leaver.

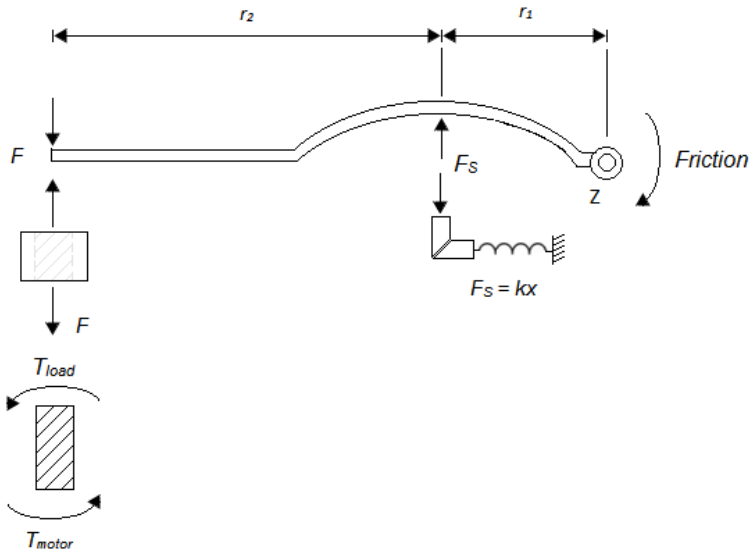

Figure 20 - Lever free body diagram

Since the force *F* was measured using the load cell, and the area of interest is the torque needed by the motor to move the lead screw, a new free body diagram of the lead screw was drawn using equations and reasoning from Jadon & Verma [70] pp.440-441. Figure 21 shows the free body diagram of the lead screw, where μN is the friction force, μ the friction coefficient (assumed as plastic-plastic to 0,4 [71]), *N* is the normal force, *F* the load on the nut, *W* is the pushing force from the screw, *p* is the pitch, *d* diameter of the screw and α is the screw pitch angle.

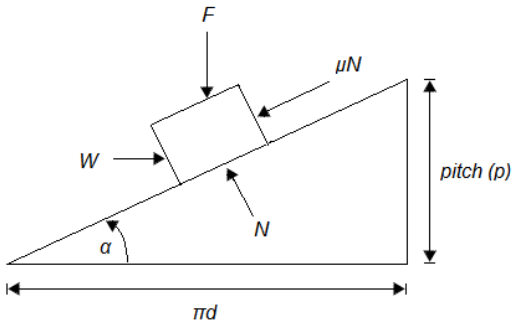

Figure 21 - Lead Screw [70]

From Figure 21 the equations (11) and (12) were derived in Jadon & Verma [70] pp.440-441. The lead screw torque T_{load}, is equal to the motor load torque $T_{motor,}$ since the screw is attached to the motor axle. The lead screw equations (11) and (12) are given as;

$$T_{UP} = F\frac{d}{2}\tan(\phi + \alpha), \tag{11}$$

$$T_{Down} = F\frac{d}{2}\tan(\phi - \alpha), \tag{12}$$

where T_{Up} is the torque for the case of raising a load, and T_{Down} is the torque for lowering a load, where in $\tan(\phi+\alpha)$ and $\tan(\phi-\alpha)$ is given as in equation (13) and (14);

$$\tan(\phi+\alpha) = \frac{\tan(\phi)+\tan(\alpha)}{1-\tan(\phi)\tan(\alpha)}, \quad (13)$$

$$\tan(\phi-\alpha) = \frac{\tan(\phi)-\tan(\alpha)}{1+\tan(\phi)\tan(\alpha)}. \quad (14)$$

$\tan(\phi)$ is as shown in equation (15);

$$\tan(\phi) = \mu, \quad (15)$$

equal to the friction constant μ and $\tan(\alpha)$ is shown in equation (17);

$$\tan(\alpha) = \frac{P}{\pi d}. \quad (16)$$

When inserting equation (15) and (16) into equation (13) and (14) the load torque, is given in equation (17) and (18), as;

$$T_{up} = F\frac{d}{2}\left(\frac{\pi\mu d+P}{\pi d-\mu P}\right), \quad (17)$$

$$T_{Down} = F\frac{d}{2}\left(\frac{\pi\mu d-P}{\pi d+\mu P}\right). \quad (18)$$

The up case (T_{up}) described in equation (17) will correspond to locking, and the down case (T_{Down}) in equation (18) corresponds to an opening of the Aperio E100 lock.

This method calculates the torque load of the mechanism but assumes the inertia of the lead screw as negligible.

4.4.1.2 Optimal motor torque

Once the load torque has been established, the next step purposed by Roos in section 3.5.1 was to check continuous torque behaviors and speed requirements. But since no steady state behavior or speed requirements exist in this application, other aspects need to be taken into account. The first thing to consider is to find a motor that operates at its optimal torque.

Most motor has an efficiency curve, in the datasheet, which is dependent on the speed and torque of the motor. Figure 22 shows an example of a curve showing that the maximum efficiency of about 69% when the motor is running with a load of ~30mNm. When selecting a motor for efficiency it is important to choose one that has its optimal torque near the actual load torque

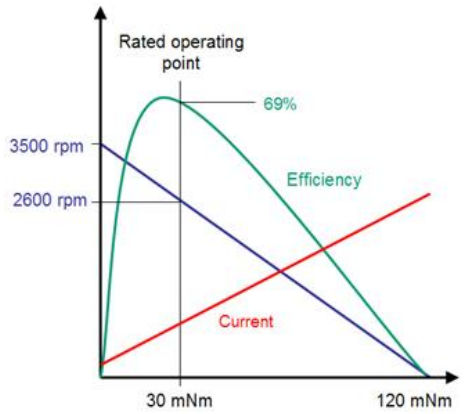

Figure 22 - Typical motor torque, speed and efficiency curve [72]

A motor with a mean torque load near the optimal efficiency will produce the least amount of losses, and therefore be desirable when optimizing the Aperio E100 prototype for energy efficiency.

4.4.1.3 Inrush current

Since the running period for the system is fairly short (100-200ms) the initial transient inrush phase will, as seen in Figure 4 in section 1.1.2, have a significant impact on the energy consumption. As discussed in section 3.6.3 the inrush current is mostly dependent on the resistance and the supply voltage. To reduce the inrush current a motor could be chosen with a higher resistance according to section 3.6.3, however with higher resistance, higher copper losses occur as described in section 3.1.1.1, making the motor less efficient.

Therefor when selecting a motor in this thesis, a lower resistance would be more desirable. The phenomenon of inrush current then needs to be dealt with using techniques such as soft starting, discussed in the research at section 3.6.3.1.

4.4.1.4 Supply voltage

A voltage source of 3V is an overhead requirement as seen in Appendix A. Therefor a motor with a nominal voltage of about 3V was required. An alternative would be to use a DC-DC boost converter to be able to use higher voltage motors. The drawback would be increased losses, as presented in section 3.3. Therefor a BLDC motor with a nominal voltage of 3V would be desirable.

4.4.1.5 Motor size

When selecting a motor an overhead requirement was that the motor fit inside the application (Appendix A). At the same time it would be desirable to have the motor as large physical size as possible to keep a higher efficiency, according to section 3.1.2.3.

According to section 3.5.1.1 the NEMA standard is a good tool to compare different motors sizes with different efficiencies. Using the NEMA tool will ensure that a highly efficient motor is selected.

4.4.1.6 Motor configuration

This section will motivate the choices of motor configuration and characteristics from the research in section 3.2.1.

A slotted motor was desirable due to its greater flux density and lower winding resistance for equal torque, compared with slotless motors. The drawback of using a slotted motor was the cogging. This effect could be eliminated by using a skew magnetization slotted armature as seen in section 3.2.1.3, however scew magnetization was unwanted due to increased losses and more complex design. In this thesis a slotted motor, without scew magnetization, due to higher flux density than slotless motors, would be desirable. The assumption was made that the gain from a higher flux density would be greater than the loss generated by cogging.

It would also, as seen in section 3.2.1.1, be suitable to have an axial flux-, instead of a radial flux motor, due to the axial flux motor having a higher efficiency and produces greater torque per size.

Outrunner motors are more desirable since they produce higher torques, according to section 3.2.1.2 than inrunners. The drawback with outrunners, compared to inrunners, is that they would be harder to fit inside the Aperio E100 lock due to the rotor being uncontained.

4.4.1.7 Sensors

When commutating a BLDC motor, knowing the rotor position is necessary. As explained in section 3.2.3 this could be done using Hall-effect sensor or back emf sensing. The drawback of back emf sensing being that the motor needs to have a certain speed before the emf can be sensed. Since in the Aperio application, the motor only turns a total of five revolutions in a complete locking or unlocking sequence, Hall-effect sensor will be essential for commutating the motor.

4.4.1.8 Selected Brushless Motor

The selected brushless motor, for this thesis, was an *EC 9.2 flat Ø10 mm, brushless, 0.5 Watt with hall sensors (*Appendix C.3) from Maxon motor*.* This motor is driven with a nominal voltage of 3V and has a maximum efficiency of 54%, winding resistance of 4.44 Ω, creating a peak inrush current of 0.675A. Furthermore it has eight connections, three for the phases and three for the Hall-effect sensors and one for GND and 5V voltage for the sensors. Hall-effect sensor pins will be connected to the microprocessor and the phase pins will be connected to a motor driver.

This motor was selected mainly since the input voltage and size fitted our requirements. The motor can produce torques higher than the required peak load torque (Appendix A), and also has Hall-effect sensors that were stated as a necessary for successful commutation. The *EC 9.2 flat Ø10 mm, brushless, 0.5 Watt with hall sensors* was the only motor found that fulfilled all the requirements, and was therefore selected. The starting current of 0.675A was higher than the requirement in Appendix A, but by using lower input voltages and slow start techniques this problem was resolved.

The Maxon motors shaft was slightly too short and had too small a diameter. This was solved by attaching an axle extension before attaching the shaft to the lead screw. This setup is illustrated in Figure 23.

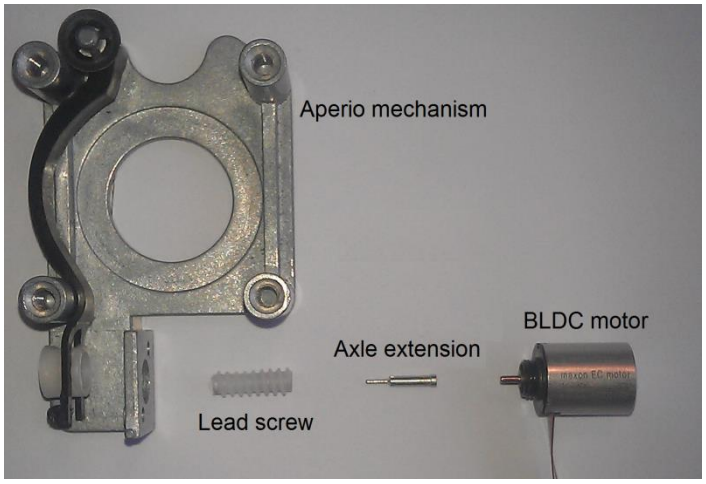

Figure 23 – BLDC Motor installation

4.4.2 BLDC drive

In this section the hardware of the motor drive to the BLDC prototype is presented. The section will also present the commutation method that was implemented.

4.4.2.1 Hardware Motor driver

To drive the motor a bipolar approach was selected due to section 3.2.2, which showed a higher torque constant in the initial phase compared to unipolar drive. The Aperio E100 lock has a short running time, and therefore the initial phase will have a significant effect on the motors performance. To drive the BLDC motor in a bipolar manner it was necessary to have a triple half bridge to control currents in both directions. Figure 24 shows a diagram of a triple half bridge connected with a BLDC, where S_1, S_3 and S_5 decides which stator that is connected to V_{cc} and S_2, S_4 and S_6 decides which stator is grounded. *A*, *B* and *C* are the three phases of the BLDC motor.

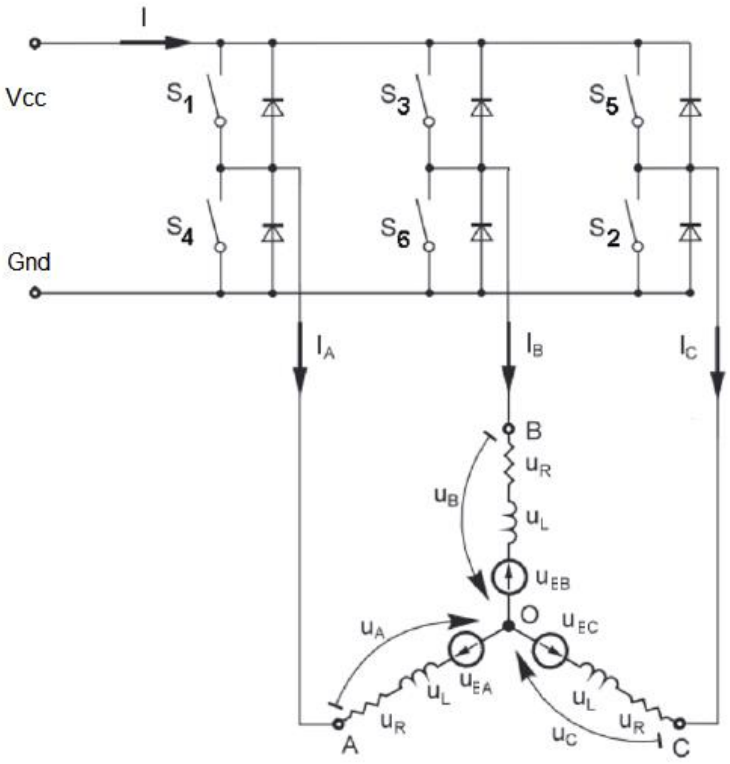

Figure 24 –Motor drive of BLDC [73]

In this thesis two dual half bridges, DRV8839EVM from Texas instrument (Appendix C.4) were connected together as a triple half bridge. There exists triple half bridge ICs, however the DRV8839EVM was most suitable since it had the right input voltage that other bridges don't.

DRV8839EVM has a maximum on resistance of 330mΩ over the input and output transistor together. The motor has a resistance of 4.4Ω which gives a ration of the voltage dissipation over the transistor as shown in equation (19) of 7.5%.

$$\frac{0.33}{4.4} = 7.5\% \tag{19}$$

The switching losses of the motor drives were assumed to be zero because no capacitive load was mentioned in the datasheet. According to section 3.1.2.4, this loss is often quite small.

4.4.2.2 Brushless commutation

To make a three-phase brushless motor run, it is necessary to implement a commutation algorithm, as seen in section 3.2.3. In this thesis a six step (trapezoidal) method was used. The six step method was selected due to its simplicity to implement and doesn't require as much processor speed as FOC. Sinusoidal commutation was discarded as the research in section 3.2.3.3 showed lower torques would be produced, even though this commutation method would reduce torque ripples. The drawback with six step commutation is that an optimal torque is not acquired as for FOC, seen in section 3.2.3. In section 3.2.3.2 the method of six step trapezoidal commutation is described.

To determine the rotor position three Hall-effect sensors located by each of the three phases was used. Table 2 shows the Hall-effect sensors high- and low configuration, for all the electrical degrees.

Table 2 – Commutation Table [74]

ELECTRICAL DEGREE	HALL 1	HALL 2	HALL 3
0-60	1	0	1
60-120	0	0	1
120-180	0	1	1
180-240	0	1	0
240-300	1	1	0
300-360	1	0	0

Figure 25 show what the phase currents I_A, I_B and I_C depends on the Hall-effect signals H1, H2 and H3.

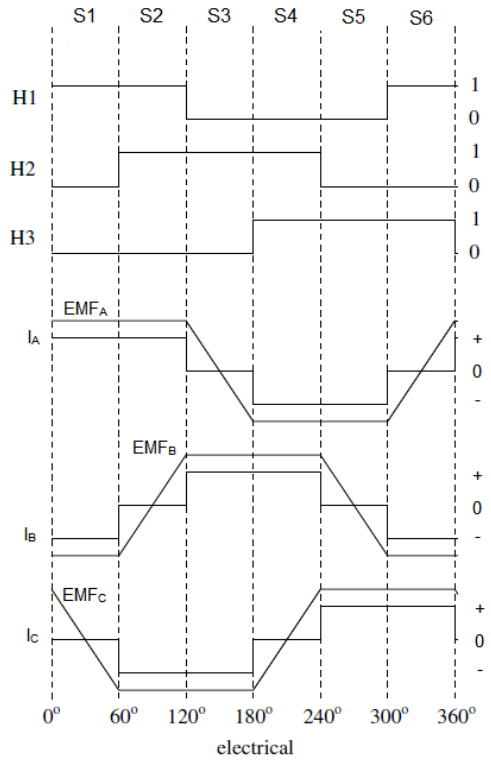

Figure 25 - Back emf, Hall, and Current sequence [4]

4.5 Modeling and Trajectory

The main method of controlling the motors was trajectory planning as discovered in the research section 3.6.1.1. This method showed that using velocity trajectory control, the energy consumption could be reduced with up to 30%, and was therefore pursued. The other trajectory method, loss minimization trajectories, described in section 3.6.1.2, was

never implemented in this thesis due to the time constraints and the complexity of the method.

In order to find the minimum energy trajectory for a specific motor, first a detailed model had to be constructed in order to test the vast number of different possible input steps. The model was then tested and verified, before the trajectories were built and implemented. The following sections will describe this process of modelling, motor response measurements for verification and finally trajectory building.

4.5.1 Modeling

This section will thoroughly describe all steps and equations involved when developing the models for the BDC and BLDC motors. Some assumptions made to simplify the modelling were:

- Constant parameters, such as *R,* resistance not affected by temperature.
- Cogging, commutation, iron, windage, and stray losses were simplified as Coulomb friction.
- Bridge losses, such as switching and resistance were excluded.
- The motor shaft and mechanism was seen as ridged, and the total inertia was a lumped inertia.
- Play in the lead screw and motor were neglected.

4.5.1.1 BDC Model equations

A brushed DC motor model is shown in Figure 26, where u_i is the input supply voltage, *i* the current through the motor, *R* the motor resistance, and *L* is the motor inductance.

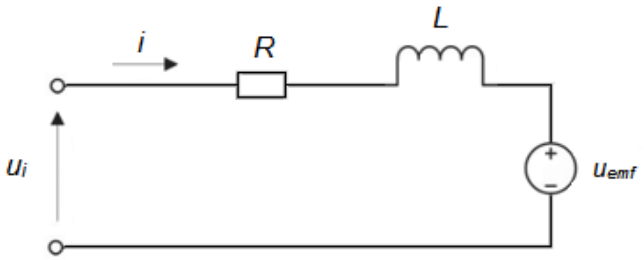

Figure 26 – Electrical DC motor circuit

The back emf voltage u_{emf} generated by the motor as it rotates is given by equation (20):

$$u_{emf} = K_{emf}\dot{\varphi}, \tag{20}$$

where K_{emf} is the motor back emf velocity constant, and $\dot{\varphi}$ the motor velocity. Equation (21) shows the voltage drops over the resistor and the inductor.

$$u_R = Ri, u_l = L\frac{di}{dt}. \tag{21}$$

The input voltage into the circuit u_i can then be written as equation (22):

$$u_i = L\frac{di}{dt} + Ri + Kemf\dot{\varphi}. \quad (22)$$

By rearranging equation (22), and solving for the current running through the motor the equation becomes as in equation (23):

$$i = \frac{u_i - L\frac{di}{dt} - Kemf\dot{\varphi}}{R}. \quad (23)$$

Equation (24) shows the torque T_m generated by the motor;

$$T_m = K_m\, i - T_l(\varphi) - T_f, \quad (24)$$

where the torque constant K_m and the load torque $T_l(\varphi)$ is a function of the rotational angle, and T_f is the coulomb friction torque.

The coulomb friction torque can be divided into two parts, dynamic and static friction. When the angular velocity is within the static friction span the friction torque increases against the applied torque to a limit of $\pm F_c$ as shown in equation (25):

$$T_f = F_C, \quad Fc = T_m\{^{+Fc}_{-Fc} \quad (25)$$

When the angular velocity then exceeds the limit, the dynamic friction b, is active giving the total friction torque in equation (25):

$$T_f = F_C + b\dot{\varphi} \quad (26)$$

Figure 27 then introduces mechanical behavior into the electrical model of the system.

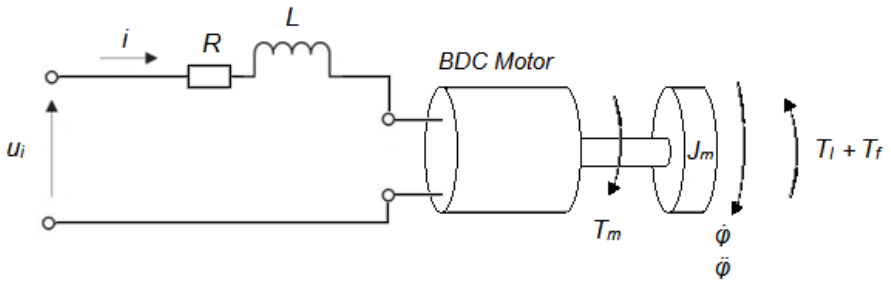

Figure 27 - Mechanical motor model

Equation (27) shows how the torque is related to the inertia, J_m and the acceleration $\ddot{\varphi}$,

$$J_m\ddot{\varphi} = T_m - T_{load}, \quad (27)$$

where T_{load} is the torque load on the motor including friction and actual axial torque load and T_m is the motor torque. The load torque was calculated in section 4.4.1.1

Putting equation (23) and (27) in (24) and solving for the acceleration, gives equation (28) as:

$$\ddot{\varphi} = \frac{\mathrm{K_m}(\mathrm{u_i} - \mathrm{L}\frac{di}{dt} - \mathrm{K_{emf}}\dot{\varphi})}{J_m \mathrm{R}} - \frac{\mathrm{T}_l(\varphi) - T_f}{J_m}. \quad (28)$$

Figure 28 shows an overview of the motor model, from an input voltage to output torque.

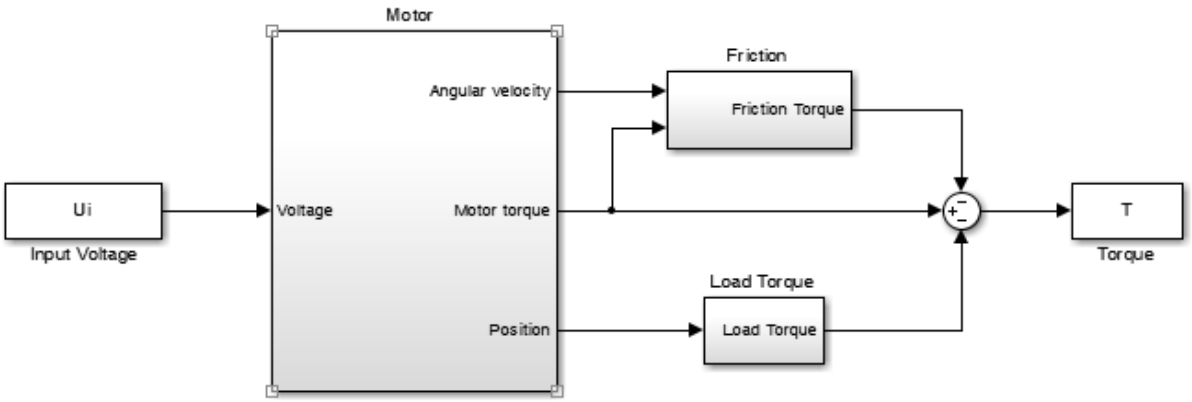

Figure 28 – BDC Prototype model

4.5.1.2 BLDC Motor Model

The brushless motor model is electrically similar to the brushed motor model where each winding consists of a resistance, inductance, and back emf. The main difference is the commutation sequence which also needs to be incorporated, as well as the sequencing of the back emf. Generation of the brushless motor model was mostly done by following a previous project by Tibor et al. [73],

As previously shown in Figure 24 in section 4.4.2.1, the configuration of a brushless motor, with its three windings, *A, B*, and *C*, as well as their respective winding currents (I_A, I_B, I_C) and voltages (u_A, u_B, u_C) was described. The voltage for each winding is given as in equation (29) (showing only winding A),

$$u_A = u_R + u_L + u_{emfA}, \quad (29)$$

where u_R is the voltage drop over the resistance R , shown in equation (30) equal to

$$u_R = RI_A. \quad (30)$$

The inductive voltage drop u_L is given by equation (31), with the inductance L, and $\frac{dI_A}{dt}$ is the change in winding current over time.

$$u_L = L\frac{dI_A}{dt}. \quad (31)$$

In a 3- phase BLDC motor the back emf voltage is related to a function of the rotor angle, and the three winding back emfs are phase shifted 120º from each other. The back emf voltages for the three phases can therefore be described as in equation (32), (33) and (34):

$$u_{emfA} = K_{emf} f(\Theta_e)\dot{\varphi} \tag{32}$$

$$u_{emfB} = K_{emf} f(\Theta_e - 2\pi/3)\dot{\varphi} \tag{33}$$

$$u_{emfC} = K_{emf} f(\Theta_e + 2\pi/3)\dot{\varphi} \tag{34}$$

The back emf constant is given by K_{emf}, and the rotor speed $\dot{\varphi}$ in rad/s. Θ_e is the electrical rotor angle. Figure 29 shows the back emf of the three phases depending on the electrical rotor angle.

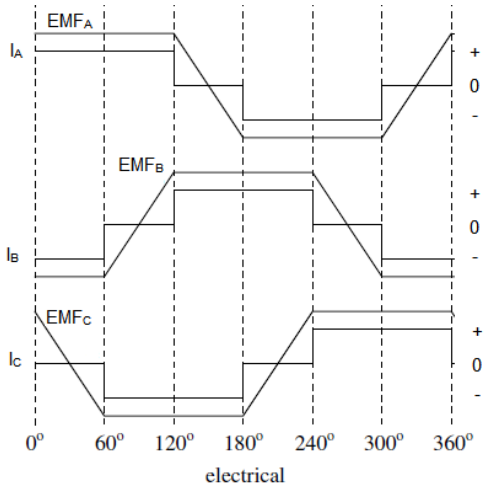

Figure 29 – Back emf, Hall, and Current sequence [4]

The electrical angle θ_e can be converted into mechanical angle, Θ_m, by, as in equation (27), multiplying by the number of pole pairs, p:

$$\theta_e = \frac{p}{2}\theta_m \tag{35}$$

The torque generated by the motor can be written as equation (36):

$$T = \frac{u_{emfA} I_A + u_{emfB} I_B + u_{emfC} I_C}{\dot{\varphi}}, \tag{36}$$

where I_A, I_B and I_C is the phase currents, u_{emfA}, u_{emfB} and u_{emfC} is the phase back emfs and $\dot{\varphi}$ the rotational speed. Adding the torque load T_L, which is calculated in section 4.4.1.1, the motor inertia J_m and friction b gives equation (37):

$$T - T_L = J\frac{d\dot{\varphi}}{dt} + b\dot{\varphi} \tag{37}$$

Equations (29) to (37) where then used to build the MATLAB Simulink model as shown in Figure 30.

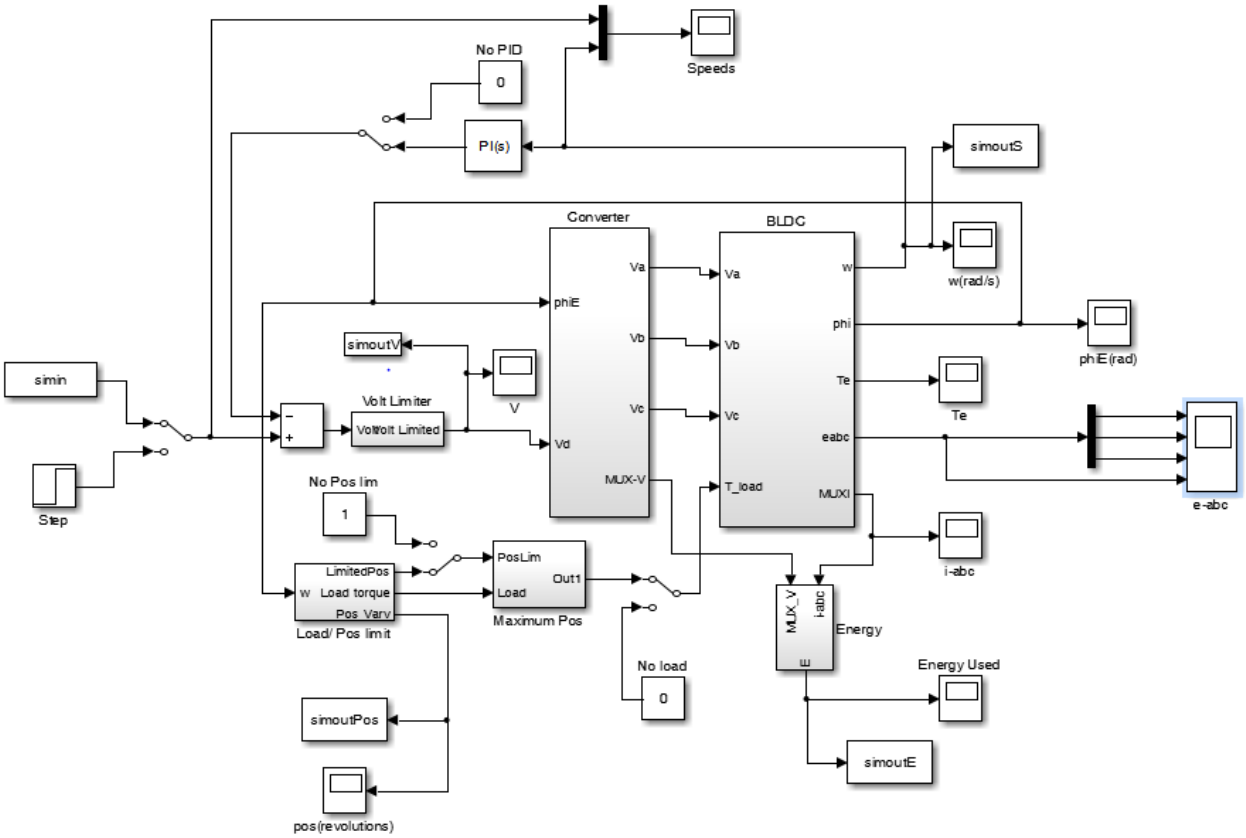

Figure 30 – BLDC Prototype model

The converter block, generates the transistor switching sequence and thereby also the sequence of phase excitation. The switching sequence was described in section 4.4.2.2 The BLDC block then uses the above described equations to build a complete motor model.

4.5.2 Motor measurements

In order to identify the different system behaviors, measurements of different components were made. Firstly the motor current needs to be measured to verify the motor behavior as well as for evaluating the energy consumption. Secondly, the no load motor speed had to be measured to verify the accuracy of the motor model. This was done using an encoder.

4.5.2.1 Current measurements

Verification of the accuracy of the current measurement was necessary, and therefore two different methods were implemented. First a current amplifier circuit, over a shunt resistor, as discussed in section 3.4, was used and secondly directly over the shunt using ASSA ABLOYs lab instruments.

The current IC amplifier LT6105 (Appendix C.5) from Linear Technology was used and soldered together as suggested on page 11 in the datasheet, with R_{in}=220Ω, R_{out}=10000Ω and a high precision shunt resistor R_{sens}=0.1Ω. This resistor configuration generated a gain, as shown in equation (38), of;

$$Gain = \frac{R_{in}}{R_{out}} \approx 45{,}45. \quad (38)$$

The sensor had a slightly linear error for small voltages, the reason being that the two R_{in} resistors weren't identical. This was solved by adding a variable resistor in series with the R_{in} resistor with the lowest resistance and tweaked until the sensor was correctly calibrated. The voltage from the amplifier was then captured on an oscilloscope and the data transferred to MATLAB. Here the voltage, over the shunt u_{shunt}, was calculated into a current i using ohms law and the amplification as in equation (39):

$$i = \frac{u_{shunt}}{Gain \cdot R_{sens}}. \quad (39)$$

The second current measurement method was used due to the fact that the LT6105 didn't present the same current profiles and levels as earlier measurements done by ASSA ABLOY. Using ASSA ABLOYs own method to measure the current of the same Aperio E100 lock would either verify the validity of the LT6105 measurements, or indicate to differences in the performance of different ASSA ABLOY Aperio E100 mechanisms.

ASSA ABLOYs method is based on measuring the voltage drop over a 0.1Ω shunt resistor, and then converting this into current using LabVIEW software. ASSA ABLOYS measurement method was not further investigated by the research group due to time limitations. The method was however important as a reference, since earlier measurements, performed by ASSA ABLOY, were executed using this method.

4.5.2.2 Speed measurement

To verify the motor model behaviors against the real motor the speed had to be measured. To make these measurements, a HEDS-5540#A01 (Appendix C.8) optical encoder from Avago Technologies was used. It is a three channel encoder and has a code wheel with the inertia of 6.0×10^{-8} m^2kg that detects 500 counts per revolution. The setup had to be slightly modified for the encoder to fit the motor shaft, see Figure 31. The encoder circuit has five inputs, three for channel output, one for source 5V and one for ground.

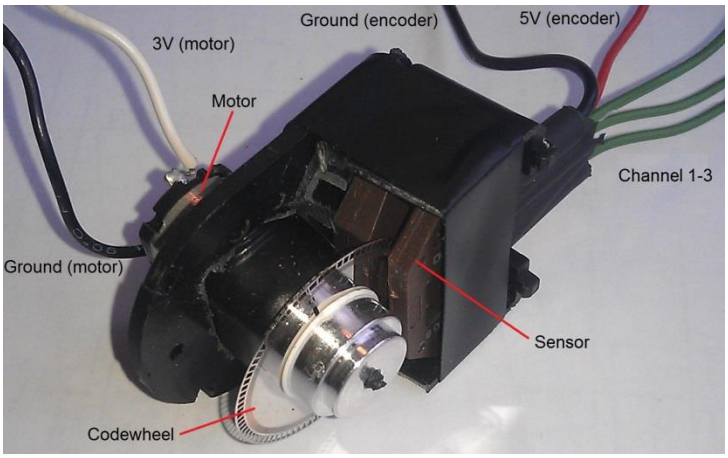

Figure 31 - Modified encoder

The software needed for the encoder was developed on the mbed LPC1768 platform. The program registered the gaps from one of the channels on an external interrupt pin and saved

the time for each pulse. This information was then transmitted via serial communication to MATLAB, where a script calculated the speed from the measured time and the angle between each encoder wheel gap.

4.5.3 Trajectory Generation

Once the models were developed and verified for both the current and speed, speed trajectory optimization could be implemented, as discussed in section 3.6.1.1. Figure 32 shows four different speed trajectories that where tested. They all consist of an acceleration phase ΔT_A, a cruise phase ΔT_C and a deceleration phase ΔT_D.

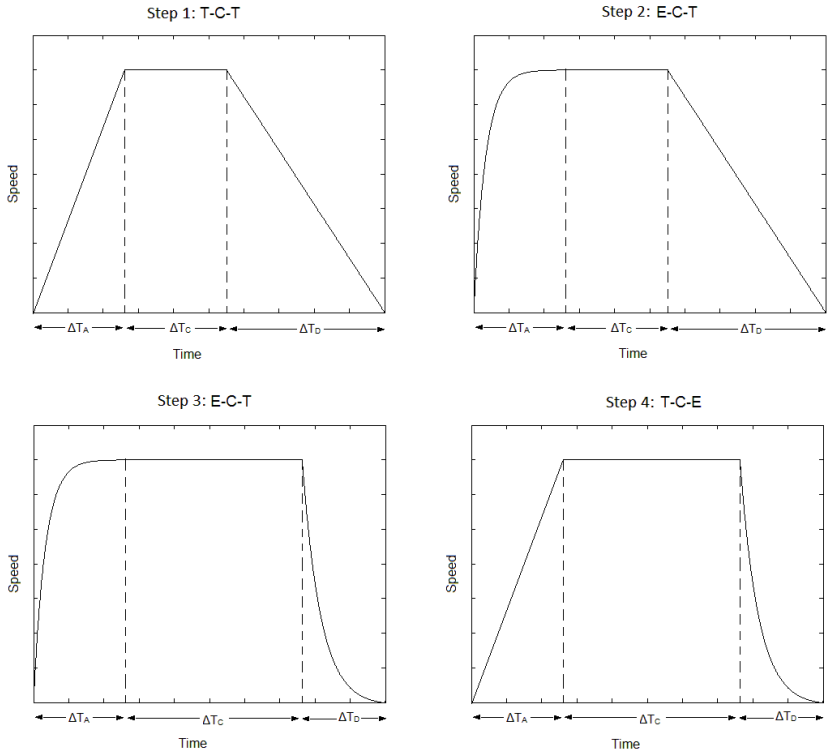

Figure 32 – Trajectory Steps

These different steps were then generated as follows:

Step 1: T-C-T (Trapezoidal – Cruise – Trapezoidal)

The first step in Figure 32 shows a trapezoidal, cruise, trapezoidal, step where both the acceleration (ΔT_A) and deceleration (ΔT_D) phases are given by linear first order equations, while the cruise phase is constant.

Step 2: E-C-T (Exponential – Cruise – Trapezoidal)

The initial acceleration phase, ΔT_A is exponentially decaying of the increasing form according to equation (40):

$$\dot{\varphi}_t = \dot{\varphi}_0(1 - e^{-ct}), \tag{40}$$

where $\dot{\varphi}_t$ is the speed at the time t, $\dot{\varphi}_0$ the desired speed, and c the scaling factor.

The intermediate cruise phase, ΔT_C is constant, and the final deceleration phase ΔT_D is a first degree linear equation.

Step 3: E-C-E (Exponential – Cruise – Exponential)
Here the acceleration phase is exponential like in step 2, described above, and the deceleration phase which is given by the equation (41):

$$\dot{\varphi}_t = \dot{\varphi}_0 \, e^{-ct}. \tag{41}$$

Step 4: T-C-E (Trapezoidal – Cruise – Exponential)
This trajectory step has a linear first order acceleration phase and an exponential deceleration phase like in step 3.

4.5.4 Trajectory Speed optimization

To optimize the different trajectories a brute force approach was used due to its simplicity to implement. This means that all possible steps for the four possible step types, for all different combinations were generated in MATLAB and simulated on the model of the system. Figure 33 shows how a typical step series was generated. Four variables where incremented step wise. The speed, $\dot{\varphi}$ was increased from a starting speed $\dot{\varphi}_s$, to a final speed, $\dot{\varphi}_f$. The cruise start time, t_1 was increased from the starting cruise time t_{1s} to the final step time t_f .The start deceleration time t_2 was increased from the value t_1 to t_f. Lastly the final t_f was increased to t_{max} the maximum time, limited in Appendix A. The entire step had a step resolution of s_{res}.

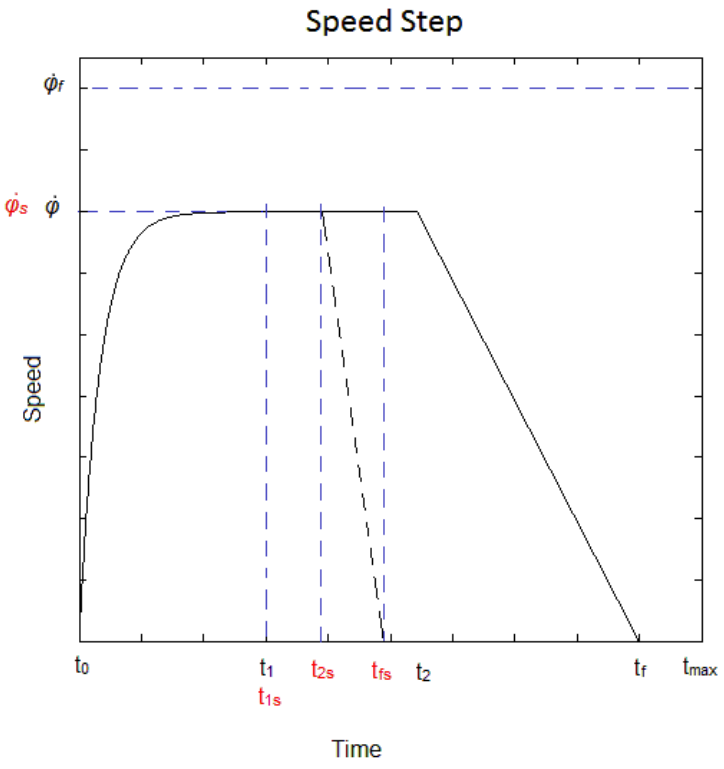

Figure 33 - Trajectory generation

Shown in Table 3 are the final values for the BDC speed trajectory values used in the simulations to generate the different possible speed trajectory steps.

Table 3 - BDC Speed trajectory values

BDC Speed Trajcetory Values	
t_0=0	Start time [ms]
t_{1s}=10	t_1 starting value [ms]
t_{2s}=20	t_2 starting value [ms]
t_f=200	End time [ms]
t_{fs}=20	tf starting value [ms]
$\dot{\varphi}_s$ =0	Starting Speed [rad/s]
$\dot{\varphi}_f$=500	Max Speed [rad/s]
s_{tim}=10	Step time between t_1, t_2, t_f [ms]
$\dot{\varphi}_{step}$=25	Speed step size [rad/s]
s_{res}=0.1	Step resolution [ms]

All the possible steps were generated and simulated on the model in MATLAB Simulink, and the energy consumed was calculated as in equation (42);

$$E = \int i\, U dt \tag{42}$$

Where *i* is the current drawn from the motor drive for the BDC motor, and *i* is the on-phase current for the BLDC motor. *U* is the motor bridge phase voltage.

A search algorithm then sorted all the results, excluding steps that failed to travel the necessary locking/unlocking distance, and showed the step with the lowest energy consumption. The voltage to achieve this speed step was then calculated and transferred into C-code as a duty cycle, voltage vector.

4.5.5 Voltage trajectories

Voltage trajectories were also generated in the same way as the speed trajectories, however replacing the velocity with voltage levels. These were then simulated on the respective models, removing the velocity feedback, running the model open loop. The same search algorithm as described previously was again used in finding the minimum energy voltage input trajectories. Table 4 shows the limitations set on the voltage trajectories generated by the MATLAB model.

Table 4 - BDC and BLDC Voltage trajectory values

BDC / BLDC Voltage Trajectory Values	
t_0=0	Start time [ms]
t_{1s}=10	t_1 starting value [ms]
t_{2s}=20	t_2 starting value [ms]
t_f=200	End time [ms]
t_{fs}=20	t_f starting value [ms]
V_0=0	Starting Voltage [V]
V_{max}=3	Max Voltage [rad/s]
s_{tim}=10	Step time between t_1, t_2, t_f [ms]
V_{step}=0.25	Voltage step size [V]
s_{res}=0.1	Step resolution [ms]

When the best possible steps were found, both for the speeds and voltages trajectories and the duty cycle voltage vector was calculated as described above, they were implemented on to the Aperio E100 prototypes, and the current were measured. This was then plotted and the total energy used was calculated. This data was then implemented into a battery life model that ASSA ABLOY uses to calculate the total battery life, including RFID and processor consumption.

4.6 mbed software

In this section the software control of the BDC- and BLDC motors are explained, as well as the input into the different motor control systems.

4.6.1 Voltage input

Three different voltage input trajectories were used, in the different motor systems, to determine what the most energy efficient control method was. The first method was to use a constant voltage supply, since the Aperio E100 lock was controlled in this way. This creates a reference of what the present current consumption was. Different constant voltages were tested in the range, 0-3V.

The second method was the 3-step velocity control, where a velocity step was the input into the model and regulated using velocity feedback. From this the minimum energy voltage trajectory is extracted. The third and final method was very similar to the velocity trajectory however this simulation is purely open loop, with a trajectory voltage step input into the model, and the minimum energy voltage trajectory was selected. Both the second and third methods generated voltage vectors that are converted into the desired motor duty cycle. These vectors were then downloaded onto the mbed processor, which open loop controls the motor.

4.6.2 BDC-code

The software of the BDC motor was developed on the mbed platform and the code structure can be seen in Figure 34. The code was based on two input voltage vectors, one for the locking trajectory and one for unlocking. The voltage vector contain all incremental voltages (duty cycles) that were generated from the MATLAB Simulink simulation. These vectors were stepped through sequentially at a frequency of 2kHz using a timer interrupt (Timer_irq). The frequency of 2kHz was used to produce steps with an accurate resolution but at the same time avoiding too large voltage vectors.

The voltage vectors control two PWM signals (PWM 1 and PWM 2). The PWM was connected to the input pins of the motor drive and during running phase, one of the PWMs was set to 0% duty cycle (grounded) while the other was set to the value of the voltage vector.

The Hall-effect sensors at the end positions of the leaver were connected to external interrupt pins (irq1 and irq2). On falling edge both PWMs were set to 100% duty cycle, which short circuits the motor driver, causing the motor to brake. A variable then attached the

opposite PWM pin to the voltage vector for the opposite direction and changed the vector from unlocking to locking. After this routine a three second delay was executed before the motor started running in the opposite direction.

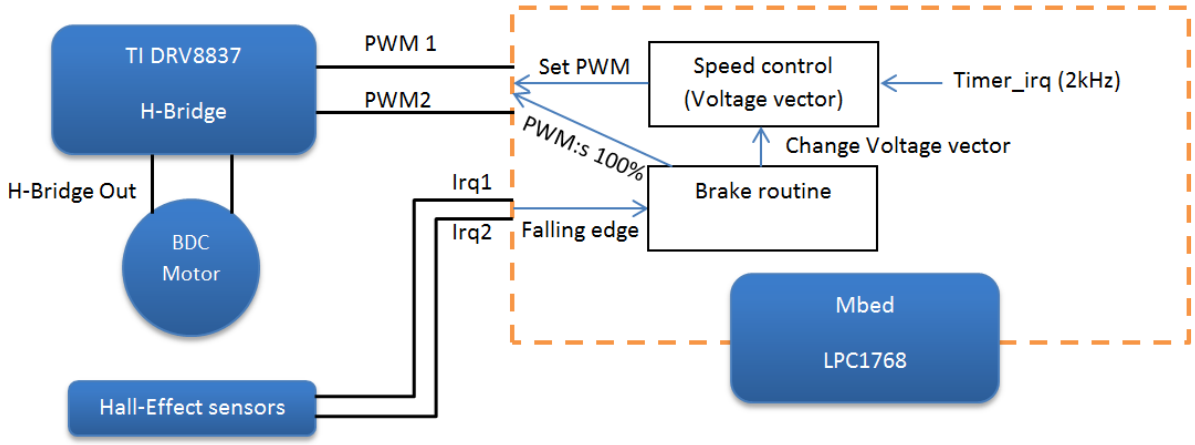

Figure 34 - Code structure of BDC motor

4.6.3 BLDC-code

The software for the BLDC motor was also developed on the mbed platform. The inputs to the motor drive were the two voltage vectors, again generated in the MATLAB Simulink simulations. One of the vectors was for locking and the other for unlocking.

The program structure, which is shown in Figure 35, had a starting sequence, in an infinite while loop, which monitored the Hall-effect sensors (irq3- 5) integrated in the BLDC motor to determine the initial rotor position. This sensing was done to know which step the commutation should start from. Every level change of the Hall-effect sensors (rising or falling edge) generated interrupts on the three external interrupt pins (irq3-5), which then changed the commutation step according to Figure 25 above in section 4.4.2.2.

The commutation activated six PWM signals (PWM 1-6) that controlled the transistors in the triple half bridge. The PWM frequency was chosen at 100kHz, due to the fact that changes of commutation step restarted the PWM at high level, causing initial inaccuracies on the voltage. This effect was reduced when the PWM frequency was increased. Five of the PWM were set to 100% or 0% duty cycle (enabling or disabling transistor switches) according to the Six-step commutation scheme. The remaining PWM was used to control the speed by varying its duty cycle depending on the voltage vector value. The voltage vector was again executed sequentially, using a timer interrupt (Timer_irq), at 2kHz as previously described in the BDC code.

The Hall-effect sensors at the end positions were connected to interrupt pins (irq 1and 2). On a falling edge, four things occurred; all six PWM signals were set to 100% duty cycle to brake the motor, the commutation was change to drive in the opposite direction for the next loop, the voltage vector is change from locking to unlocking and the starting sequence was again activated.

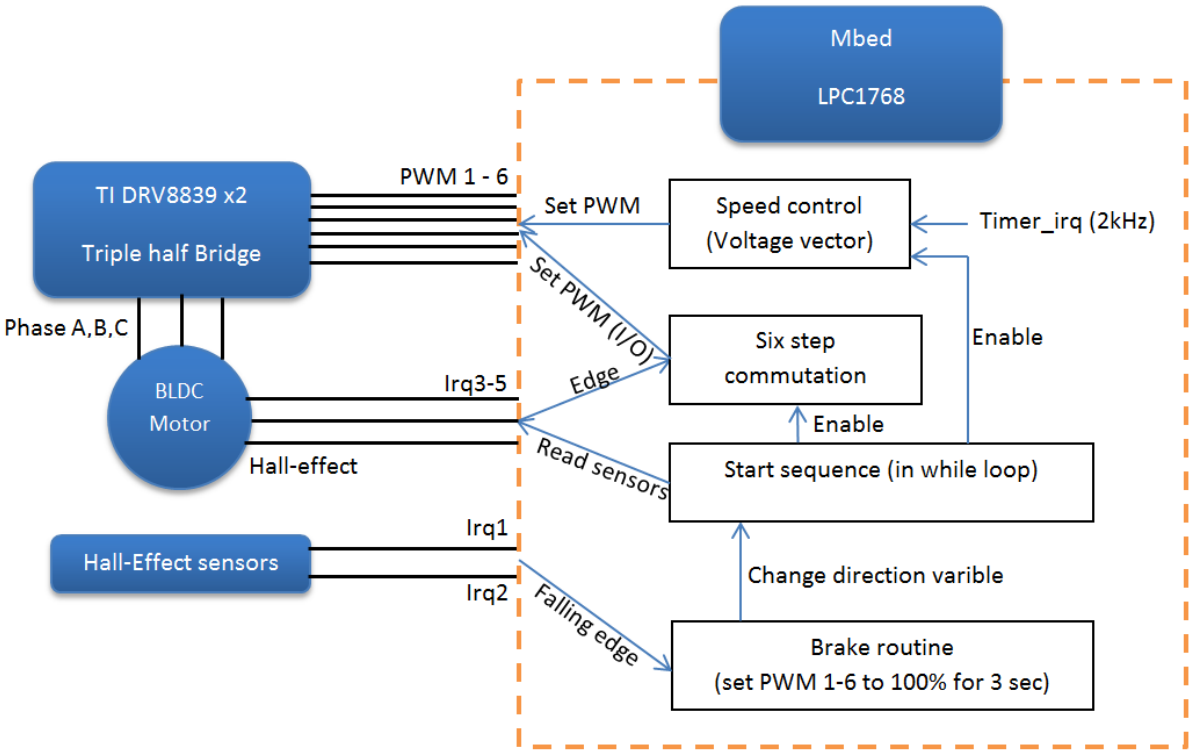

Figure 35 – Code structure of BLDC motor

A complete circuit diagram of how the BLDC motor, half bridges, the Aperio E100 Hall-effect sensors and the mbed processor were connected is shown in Appendix B.

5 Results

This chapter will present all the results from the different measurements and verifications that were undertaken in this thesis. These consist of load measurements, current sensor measurement and calibration, model verification, and finally the energy consumptions of the current Aperio E100 lock, the improved BDC prototype as well as the new BLDC implementation.

5.1 Load Measurement

The results from the force load measurements, using the Phidgets Micro Load Cell, are shown in Figure 36. It shows an increasing force when the leaver is pushed down against the locking pin, with a maximum force of 0,42N.

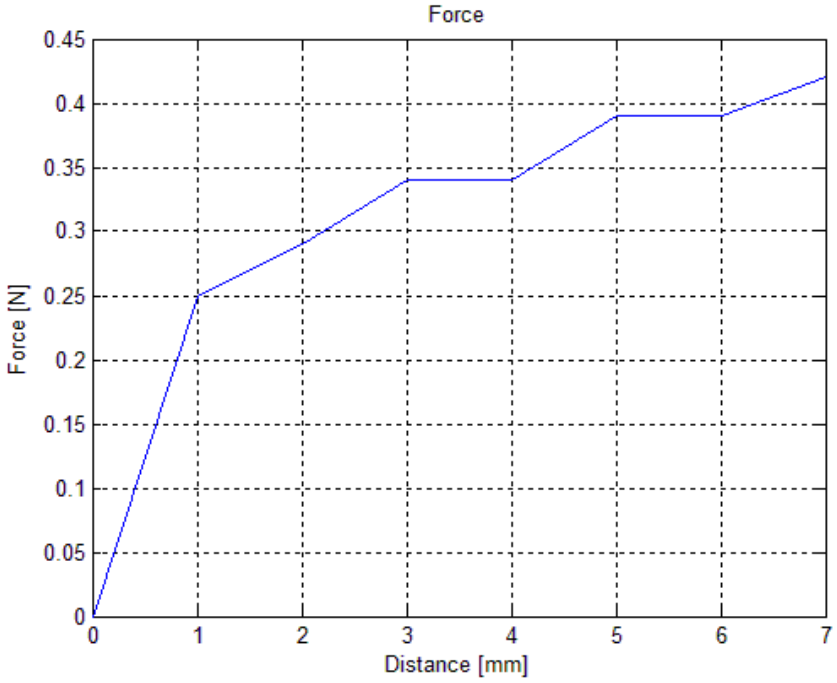

Figure 36 - Force measurements

Figure 37 then shows the calculated load torques for the locking and opening cases of the mechanism, described in section 4.4.1.1, calculated from the force measurements, dependent on the distance moved by the leaver. It gives a maximum torque for the locking sequence of 0,44mNm and 0,28mNm for the opening sequence.

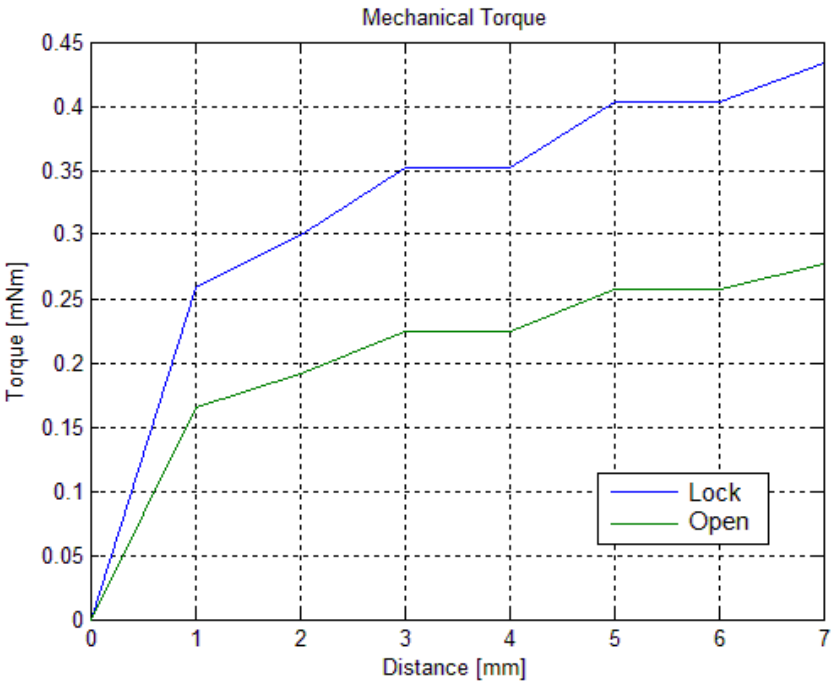

Figure 37 - Motor torque

5.2 Current sensor verification

The result of the current measurement of whole Aperio E100 system using the LT6105, for the locking and opening sequence, are shown in Figure 38.

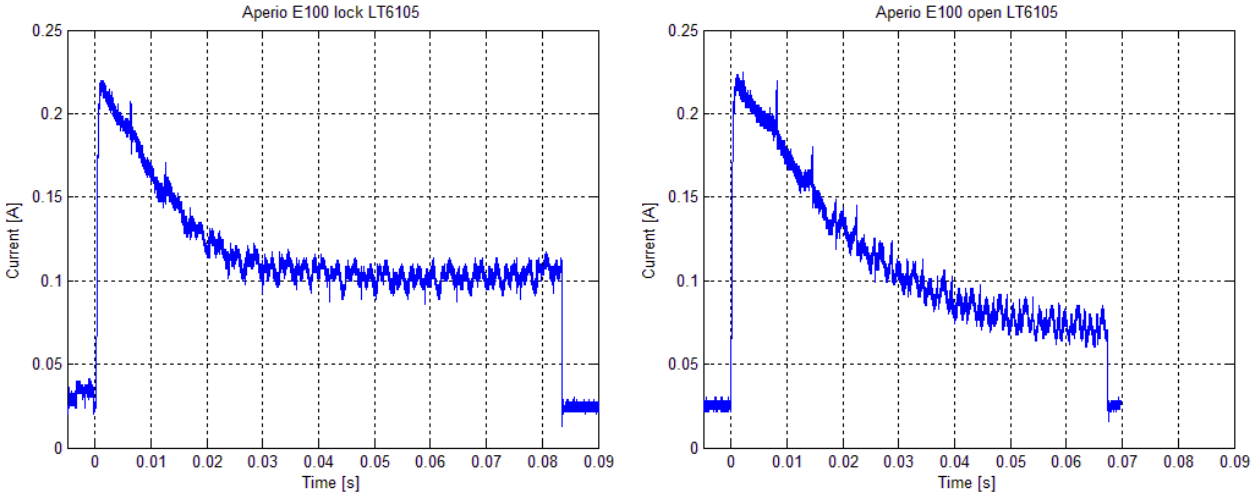

Figure 38 – Current a) Locking sequence b) Opening sequence, of Aperio E100 with LT6105

To verify the accuracy of the current measurements of the LT6105, the same Aperio E100 product was measured using the ASSA ABLOYs LabVIEW setup. The measurement of the LabVIEW test can be seen in Figure 39.

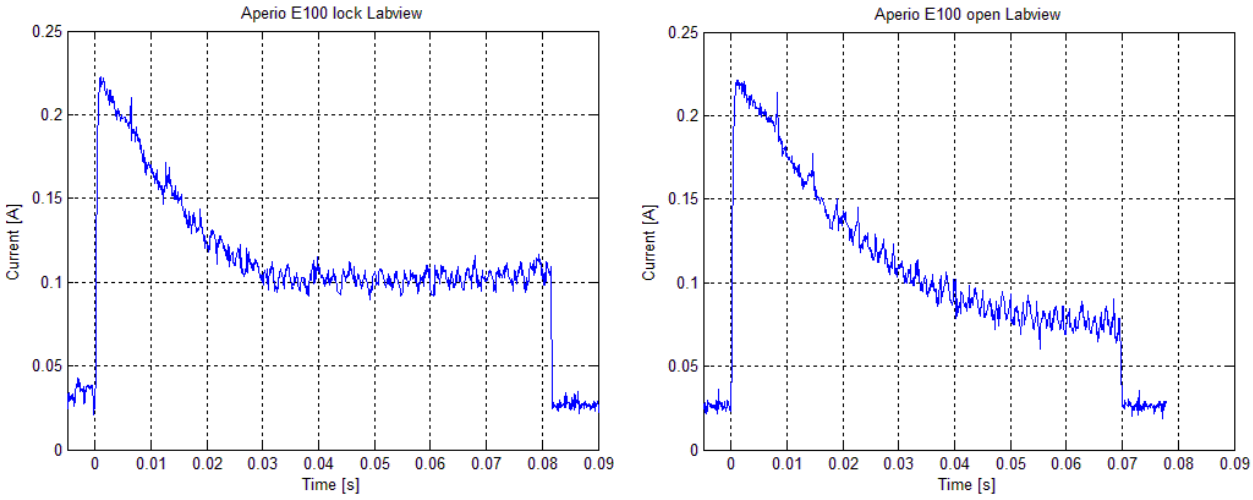

Figure 39 – Current a) Locking sequence b) Opening sequence, of Aperio E100 with LabVIEW

From the figures (Figure 38 and Figure 39) it can be seen that the measurements show a similar result but have a slight time difference, as shown in Figure 40, for the locking phase the LT6105 was about 2ms slower, and for the opening it was about 3ms faster.

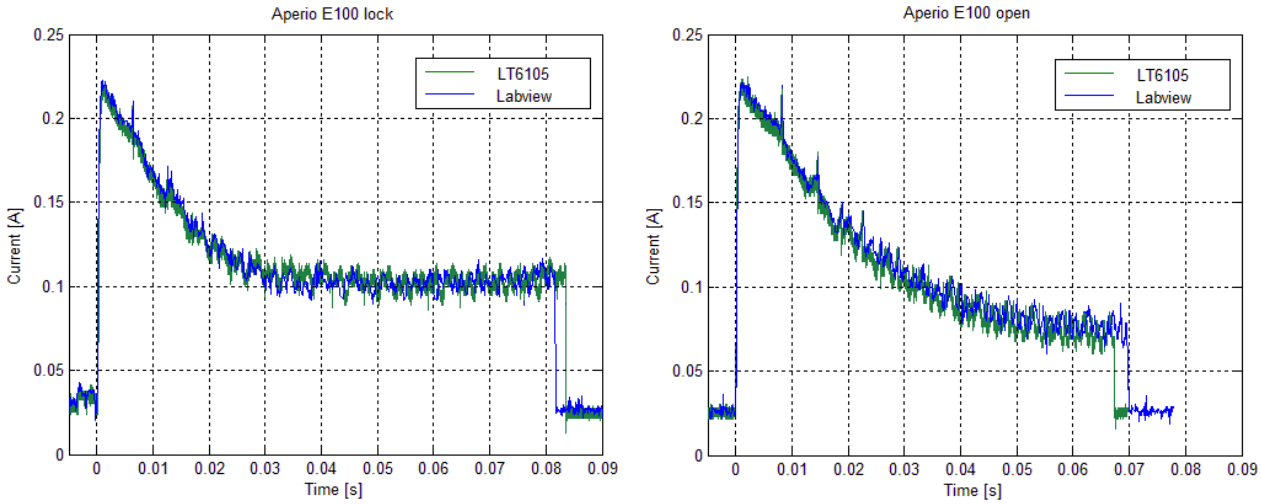

Figure 40 - Current a) Locking b) Opening, of Aperio E100 Comparing LT6105 with LabVIEW

When comparing these measurements with the old measurements done by ASSA ABLOY seen in Figure 41 it clearly shows a large current peak difference of 70mA (for locking) and a completely different locking dynamic.

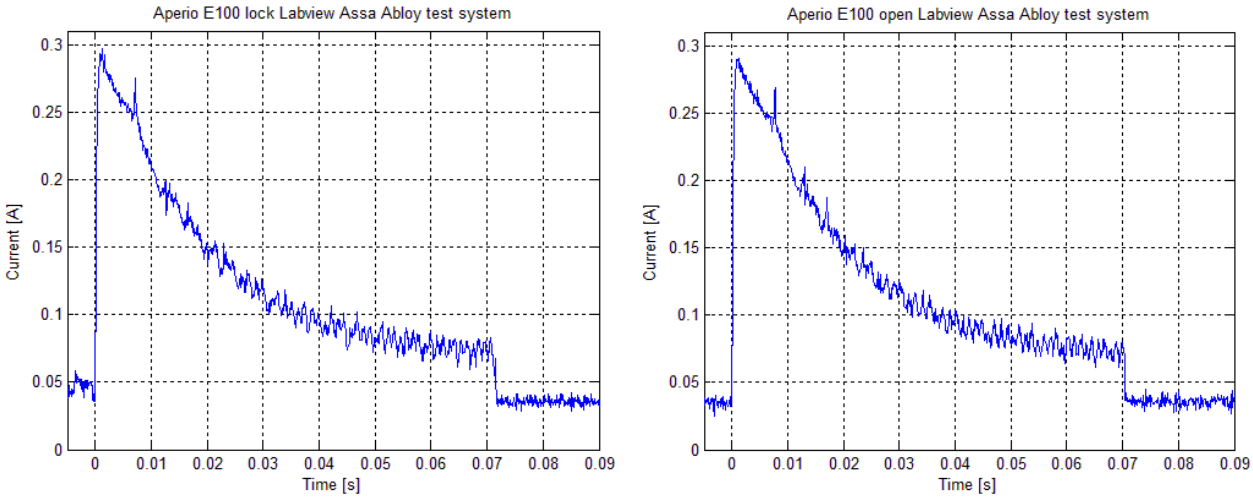

Figure 41 – Current a) Locking sequence b) Opening sequence, of old Aperio E100 with LabVIEW

5.3 Model Verification

As described previously in section 4.5 the validity of the different models needed to be investigated before the trajectory step were implemented. This following section will present the results of this verification of both the BDC and BLDC models, with and without the load, for both speed and current responses.

5.3.1 BDC Model verification

Since there were unknown parameters in the motor model, and the data sheet for the motor in the Aperio E100 system was very limited, a verification of the motor model accuracy against the real motor was necessary. This was done by comparing both the speed and current responses of the motor and the model at the same time, when inputting a 3V step, during a no load case. This was also done with the load, however only the current was measured as there was insufficient space to fit an encoder in the Aperio E100 locking housing.

5.3.1.1 No load speed verification

The speed of the motor in the no load case was measured using an encoder described in section 4.5.2.2. Parameters such as motor inertia, inductance, and both dynamic and coulomb friction constants were matched to the response of the real motor. Figure 42 shows the measured motor speed in blue, and the model speed in black (inside the blue line).

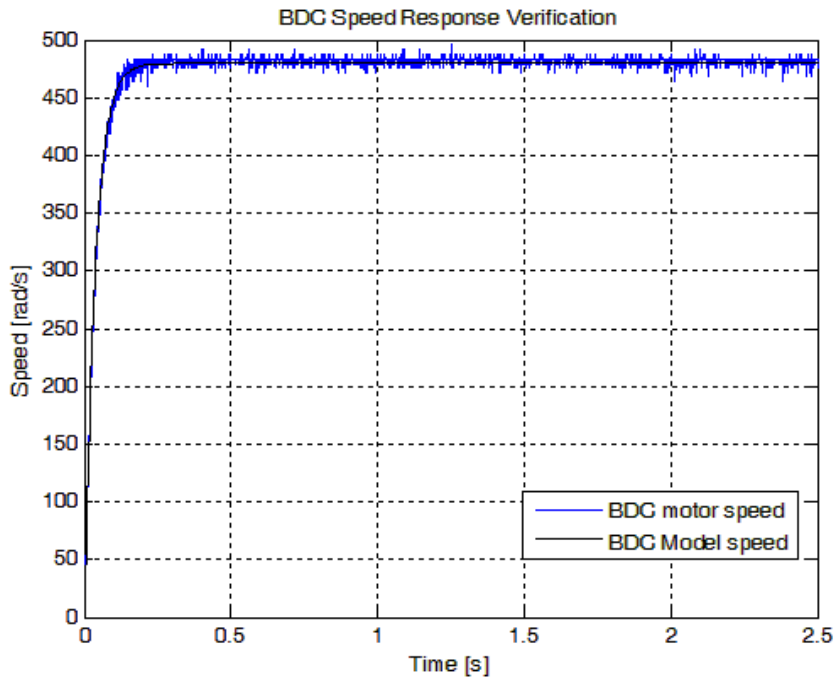

Figure 42 – BDC: motor model speed verification

5.3.1.2 No load current verification

During all the speed verification tests mentioned above the current was also monitored using current measurements mentioned in 4.5.2.1 and verified against the model. Figure 43 shows the no load current response to a 3V input step. Again the measured motor is shown in blue, and the model response in black.

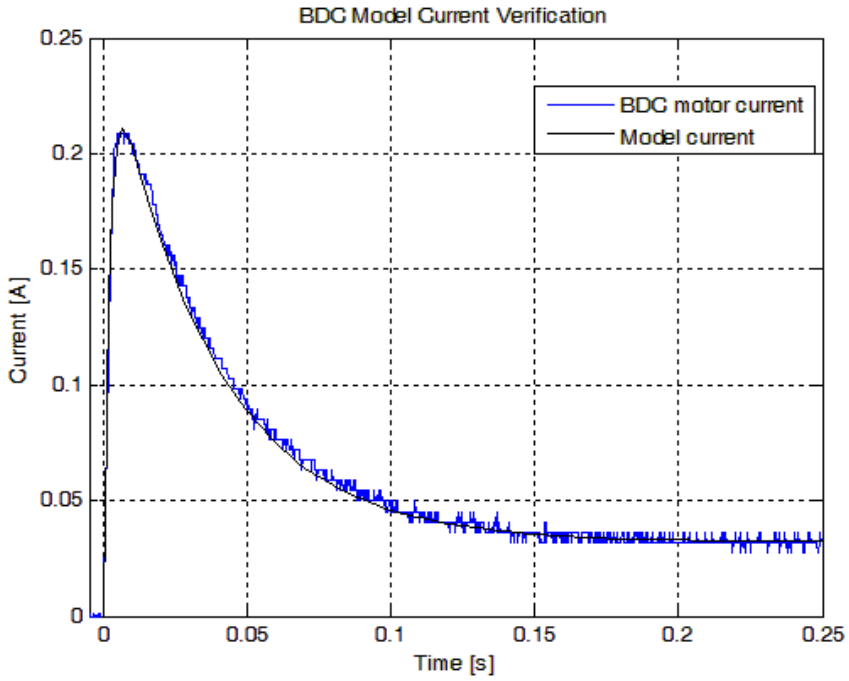

Figure 43 – BDC: motor model current verification

In both the figures above for the current and speed responses, an average curve was plotted for the real measured values as these were noisy, making the actual level hard to distinguish.

5.3.1.3 BDC model with load verification

Once the motor model was verified for the no load case, the mechanical load of the locking mechanism was added to the model and this was also verified. Figure 44 shows the current response of the model against the real system during an opening operation. As shown in the figure the current follows relatively well and the peak up to stall torque at the end can be explained by the lead screw reaching a physical end limit in the system however the voltage not being switched off .

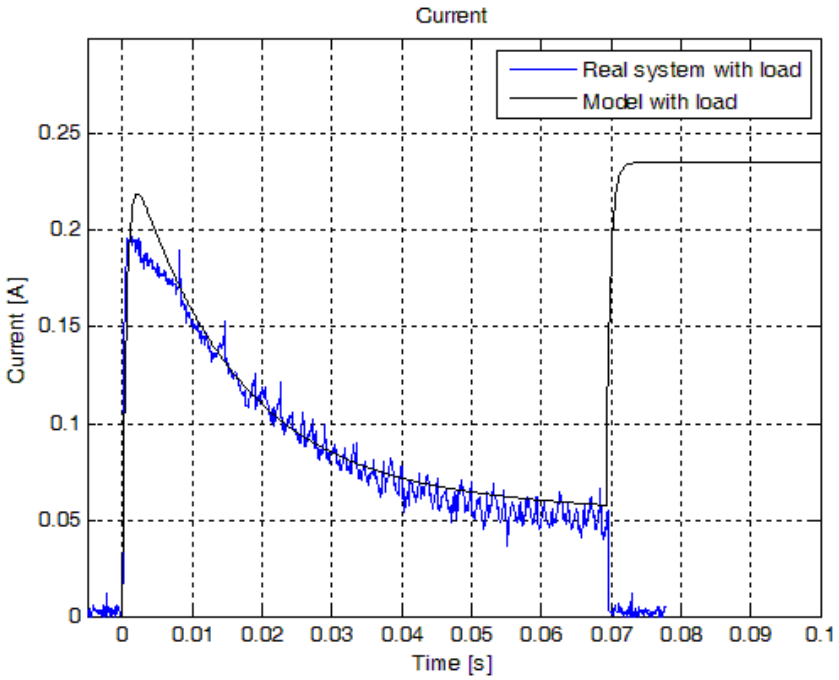

Figure 44 – BDC: Load model verification: Opening

Figure 45, below shows the current response for a locking operation. Again some errors exist between the model and real system, and the stall current at the end is again explained by the lead screw running into its end position.

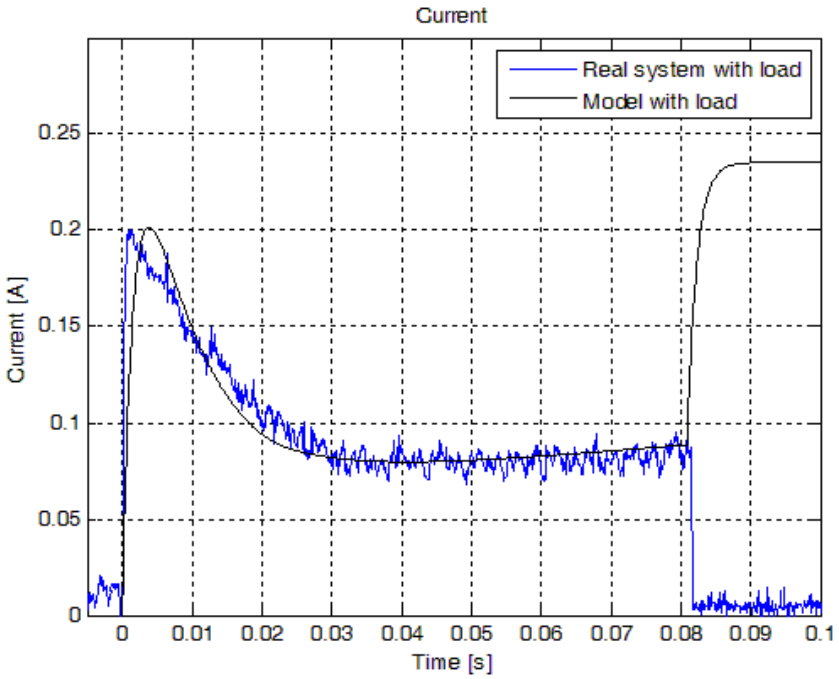

Figure 45 – BDC: Load model verification: Locking

5.3.2 BLDC Model verification

The verification of the BLDC motor model was carried out in the same way as the BDC model described above.

5.3.2.1 BLDC No load verification

Similarly to the model verification for the BDC motor, the BLDC Maxon motor was also verified against its model. Figure 46 shows the speed response of the BLDC motor in blue and the model in black. This speed curve was also an averaged due to noise induced in the encoder.

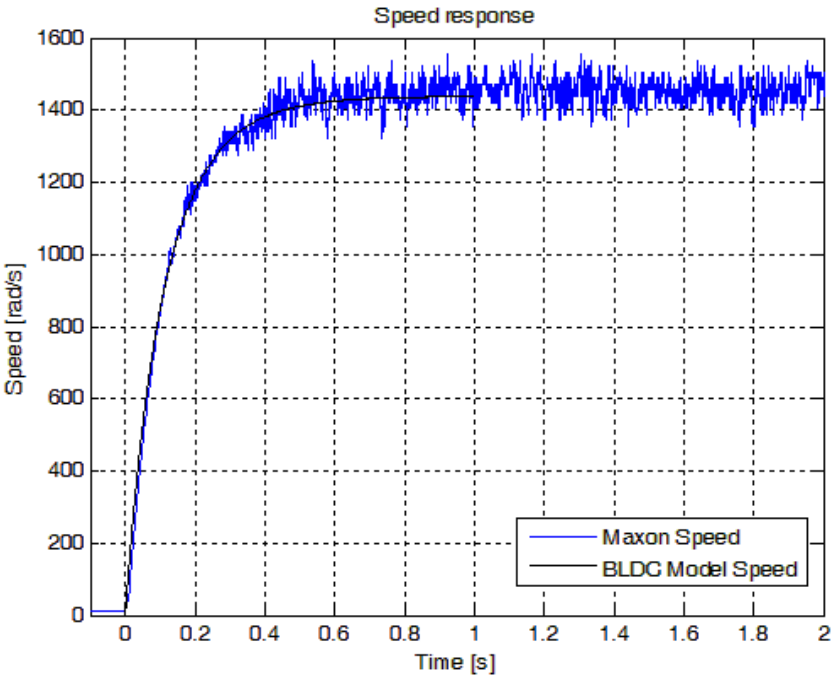

Figure 46 – BLDC: model speed verification

During the speed verification the current was also measured and is plotted below in Figure 47. Both these curves were averaged to facilitate a comparison of the performances.

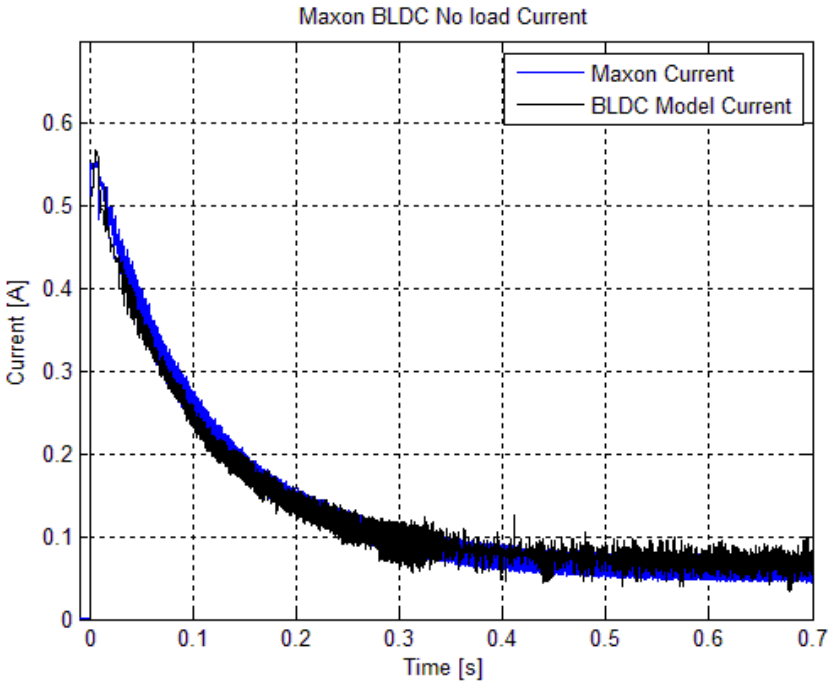

Figure 47 – BLDC: model current verification

5.3.2.2 BLDC model with load verification

To verify the complete BLDC system model, the load was added. The model current profile was compared to the real systems as in Figure 48, where the comparison, between the motor in blue and the model in black, is shown for the opening sequence and in Figure 49 for the locking sequences.

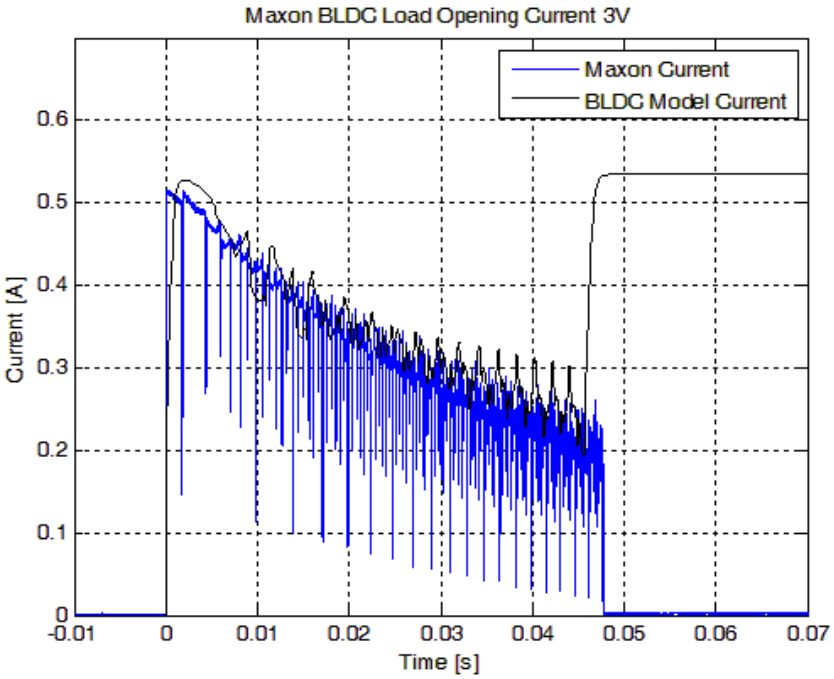

Figure 48 – BLDC: Load model verification: Opening

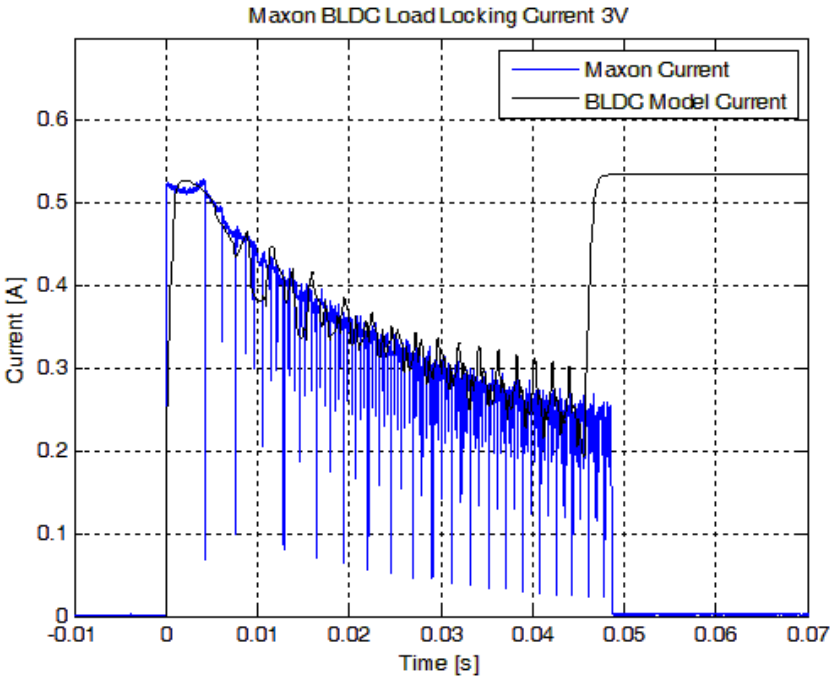

Figure 49 – BLDC: Load model verification: Locking

5.4 Energy result

In this section the results of the total energy consumption for the different input trajectories and running cycles is presented. First the energy consumption of the current Aperio E100 system is presented, followed by the BDC results, and finally the BLDC prototype results.

Some current measurements in this section also contains a green plot which is a mean value of the current, this is used to show a more representative look of the current however when calculating the total energy no mean value was used.

5.4.1 BDC

Figure 50 shows the result of the Aperio E100 locking sequence, showing a) the 3V constant input voltage and b) the measured current.

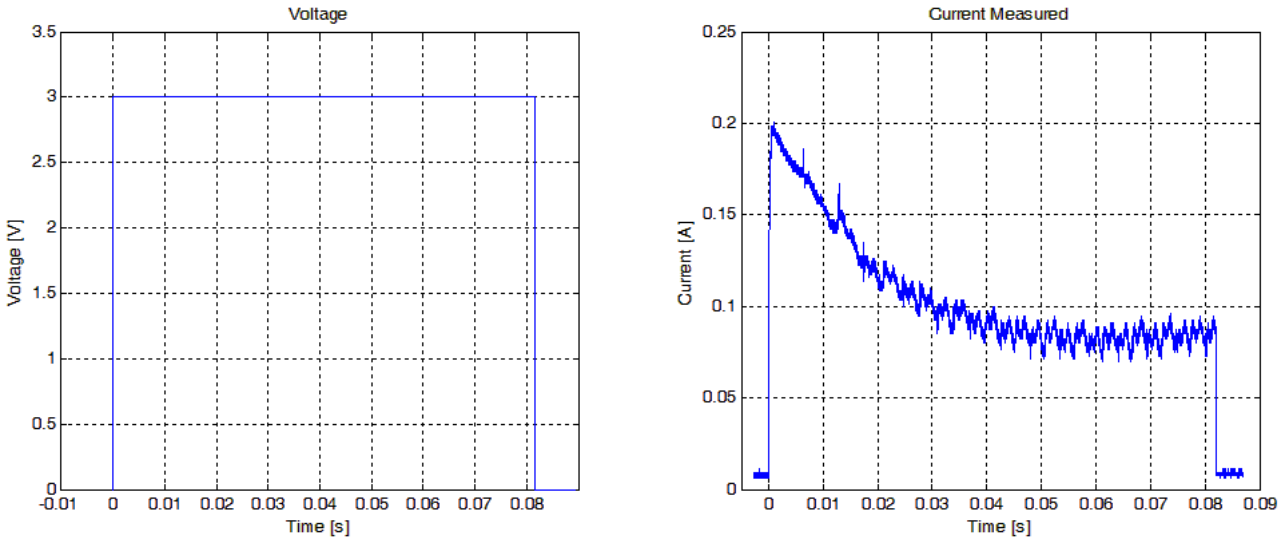

Figure 50 - Aperio E100: Locking a) Constant 3V input b) Current output

The calculated total energy for the E100 is shown in Figure 51, where the total energy consumed during a locking sequence was 25,8mJ.

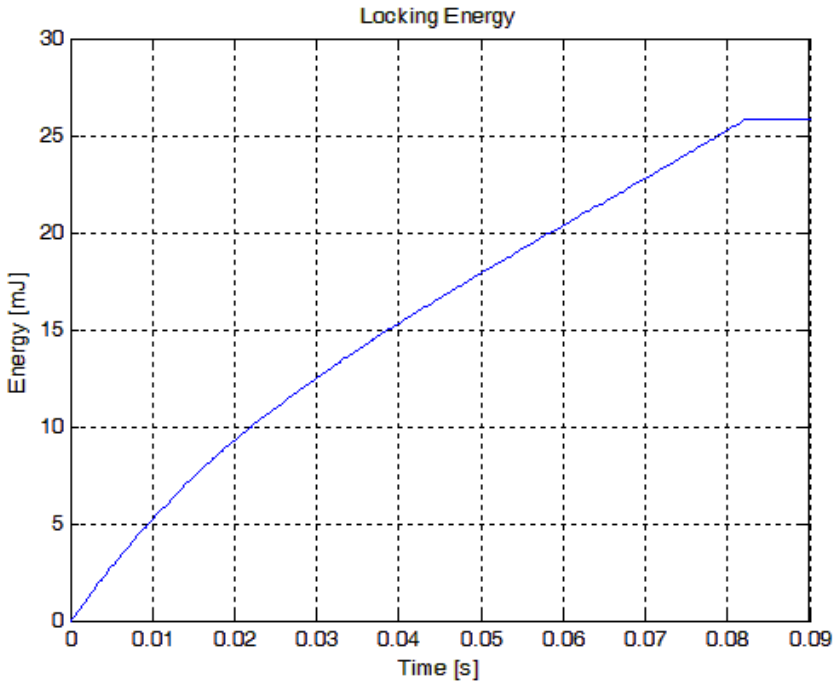

Figure 51 – Aperio E100: Energy: Locking

Figure 52 shows the results of an opening sequence of the Aperio E100 with a) 3V input voltage, and b) the measured current.

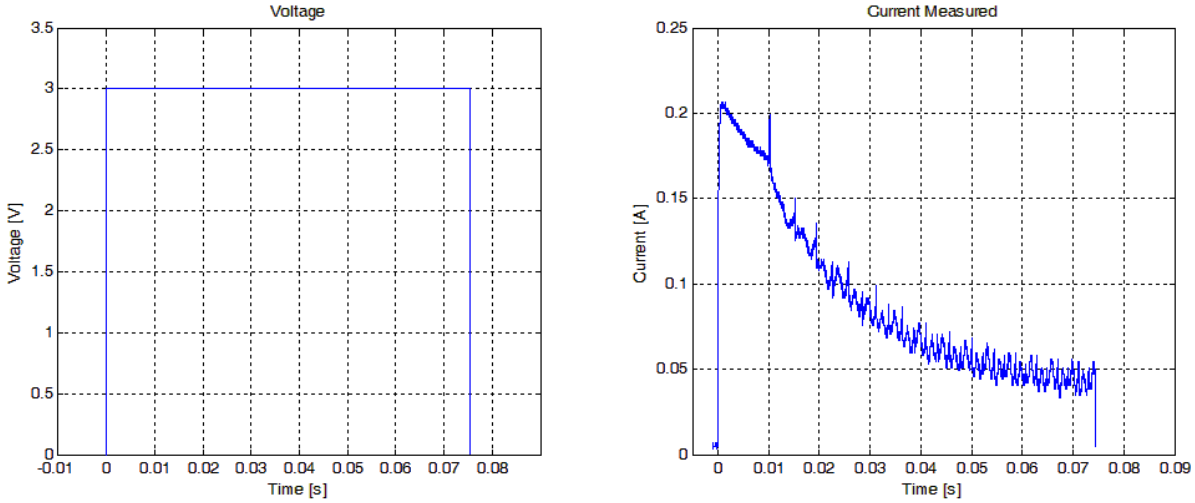

Figure 52 - Aperio E100: Opening a) Constant 3V input b) Current output

The calculated energy of the opening sequence is shown in Figure 53 and gave a total consumption of 20mJ.

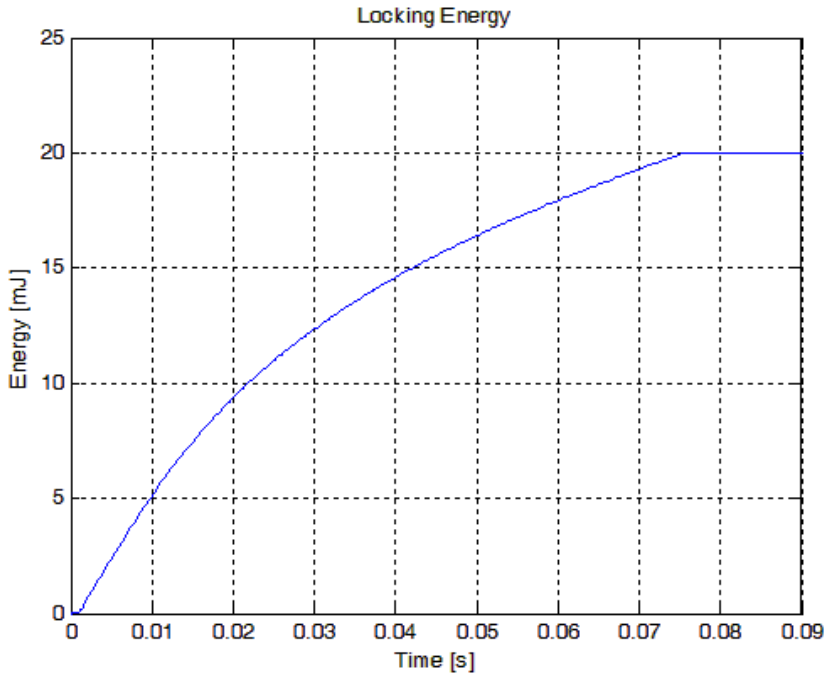

Figure 53 – Aperio E100: Energy: Opening

5.4.2 BDC Trajectories

This section describes the three different trajectories that were implemented on the BDC system. These were constant voltage, speed- and voltage trajectory.

5.4.2.1 Constant voltage

The first trajectory method implemented on the BDC system was to measure the energy during constant voltage level inputs. This was done using a PWM signal with a constant duty cycle for both the locking and unlocking sequences. The results are showed in Table 5.

Table 5 – Energy of constant PWM duty cycle: BDC

Duty cycle	Lock (energy)	Open (energy)
70	26,3mJ	-
80	21.5mJ	14.9mJ
90	21.6mJ	16.7mJ
100	25.8mJ	20.0mJ

For duty cycles under 70% the motor did not manage to travel the complete distance between the two states, locked or unlocked in neither direction, and for the duty cycle 70% the opening sequence didn't start either. The corresponding running times for the different duty cycles in Table 5 are shown in Table 6.

Table 6 – Running time of constant PWM duty cycle: BDC

Duty cycle	Lock (time)	Open (time)
70	210ms	-
80	119ms	90ms
90	91ms	73ms
100	82ms	72ms

The results from Table 5 and Table 6, the trade-off between the duty cycle, energy consumption and time for the BDC motor are shown Figure 54. The locking and opening times can be seen to decrease with an increased duty cycle. The energy consumption for the opening phase increased with increased duty cycles, whilst a local minimum for the locking phase could be seen at a duty cycle of 80%.

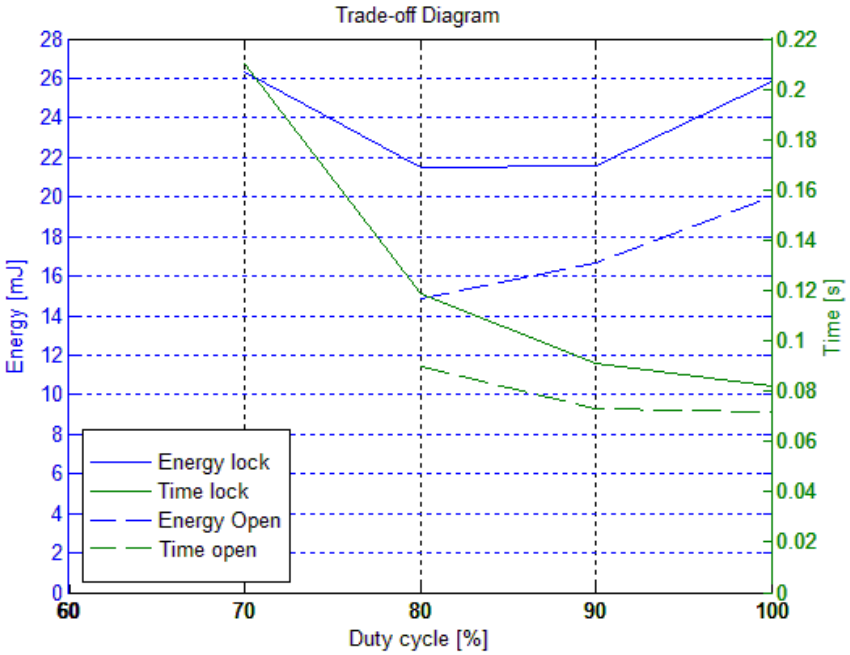

Figure 54 – BDC: Duty, energy and time trade-off

5.4.2.2 Speed trajectory

The voltage step result from the speed trajectory simulation, for the locking sequence of the BDC motor, is shown in Figure 55a. When this step was implemented into the mbed software, a current over time profile (shown in Figure 55 b) gave a peak current of 200mA and a runtime of about 0.1s.

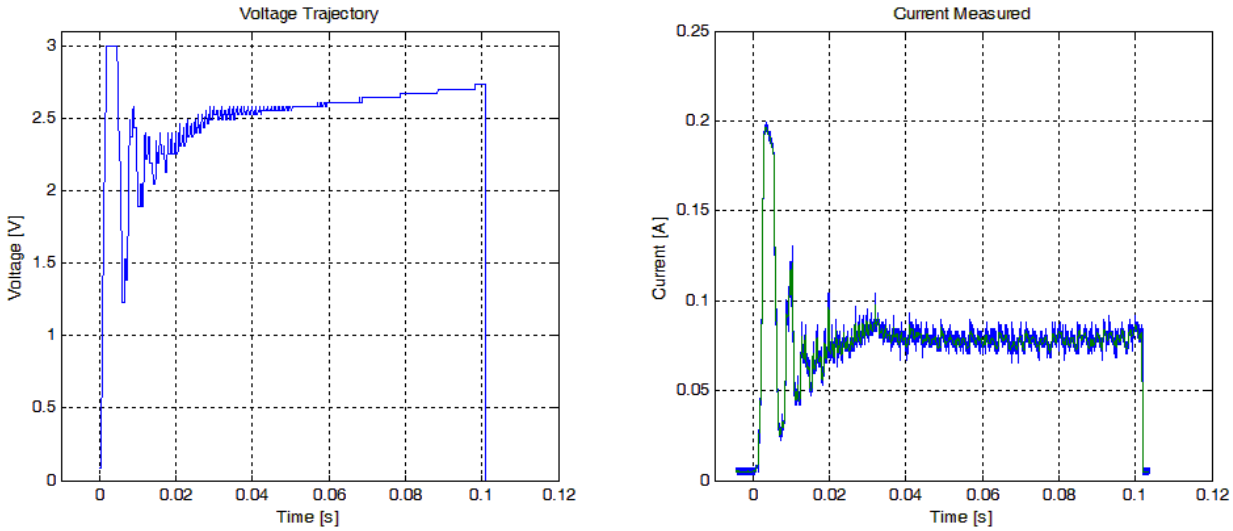

Figure 55 – BDC: Speed trajectory profile: Locking a) Voltage input b) Current output

Figure 56 shows the calculated energy of this locking sequence. The energy consumed for this step was 20.4mJ.

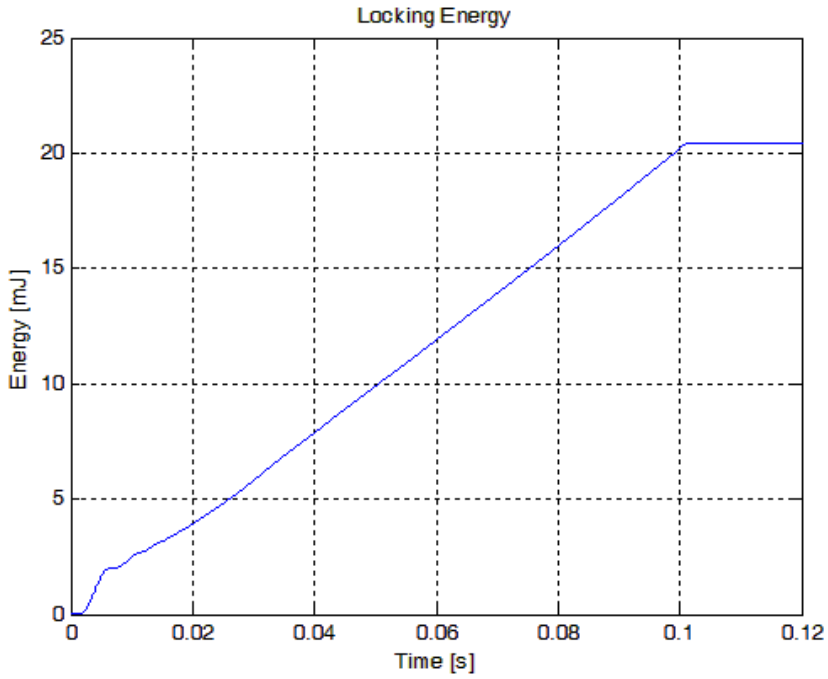

Figure 56 –BDC: Energy of trajectory: Locking

This result compared to E100, seen in Figure 51, shows a decrease of energy consumption, according to equation (43) by;

$$1 - \frac{20,4}{25,8} \approx 21\%. \qquad (43)$$

Figure 57a) shows the voltage step that was generated from the speed trajectory simulations for the opening sequence and b) the current output. When this voltage step was implemented in the software the current profile, shown in Figure 57, gave a peak current of 200mA and a running time of 120ms.

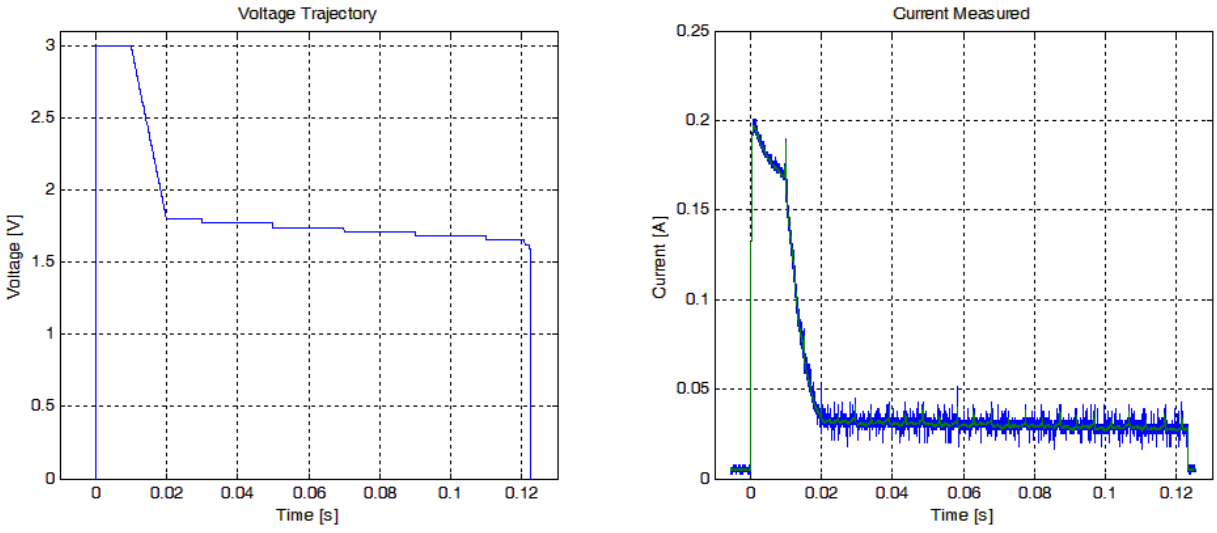

Figure 57 –BDC: Speed trajectory profile: Opening a) Voltage input b) Current output

The calculated energy, shown in Figure 58, gave a consumption of 12,6mJ.

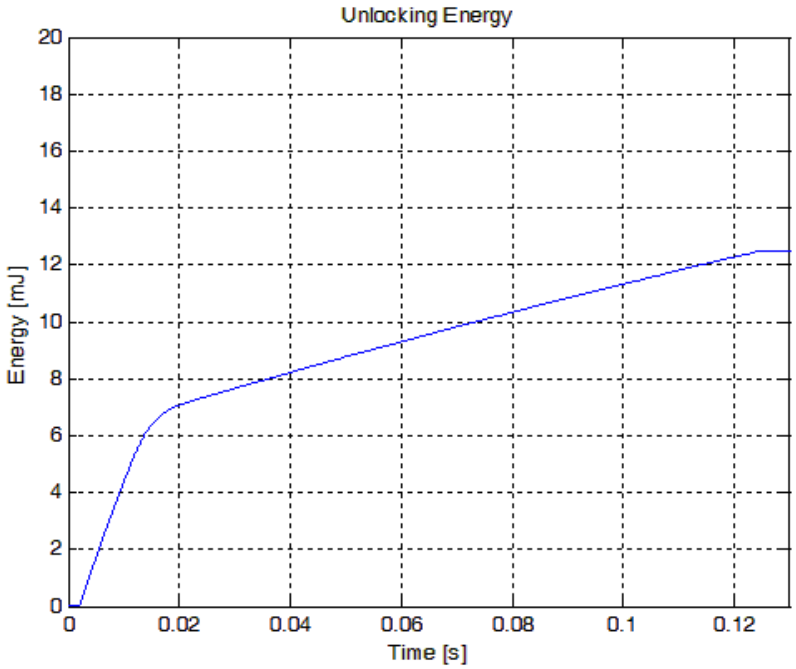

Figure 58 – BDC: Energy of trajectory: Opening

This compared to the Aperio E100 system produced, as seen in Figure 52, a total consumption reduction according to equation (44) of;

$$1 - \frac{12,6}{20,0} \approx 37\%. \qquad (44)$$

5.4.2.3 Voltage trajectory

After the speed trajectory a voltage trajectory was implemented. Figure 59 a) shows the voltage step that was generated by the trajectory simulation for an opening sequence. This voltage step was implemented in the software and the current profile, shown in Figure 57, gave a peak current of 165mA and a running time of 95ms.

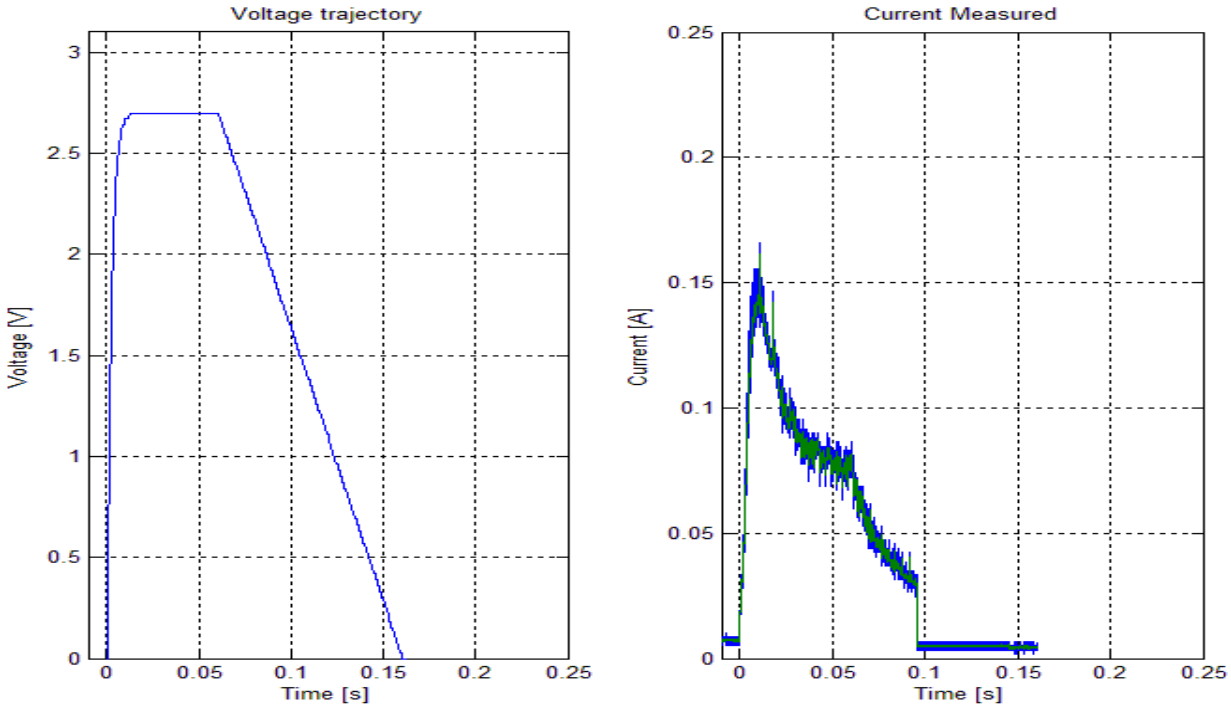

Figure 59- BDC: Voltage trajectory profile: Locking a) Voltage input b) Current output

The calculated energy is shown in Figure 60, presenting a consumption of 18,9mJ.

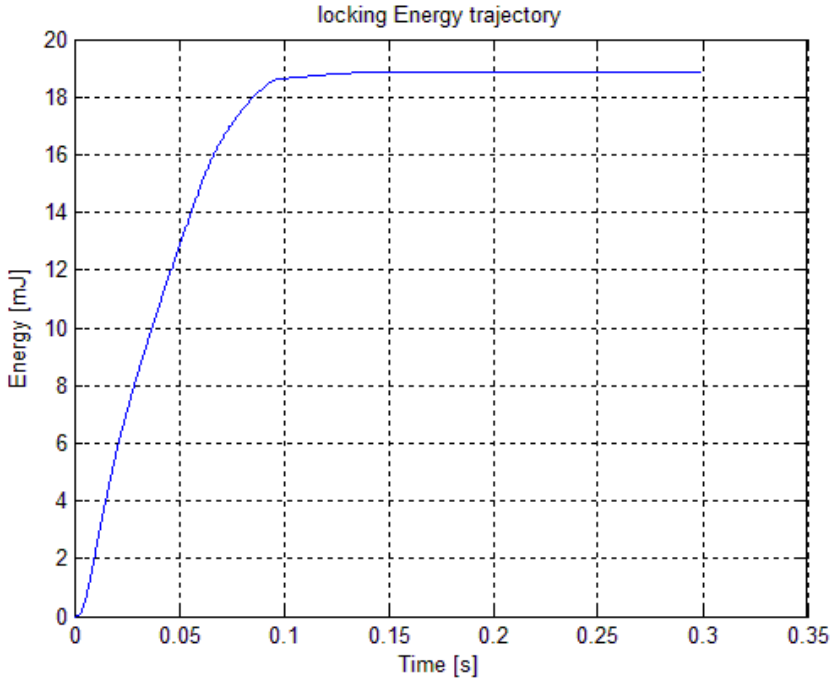

Figure 60 – BDC: Energy of voltage trajectory: Locking

This compared to the Aperio E100 system gave, the total consumption reduction according to equation (45) of:

$$1 - \frac{18,9}{25,8} \approx 27\%. \quad (45)$$

Figure 61 shows a) voltage trajectory input step that was generated from the voltage trajectory simulations for the opening sequence and b) current response. This voltage step was then implemented in the software. The current profile, shown in Figure 61 presented a peak current of 125mA and a running time of 91ms.

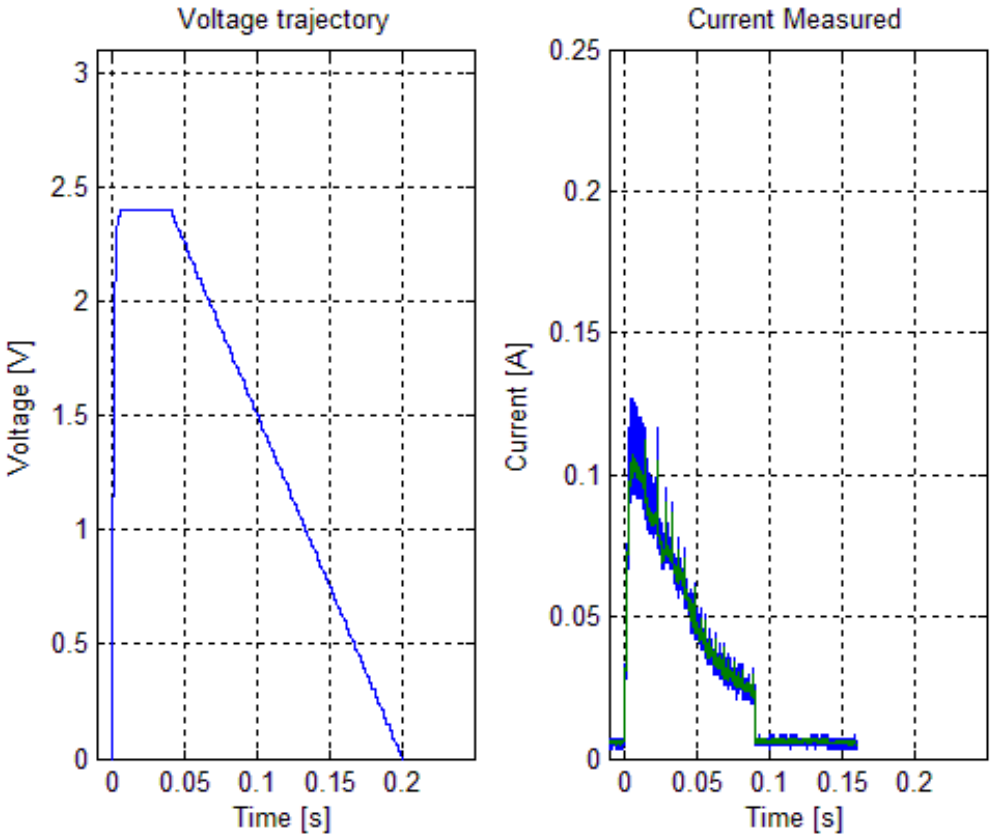

Figure 61 – BDC: Voltage trajectory profile: Opening a) Voltage input b) Current output

Shown below in Figure 62 is the calculated energy from the trajectory input step for the unlocking of 11.9mJ.

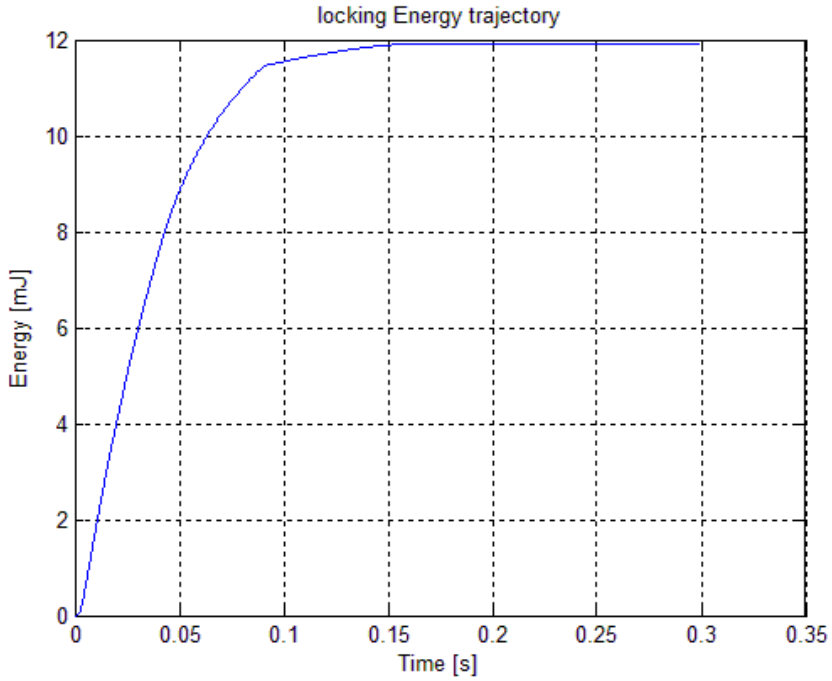

Figure 62 – BDC: Energy of voltage trajectory: Opening

When comparing this consumption to the Aperio E100 system, a total consumption reduction was given according to equation (46) of;

$$1 - \frac{11,9}{20.0} \approx 41\%. \tag{46}$$

The overall energy consumption reduction of the locking and opening sequence of the BDC system using the voltage trajectory is then according to equation (47).

$$1 - \frac{18.9+11,9}{25.8+20,0} \approx 33\%. \tag{47}$$

5.4.3 BLDC Trajectories

For the BLDC system only the constant PWM and voltage trajectories were implemented, the results are presented below. Speed trajectories were omitted since unusable voltage vectors were generated by the simulation model.

5.4.3.1 Constant voltage

Similarly to the BDC motor, the BLDC motor was also tested at constant voltage input steps, and the times and energies recorded. The results of these tests are shown in Table 7 and Table 8.

Table 7 – Energy of constant PWM duty cycle: BLDC

Duty cycle	Lock (energy)	Open (energy)
17	-	0,81mJ
30	5,5mJ	2,5mJ
45	8.3mJ	6.0mJ
60	15.2mJ	12,5mJ
75	25.0mJ	22.0mJ

The tables show that below 17% duty cycle for the opening sequence, and 30% for locking sequence, the motor could not produce enough torque to travel to the next state. Over 75% duty cycle and the motor ran too fast, making the braking sequence too slow and the motor leaver running past the Hall-effect sensors. This behavior was damaging to the mechanism and a voltage limit was therefore set at 75% duty cycle for constant voltages. Table 8 shows the corresponding running times for the results in Table 7.

Table 8 – Running time of constant PWM duty cycle: BLDC

Duty cycle	Lock (time)	Open (time)
17	-	138ms
30	153ms	82ms
45	89ms	67ms
60	72ms	60ms
75	61mJ	55ms

Summarizing the results from Table 7 and Table 8, a trade-off diagram between duty cycle, energy consumption and time was developed as shown in Figure 63. Both the locking and opening sequences show that a lower duty cycle reduces the energy consumption whilst increasing the time.

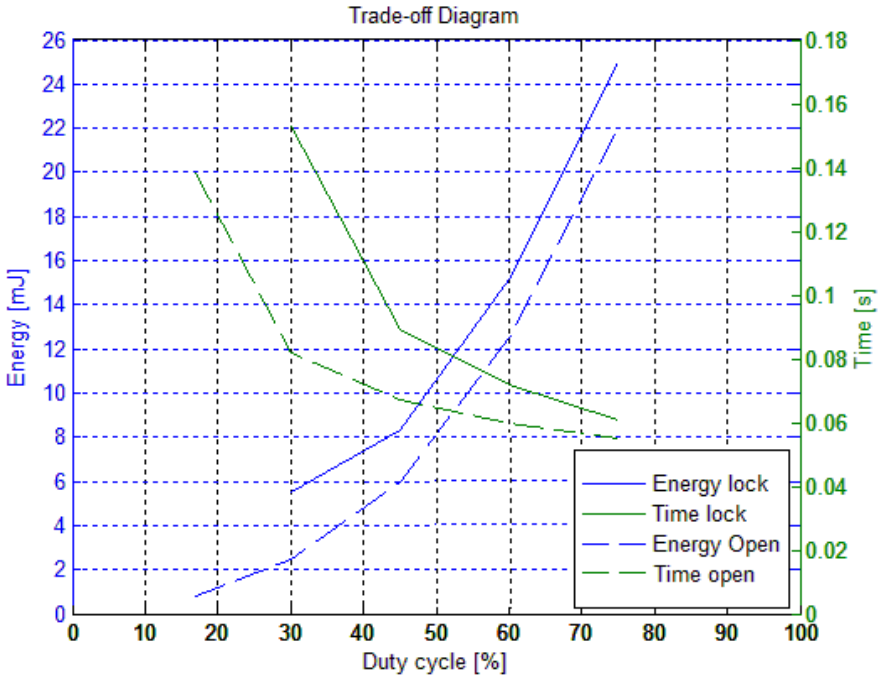

Figure 63 - BLDC: Duty, energy and time trade-off

5.4.3.2 Voltage trajectories

After the reference values of what the constant energy consumptions where for the BLDC motor, voltage trajectories were implemented from the simulation. An optimized voltage trajectory is shown in Figure 64 where a) input voltage and b) current output, for the locking sequence, is show.

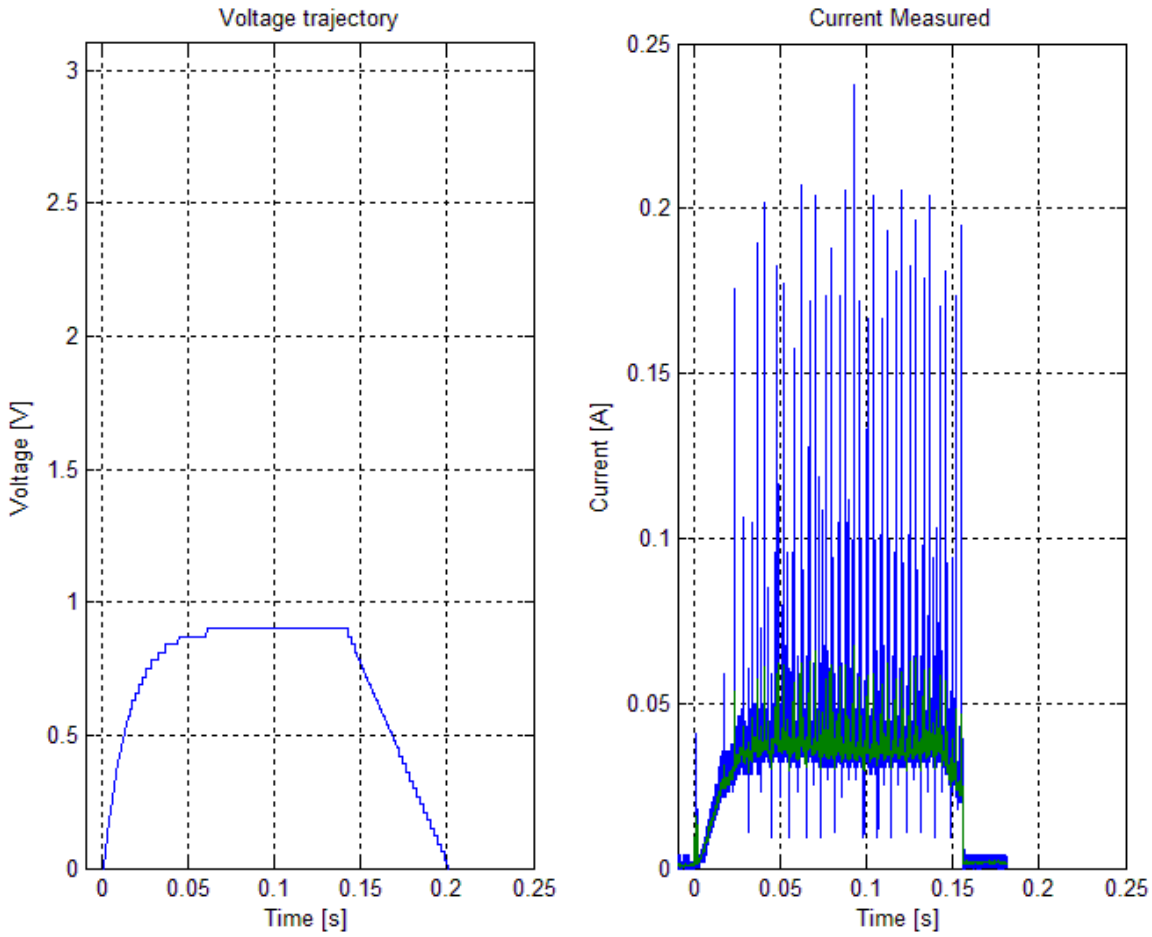

Figure 64 – BLDC: Voltage trajectory profile: Locking a) Voltage input b) Current output

This gave fast current peaks around 200mA and a running time of 153ms. Calculating the energy from the results in Figure 64 gave a consumption of 4,43mJ as seen in Figure 65.

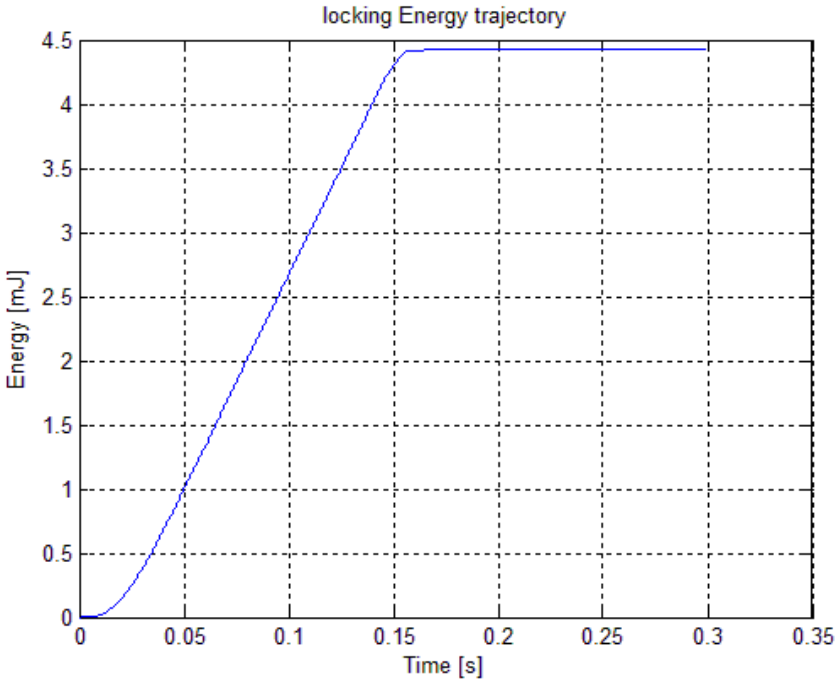

Figure 65 – BLDC: Energy of Voltage trajectory: Locking

When comparing this result with the Aperio E100 an energy consumption reduction of 83% as seen in equation (48) was achieved.

$$1 - \frac{4{,}43}{25{,}8} \approx 83\%. \qquad (48)$$

The same method was used to produce an input voltage step for the opening sequence. Figure 66 shows the a) input voltage and b) output current for this sequence.

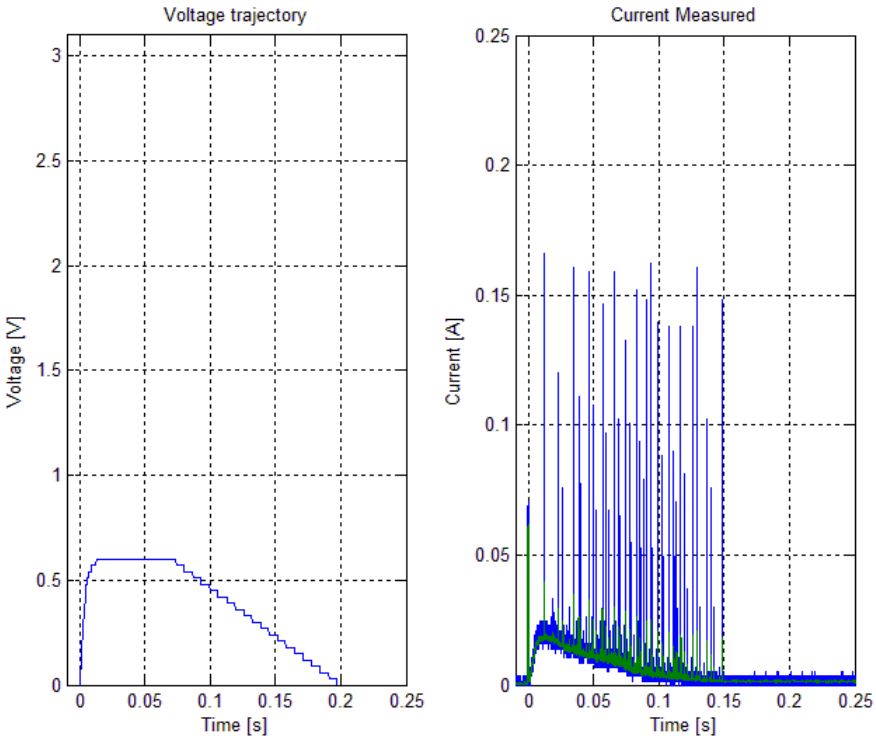

Figure 66 – BLDC: Voltage trajectory profile: Opening a) Voltage input b) Current output

This gave fast current peaks of around 160mA and a running time of 150ms. Calculating the Energy from the results in Figure 66 gave a consumption of 0.69mJ as seen in Figure 67.

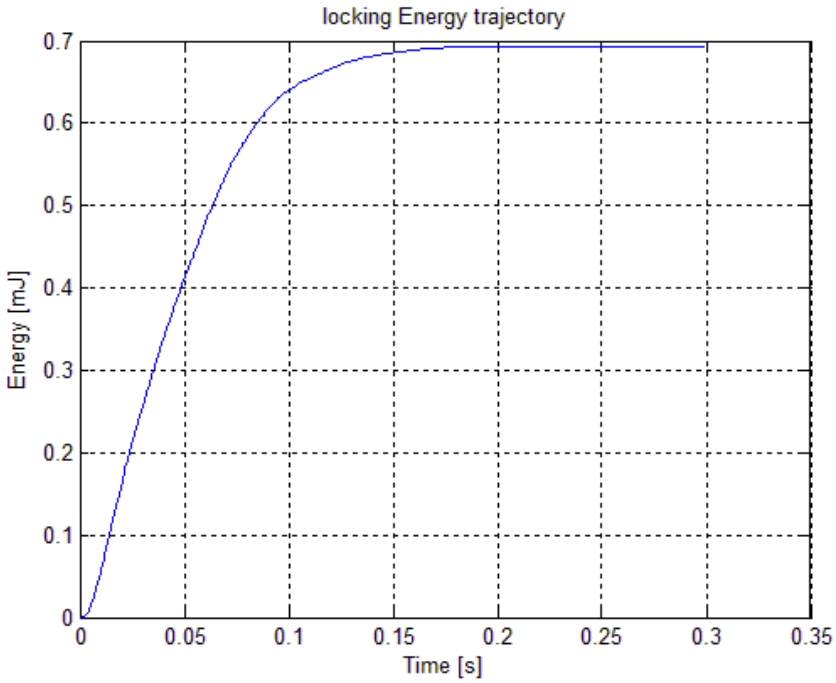

Figure 67 – BLDC: Energy of Voltage trajectory: Opening

The reduction of the voltage trajectory opening sequence compared to Aperio E100 gives an energy reduction of 97% as seen in equation (49).

$$1 - \frac{0{,}69}{20{,}0} \approx 97\%. \tag{49}$$

The overall energy consumption reduction of the locking and opening sequences is according to equation (50).

$$1 - \frac{4.43+0{,}69}{25.8+20{,}0} \approx 89\%. \tag{50}$$

Shown in Figure 68 and Figure 69 are the final results of the current and voltage responses of the Aperio E100 system and the BLDC voltage trajectory optimized system. Both figures show significantly reduced currents and voltages.

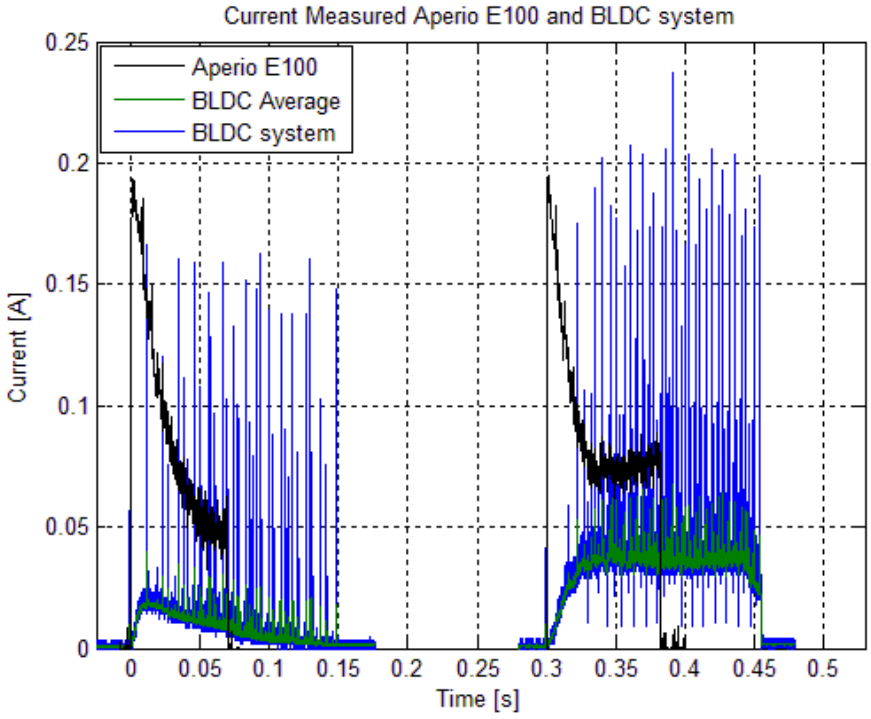

Figure 68 – Current: Opening and Locking Aperio E100 and BLDC

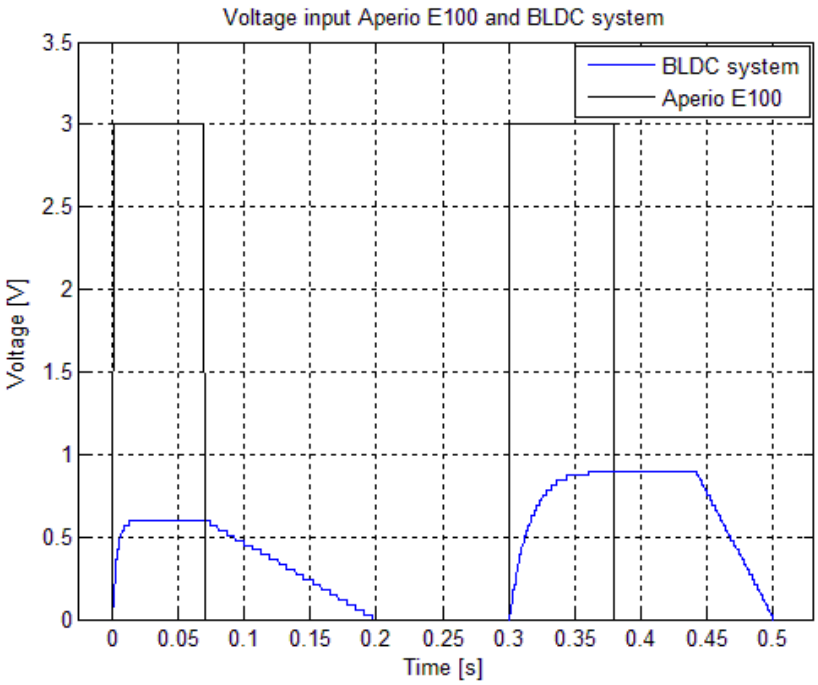

Figure 69 - Voltage: Opening and Locking Aperio E100 and BLDC

5.4.4 Extension of battery life

With the help from the ASSA ABLOY team the total extension of the battery lifetime could be calculated from the motor consumptions presented previously. These are shown below in Figure 70, where the battery life is presented in months on the x-axis, and the motor energy consumption is shown as a percentage of the entire system on the y-axis. The current Aperio E100 system has a battery life of 40 months, where 34% of the total consumption is accounted for by the motor. The improved BDC system had a lifetime of 48 months, with a motor consumption of 21% of the total. Finally the BLDC system had a lifetime of 57.6 months with the motor consumption accounting for just 6% of the total energy consumption. These calculations were carried out assuming 55 opening and locking sequences were executed per day. This method of measuring the battery life is a well-tested tool used by ASSA ABLOY and experts at the company vouched for their accuracy. These tests were therefore not further investigated.

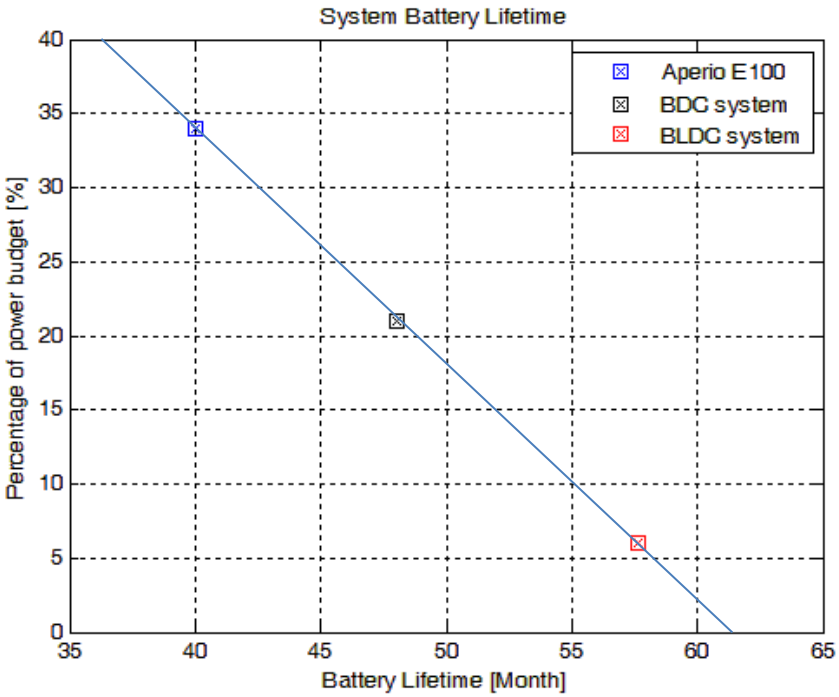

Figure 70 - Battery Life

6 Conclusion

This thesis has shown that it is possible to drive a low voltage motor more efficiently using firstly more intelligent control. In the case of the Aperio E100 BDC system an energy consumption reduction of totally 33% was achieved by implementing energy optimized voltage trajectory input steps for both the locking and unlocking of the system, instead of a constant 3V supply. The thesis also showed that improving the hardware, using a BLDC motor, together with the voltage trajectory control method, a total reduction in the energy consumption of 89% could be achieved. In total this could lead to an extension of the battery life for the Aperio E100 system with 17,6 months to a total of 57,6 months. The hypothesis of a reduction in the motor and driver consumption with 50% was surpassed by using voltage trajectory control on the BLDC motor.

7 Discussion and Future work

This chapter will present a discussion of the results, as well as a recommendation of future work.

7.1 Discussion

The discussion of the results is broken down into hardware and software choices, measurements and verification, trajectory generation method, energy results and finally reliability.

7.1.1 Hardware and software choices

The hardware and software choices were a major part of this thesis and some advantages and drawbacks of the choices are discussed below.

7.1.1.1 Motor selection/design

When selecting a BLDC motor for this thesis, there were not many options available on the market that fulfilled the requirements for this project. It was hard to find motors with a low input voltage that could supply the required torque and at the same time have integrated Hall-effect sensors. This forced the choice to the *EC 9.2 flat Ø10 mm, brushless, 0.5 Watt with hall sensors.*

Since it was hard to find motors that fulfilled all the requirements for this thesis, the NEMA standard of efficient motors was overlooked. The Maxon motor did not have a data sheet showing the optimal torque/efficiency curves discussed in 4.4.1.2, therefore this check could also not be done. The motor was therefore considered over dimensioned for the task, being able to produce a stall torque of 1.22mNm whilst the calculated maximum torque was 0.43mNm.

The price of the motor was also a bit high, when comparing with for example piezo motors (which were considered too expensive in section 2.2.4). The discussion that was held with the supervisors at ASSA ABLOY was that BLDC motors have a lot more suppliers and therefore it may be easier to get an advantageous large scale production price in the future.

Another downside of the BLDC motor was that the Hall-effect sensors at least need 4V supply (5V in this project). This is higher than supply volt max at 3V. The reason of using this motor anyway was that it in all other aspect was the best choice and the higher supply voltage of the sensors will not have any effect of the energy results.

7.1.1.2 Mechanical setup

For the mechanical setup of the BLDC motor it was necessary to add a shaft adapted to extend the axle and increase its diameter to fit the lead screw gear. This gave the shaft some play that decreased the reliability and introduced inconsistencies, which surely decreased the overall efficiency of the system. The BLDC motor was also not properly fastened to the Aperio mechanism which also led to some minor play to the system. This was due to time constraints.

Another factor that could have influenced the results was the fact that the prototype build had a lot of loose and long wiring, mounted on different experiment cards and breadboards. This of course made the system vulnerable to electromagnetic interference, EMI and adds extra impedance.

In this thesis the electrical component sizing was selected to facilitate the soldering. Although most of the components, such as the motor driver and connectors (not mounted on evaluation board) were in fact small enough, and if designing an optimized IC the electrical system would fit inside the lock housing.

7.1.1.3 Mbed

The mbed platform was excellent for rapid prototyping and was very sufficient for the thesis. Although all the predefined functions that existed in the mbed library did not fit all the thesis needs. For example, the predefined PWM function has a constant period, always finishing a period before switching the duty cycle, causing delays. This wasn't a very large problem though since it was possible to define new PWM signals by altering the processors registers.

The mbed processor used in this thesis was oversized, too powerful for this project, and in a production view too expensive. The measured maximum current consumption of the mbed processor was 135mA, with all peripherals switched on, and 100mA with only the timers and PWMs needed for the project. Both these figures were well above what the current Aperio E100 processor draws approximately 50mA.Therfore excluding the mbed processors consumption from the total, presents a misleading result.

The BLDC motor required more processor power than the Aperio E100 due to the PWM signals and more I/O ports, which require more peripherals. The Aperio E100 processor Atmega168PA doesn't provide any peripheral consumption tables. Therefor a similar processor, the STM32L151xE:s datasheet (Appendix C.9) was investigated to approximate the consumption of extra peripherals. If all GPIO pins, clocks and ADC peripherals were on, these would consume about 28mA if a 96MHz clock was used as was the case of the mbed processor (This clock speed is however not provided for the STM32L151xE processor, but is used as a comparison). Some of these peripherals were already used for the Aperio E100 as well, however it shows that an investigation into the processor's consumption in parallel with the motor drive's was preferable. However the scope of this thesis didn't include the processor consumption and was therefore never considered for power efficiency.

7.1.1.4 Motor bridges selected

The motor bridges selected in section 4.3.2 for the BDC motor and 4.4.2.1 for the BLDC motor both contained losses. In the case of the BDC driver a voltage drop of 2,5% was estimated and for the BLDC 7,5%. Reducing these losses over the bridge would increase the efficiency of the motor, and could thereby reduce the total energy consumption of the system.

7.1.2 Measurements

The different measurements made in this thesis work all had errors which led to errors in the model which was later used to generate the trajectories. Reducing these initial errors would produce a better model, leading to better trajectory results. Below the force, current, and speed measurements are discussed, as well as the impact of these on the model.

7.1.2.1 Load measurement

The method of calculating the load torque using a load cell to measure the static force, and calculating the torque may not be the most exact method. If this thesis had more time and more focus towards measuring techniques. It would have been preferable to measure the torque directly instead of the force, in order to avoid errors introduced by having to measure the pitch as well as inaccuracies in the assumed values used for the friction constant.

7.1.2.2 Current measurement

The results from the current verification showed almost the same result using the LT6105 as the ASSA ABLOYs LabVIEW current measurement method. There were small but negligible deviations of the time behavior between the measurement methods. These could be due to small impedance differences or slightly different running distances of the motor, caused by play in the mechanism, for the different cycles. It could also be caused by minute differences in the perpendicularity of the locking pin, altering the required torque.

However, old current measurements performed by ASSA ABLOY, previously to this project, showed a significant difference to these new measurements. This shows that there exists major performance deviation between different Aperio E100 locks. The reasons for this may be due to manufacturing inconsistencies of the mechanism or motor, it could also be due to the fact that the ASSA ABLOY test team makes very many tests on their systems which may wear out the mechanism or motor compared to the thesis groups Aperio E100 lock, which was new.

These deviations between different Aperio E100 systems may be a problem if an optimal trajectory is to be implemented because all the systems have to be modeled differently. A solution to this is to use safety margins.

7.1.2.3 Speed measurement

The major problem with the speed measurement and verification in this thesis was finding an encoder that could fit the small motor axle. The encoder chosen was a bit too large and had to be altered to fit the motor. This introduced noise into the speed measurements as the code wheel was no longer completely centered on the axle.

7.1.2.4 Model verification

As a result of all the inconsistencies and errors in the measurements discussed above, the model did not truly represent the real world motor dynamics. Alterations to model parameters had to be made to the model. The model also overlooked some losses, such as cogging for the BLDC motor which caused the simulations to run extremely slow. However, even though the model didn’t represent the real motor and system exactly it was considered to be a good representation of the real system dynamics.

7.1.3 Trajectories

In the research for this thesis two trajectory methods; speed, and loss minimization were introduced. This thesis however, only implemented speed and voltage trajectories due to the complexity of the loss minimization method.

The trajectories simulated on the model performed very well compared to the current system, however it must be noted that there was room for improvement here as well. The resolution

of the different trajectories that were created was limited, both in the time and speed/voltage domains. This was done to reduce the simulation times to a manageable level. Reducing these steps, and thereby increasing the resolution, making sure all intermittent steps were tested, could improve the result. The speed and voltage trajectories are discussed in more detail below.

7.1.3.1 Speed Trajectory

The speed trajectories generated, all produced a high starting current as the model feedback created large reference speed errors, causing the voltage to saturate to 3V. This gave a large inrush current which corresponded to most of the energy consumption. It worked better for the BDC motor system since it required a higher starting voltage to initiate motion. The high inrush current was the reason for implementing a slow starting voltage trajectory method. This problem could be reduced by implementing a better feedback controller to alter the input voltage.

7.1.3.2 Voltage Trajectory

Since the performance of the trajectories calculated, all used the model, errors in this model inevitably introduced errors into the calculated trajectories energy consumption. This could be seen with some of the minimum energy steps not actually reaching the end position when inputted into the system. As well as sometimes steps were getting cut of early by the braking function implemented on the processor. Figure 59 and Figure 61 shows this happening to the BDC motor and Figure 64 and Figure 66 show it for the BLDC motor. The result of the voltage still being on, after the motor has reached its end position, is unnecessary energy consumption due to the constant motor bridge current draw. All the trajectory steps could obviously be further optimized if the model error was reduced, and steps no longer were cut off.

For both the BDC and BLDC motor systems, the voltage trajectory presented the better result than the speed and constant voltage trajectories. This could be due to this trajectory giving a smoother slow start, as well as a gradual deceleration using all the momentum of the motor, and wasting as little as possible to braking.

For both the speed and voltage trajectories only the minimum energy step was found and implemented on the motor. The steps that always showed the minimum energy were the E-C-T (exponential acceleration, cruise, trapezoidal deceleration) so only this step type was implemented. It would have been interesting to evaluate and implement the other step types, T-C-T, E-C-E and T-C-E as well. However, due to time constraints and long implementation times this had to be overlooked.

7.1.4 Energy results

The results showed that a 33% energy reduction could be achieved with the current BDC system as well as a significant energy reduction of 88% for the BLDC system compared with original Aperio E100 system. Both these reductions were achieved by using the same method of voltage trajectories.

7.1.4.1 Comparison between BLDC and BDC

The main reason that the BLDC motor outperformed the BDC motor is that it has a higher efficiency and also a lot smaller losses such as cogging and internal brush friction. The

BLDC motor also has a much lower resistance (approximately a third) which lowers the armature copper losses.

The Brushed DC motor required a lot higher input voltage to start moving which resulted in a high inrush current. The combination of a higher; overall current, as well as voltage, were two factors that increase the total energy consumption of the BDC system.

7.1.4.2 Torque ripple

As seen in the result plots from the BLDC motors, there are quite a lot torque ripples. These were mainly caused by the PWM switching in the motor drive, used to achieve variable speed drive, but could also be due to the commutation.

7.1.4.3 Trade-off diagram

The trade-off diagrams (Figure 54, Figure 63) presented in section 5.4 shows the correlation between the operating time, energy consumption and required voltage. Generally the energy was decreased and the operating time increased with reduced PWM duty cycle. The BDC motor (Figure 54) locking sequence, however showed an energy increase at lower duty cycles than 80%, caused by the static friction in the motor which becomes predominant at lower torques and speeds. This is not shown for the opening sequence nor for the BLDC motor (Figure 63). This is explained by the resolution of the different duty cycles tested, had these steps been smaller, this behavior could also been observed here.

7.1.4.4 Extended battery life

The battery lifetime calculations shown in Figure 70 in section 5.4.4 showed a total increase in the battery life between the original Aperio E100 system and the BLDC system with 44%. This was done whilst the motor component of the entire consumption was reduced by 82% from the Aperio E100s 34% to the BLDCs 6%. The figure however also shows the maximum battery life possible as about 62 months, and in order to increase this number, other consumptions in the system such as the RFID communication and the processor energy need to be reduced.

7.1.5 Reliability

Due to the changing characteristics and minor play in the mechanical system of the Aperio E100, reliability that a step always worked was not certain. This could be improved by enhancing the fastening of the motor and lead screw, or by adding safety margins to the voltage steps and a contingency plan if the system didn’t perform as expected.

7.2 Future work

As presented previously in the discussion there is still room for improvement for the Aperio E100 system and some of these are presented here.

7.2.1 Motor selection

Due to the difficulty in almost any application of finding a motor that are optimized for the specific system, other methods could be used. An alternative of selecting a motor would be to design and build the motor oneself, using optimization algorithms as presented in the section 3.5.2. A method of doing this is described by Roos [75], where a complete method of

developing mechatronic products is discussed, the main goal being to develop all the components in a system together instead of individually.

7.2.2 Control

As discussed previously in section 7.1.3.1 there was a problem with the voltage step saturating to 3V for the speed trajectory. This was caused by the controller being improperly tuned and could therefore be further developed by focusing on controller techniques for the velocity feedback within the modeled motor system. If this were improved the speed trajectory model may produce better results than were achieved in this thesis.

7.2.3 Ripples/ soft switching

Even though the thesis showed good results, there was still a problem with torque ripples as seen in Figure 68. A way of reducing these peaks would be to use a soft switching approach, as discussed in section 3.2.2.4 in the frame of reference.

7.2.4 Irregular system performance

To solve the problem with changing dynamics of the mechanism, a timer fail routine could be implemented into the software, which runs the motor again if it fails to reach the next state. To make a smart system the program could also use machine learning techniques, where the software analyses the performance of the lock and alters the duty cycle (add or subtract to all duty cycles in the Voltage vector). This information could also be used by technicians evaluating the health of the locks as a pre-maintenance function.

7.2.5 Aperio E100 component consumption

As discussed previously the battery life can only be extended to about 62 months by reducing the motor consumption to zero. In order to extend beyond this other components such as the RFID and the processor consumption need to be reduced and this could be an area of future work that would be interesting to investigate.

The processor used in the thesis was oversized and had a minimum running current twice that of the processor in the Aperio E100 system. To get more precise results of the possible total reductions in consumption using the voltage step trajectories, these would have to be implemented on the Aperio processor, or a new investigation into energy efficient processors needs to be carried out.

7.2.6 Mechanism

Alterations to the locking mechanism were out of scope in this thesis due to time constraints and security concerns. However changes to the lead screw pitch or design alterations to the leaver could change the torque needed by the motor, giving more degrees of freedom when selecting a motor.

8 Bibliography

[1] A. ABLOY, "Aperio E100," ASSA ABLOY, [Online]. Available: http://w3.assaabloy.co.uk/images/catalog/ikon/Print_Farbe/APERIO/PDF/Aperio_online_overview.pdf. [Accessed 12 5 2014].

[2] KTH, "Master Thesis Projects at the department of machine design," 2013.

[3] R. Condit, "Brushed DC Motor Fundamentals," Microship Technology Inc..

[4] M. Nikolic, J. Kovacevic, N. Pjevalica, I. Papp and N. Milivojevic, "Real Time FPGA Implementation of Brushless DC Motor Control Using Single Current Senso," in *SISY2013*, Subotica, 2013.

[5] J. Cross, G. C. R. Sincero and P. Viarouge, "Design Method for Brush Permanent Magnet DC Motors," 2009.

[6] F. Aghili, "Fault-Tolerant Torque Control of BLDC Motors," *IEEE Transactions on Power Electronics,* vol. 26, no. 2, pp. 355-364, 2011.

[7] H. Wang, "Design and Implementation of Brushless DC Motor Drive and Control System," in *International Workshop on Information and Electronics Engineering*, 2012.

[8] I. Bodea and S. A. Nasar, "Chapter 2 - Introduction to Linear Electric Actuators and Generators," in *Linear Electric Actuators and Generators*, pp. 33-44.

[9] R. Crowder, Electric Drives and Electromechanical Systems: Applications and Control, 2006.

[10] M. Rakesh and P. V. R. L. Narasimham, "Different Braking Techniques Employed to a Brushless DC Motor Drive used in Locomotives," *IEEJ,* vol. 3, no. 2, pp. 784-790, 2012.

[11] J. McMahon, "Piezoelectric Motors equipment Performance," *Control Engineering,* vol. Aug, p. 48(M5), 2010.

[12] H. X. Nguyen, C. Edeler and S. Fatikow, "Contact mechanics modeling of piezo-actuated stick-slip microdrives," *Physical Mesomechanics,* vol. 15, no. 5-6, pp. 280-286, 2012.

[13] S.-S. Jeong, S.-K. Cheon, J.-K. Park and T.-G. Park, "Design and Fabrication of Three Touch Point Thin Ultrasonic Rotary Motor," 2013.

[14] B. Shah, "Field Oriented Control of Step Motors," 2000.

[15] F. Claeyssen, N. Lhermet and T. Maillard, "Magnetostrictive Actuators compared to Piezoelectric actuators," 2002..

[16] F. Claeyssen, N. Lhermet and T. Maillard, "Magnetostrictive Elastic Wave Type Linear Motion with TERFENOL-D," in *European Workshop on Smart Structures in Engineering and Technology SPIE Vol 4763*, 1997.

[17] A. M. Pawlak, Sensors and Actuators in Mechatronics: Design and Applications, 2006.

[18] O. E. Struman, "Self-latching solenoid actuator". Patent US3683239 A, 8 August 1972.

[19] I. Yatchev, K. Hinov and V. Gueorgiev, "Dynamic Characteristics of a Bistable Linear Actuator with Moving Permanent Magnet," *Serbian Journal of Electrical engineering,* vol. 1, no. 2, pp. 207-214, 2004.

[20] F. Claeyssen, N. Lhermet and T. Maillard, "Magnetostrictive Actuators compared to Piezoelectric actuators," 2002.

[21] J. B. Grimbleby, "A Simple Algorithm for closed_loop control of Stepping motors," *Electr. Power Appl.,* vol. 142, no. 1, pp. 5-13, 1995.

[22] Brushed DC Motor Fundamentals http://educypedia.karadimov.info/library/00905a.pdf pp.1-2.

[23] A. Hughes, Electric Motors and Drives, 2005.

[24] C. De Angelo, G. Bossio and G. García, "Loss Minimization in DC Motor Drives".

[25] E. S. Sergaki, G. S. Stavrakakis and A. D. Pouliezos, "Optimal Robot Speed Trajectory by Minimization of the Actuator Motor Electromechanical Losses," 2002.

[26] A. Kusko and D. Galler, "Control Means for Minimization of Losses in AC and DC Motor Drives," 1983.

[27] U. A. Bakshi and M. V. Bakshi, Electromechanical Energy Conversion & D.C. Machines, 2009.

[28] J. Shi and T.-C. Li, "New Method to Eliminate Commutation Torque Ripple of Brushless DC Motor With Minimum Commutation Time," 2013.

[29] A. N. Bando, Electrical Machines: Theory and Practice.

[30] A. Krawczyk, S. Wiak and X. Lopez-Fernandez, Electromagnetic Fields in Mechatronics, Electrical and Electronic Engineering, 2006.

[31] U.S. Department of Energy, "Buying an Energy-Efficient Electric Motor".

[32] S. K. Bhattacharya and B. Singh, Control Of Electrical Machines, 1996.

[33] C.-L. Xia, Permanent Magnet Brushless DC Motor Drives and Controls, First Edition., 2012.

[34] I. Bataresh, "4 - The Power MOSFET," in *Power Electronics Handbook (Third Edition)*, 2011, p. 51.

[35] K. Yilmaz, "Comparison of axial flux and radial flux brushless DC motor topologies for control moment gyroscope wheel application," 2009.

[36] D. Hanselman, Brushless Permanent Magnet Motor Design: Second edition, 2006.

[37] I. V. Mitchell, J. Coey, D. Givord, I. Harris and R. Hanitsch, Concerted European Action on Magnets (CEAM), 1987.

[38] R. R. Pittman, "machine design," 1 May 2000. [Online]. Available: http://machinedesign.com/technologies/slotless-motors-smooth-way.

[39] J. F. Gieras, Permanent Magnet Motor Technology: Design and Application, Third Edition, 2010.

[40] G. Yan and F. O. Serteller, "Brushless direct current (BLDC) machine Bipolar – Unipolar Driving Circuit education study," 2010.

[41] G. H. Jang, M. G. Kim and H. Y. Kim, "A bipolarstarting and unipolar-running method to drive a brushless dc motor in high speed with large starting torque".

[42] A. Smith, "Calculating power loss in switching MOSFETs," 8 1 2011. [Online]. Available: http://www.eetimes.com/document.asp?doc_id=1278970. [Accessed 5 2014].

[43] M. M. Shahbazi, S. M. Madani and A. Ebrahimi, "New Resonant Pole Inverter for Battery Fed Brushless DC Motor Drive".

[44] Z. Y. Pan and F. L. Lou, "Novel Soft-Switching Inverter for Brushless DC Motor Variable Speed Drive System," *Transactions on Power Electronics,* vol. 19, no. 2, pp.

280-289, 2004.

[45] G. R. Herrington, "Trapezoidal or sinusoidal commutation control of brushless d.c.motors with pulse width modulation amplifiers," *SPIE Acquisition, Tracking, and Pointing,* vol. IV, no. 1304, 1990.

[46] J. P. John, S. Suresh Kumar and Jaya B., "Space Vector Modulation based Field Oriented Control Scheme for Brushless DC Motors," in *ICETECT 2011*, 2011.

[47] C. Chan, J. Jiang, W. Xia, K. Chau and M. Zhu, "Optimal-Efficiency Control for Constant-Power Operation of Phase-Decoupling Permanent-Magnet Brushless Motor Drives," in *IEEE Applied Power Electronics Conference and Exposition - APec*, 1996.

[48] C.-W. Hung, J.-T. Su, C.-W. Liu, C.-T. Lin and J.-H. Chen, "Fuzzy Gain Scheduling PI Controller for a Sensorless Four Switch Three Phase BLDC Motor," 2010.

[49] A. Ungurean, V. Coroban-Schramel and I. Boldea, "Sensorless control of a BLDC PM motor based on I-f starting and Back-EMF zero-crossing detection," in *12th International Conference on Optimization of Electrical and Electronic Equipment, OPTIM*, 2010.

[50] D. Czarkowski, "DC-DC Converters," in *Power Electronics Handbook (Third Edition)*, 2011, pp. 249-263.

[51] V. Pop, H. Bergveld, D. Danilov, P. Regtien and P. Notten, Battery Management Systems: Accurate State-of-Charge Indication for Battery Powered Applications, 2008.

[52] K. Sozanski, Digital Signal Processing in Power Electronics Control Circuits, 2013.

[53] F. Roos, H. Johansson and J. Wikander, "Optimal selection of motor and gearhead in mechatronic applications," 2005.

[54] J. E. Poulin, "Practical Considerations in DC Motor and Amplifier Selection," *Transactions on Industry Applications,* Vols. IA-20, no. 5, 1984.

[55] G. A. McCoy, T. Litman and J. G. Douglas, Energy-Efficient Electric Motor Selection Handbook, 1993.

[56] K. George, S. K S and S. Gopinath, "Finite Element Modeling of Five Phase Permanent Magnet BLDC Motor for High Power Density Application]," *International Journal of Power Electronicvs and Drive systems (IJPEDS),* vol. 3, no. 4, pp. 384-391, 2013.

[57] L. Zhang, D. Luo, L. Su, D. Cao and Z. Luo, "Design of a DC Motor Soft Start Based on AVR Microcontroller," *Applied Mechanics and Materials,* Vols. 55-57, pp. 382-397, 2011.

[58] M. Markovic, P. Ragot and Y. Perriard, "Design optimization of a BLDC motor: a comparative analysis," 2007.

[59] A. Rahideh, T. Korakianitis, P. Ruiz, T. Keeble and M. Rothman, "Optimal brushless DC motor design using genetic algorithms.," *Journal of Magnetism and Magnetic Materials,* vol. 322, no. 22, pp. 3680-3687, 2010.

[60] F. Messine, B. Nogarede and J.-L. Lagouanelle, "Optimal Design of Electromechanical Actuators: A New Method Based on Global Optimization," *IEEE Transactions on Magnetics,* vol. 34, no. 1, pp. 299-309, 1998.

[61] M. Markovic, V. Muller, A. Hodder and Y. Pierrard, "Optimal design of an in-wheel BLDC motor for a kick scooter," 2010.

[62] "Finite Element Method Magnetics Software," [Online]. Available:

http://www.femm.info/wiki/Download. [Accessed 4 2014].

[63] D. Ishak and A. H. A. Hassan, "Analytical modeling of permanent magnet excited brushed dc motor for low-cost applications," in *ISMA08*, Amman, 2008.

[64] C. H. Kim and B. K. Kim, "Energy-Saving 3-Step Velocity Control Algorithm for Battery-Powered Wheeled Mobile Robots," in *International Conference on Robotics and Automation*, Barcelona, 2005.

[65] C. H. Kim and B. K. Kim, "Minimum-Energy Translational Trajectory Generation for Differential-Driven Wheeled Mobile Robots," *Intell Robot Syst,* pp. 367-383, 2007.

[66] R. Saidur, S. Mekhilef, M. Ali, A. Safari and H. Mohammed, "Applications of variable speed drive (VSD) in electrical motors energy savings," *Renewable and Sustainable Energy Reviews,* vol. 16, pp. 543-550, 2012.

[67] A. Watanabe and S. Yuta, "Efficient Feedforward Current Control Method of Brushless DC Motor," in *The 11th IEEE International workshop on Advanced Motion Control*, Nagaoka, 2010.

[68] Z. Lü and F. Sun, "Soft-Start Circuitry for DC Motor," 2011.

[69] L. Tie and J. Le-jia, "Adaptive Neuro Fuzzy based Soft Starting of DC Motor," in *International Conference on Electrical and Control Engineering*, 2010.

[70] V. K. Jadon and S. Verma, Analysis and Design of Machine Elements, 2010.

[71] Engineering-abc.com. [Online]. Available: http://www.tribology-abc.com/abc/cof.htm. [Accessed 15 4 2014].

[72] "Johnson Electric," Johnson Electric, 2014. [Online]. Available: http://www.johnsonelectric.com/en/resources-for-engineers/automotive-applications/motion-technology/ec-motor-brushless.html.

[73] B. Tibor, V. Fedák and F. Ďurovský, "Modeling and Simulation of the BLDC Motor in MATLAB GUI," 2011.

[74] A. Tashakori, M. Ektesabi and N. Hosseinzadeh, "Modeling of BLDC Motor with Ideal Back-EMF for Automotive Applications," in *World Congress on Engineering*, London, 2011.

[75] F. Roos, "Integrated Design of Mechatronic Servo Systems," 2007.

9 Appendices

9.1 Appendix A Requirements

Overhead requirements:	
Constant supply voltage:	3V
Maximum current peaks:	<500mA
Motor Size (Length, Width, Height):	20, 15, 12 (mm)
Unlocking time:	300ms
Linear motor requirements:	
Minimum stroke (distance of motion):	10mm
Holding torque of load: measured to:	0.42Nm
Calculated requirements:	
Maximum torque required:	0.43mNm
Limiting requirements:	
No battery management	-
No change of the existing locking mechanism and gearing.	-
No energy harvesting	-

9.2 Appendix B

BLDC- Prototype Circuit diagram

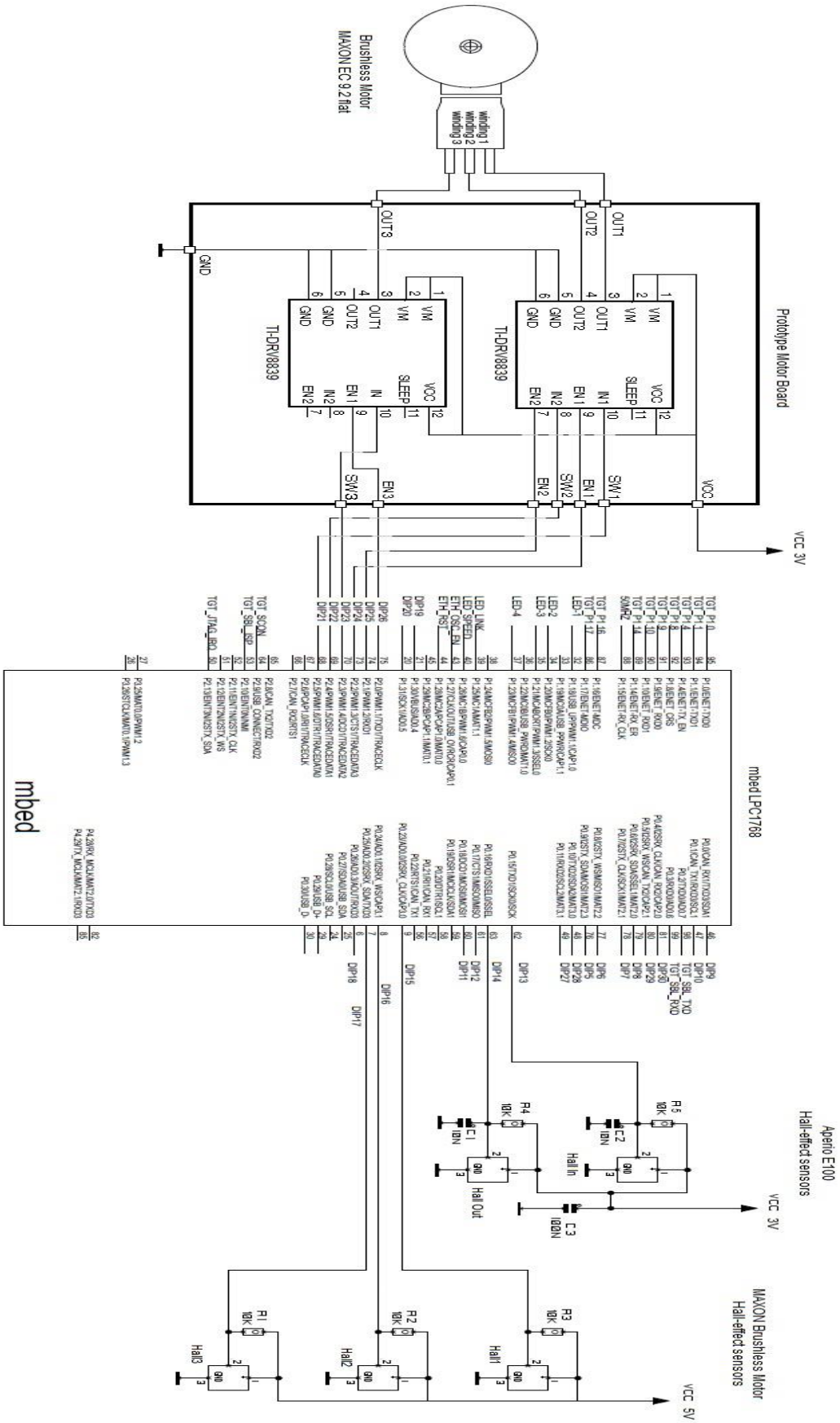

9.3 Appendix C
Datasheets

C.1 BDC: QX-FF-030

C.2 BDC motor drive: DRV8837EVM

C.3 BLDC: EC 9.2 flat 10mm, brushless, 0.5 Watt with Hall sensors

C.4 BLDC motor drive: DRV8839

C.5 Current sense amplifier: LT6105

C.6 PhidgetsBridge

C.7 Phidgets loadcell

C.8 Encoder: HEDS-5540#A01

C.9 Processor: STM32L151xE

C.10 Processor: LPC1768